Radiative tail in π_{e2} decay and some remarks on $\mu-e$ universality

E. A. Kuraev
Bogoliubov Laboratory for Theoretical Physics, JINR, 141980 Dubna, Russia

(Submitted 25 November 1996)
Pis'ma Zh. Éksp. Teor. Fiz. **65**, No. 2, 119–122 (25 January 1997)

The results of lowest-order perturbation theory calculations of the photon and positron spectra in radiative π_{e2} decay are generalized to all orders of perturbation theory using the structure-function method. An additional source of radiative corrections to the ratio of the positron and muon channels of pion decay, due to emission of virtual and real photons and pairs, is considered. It depends on details of the detection of the final particles and is large enough to be taken into account in theoretical estimates with a level of accuracy of 0.1%. © *1997 American Institute of Physics.* [S0021-3640(97)00102-3]

PACS numbers: 13.40.Hq, 13.40.Ks, 12.15.Lk, 14.40.Aq

As a first step in the calculation of the spectra of radiative pion decays we reproduce the results obtained by Berman and Kinoshita,[1] treating the pion as a point-like particle. Kinoshita[1] calculated the positron energy spectrum in radiative pion decay:

$$\frac{\mathbf{d}\Gamma}{\Gamma_0\mathbf{d}y}=\frac{\alpha}{\pi}\left[\frac{1+y^2}{1-y}\,(L-1)-1+y-\frac{1}{2}\,(1-y)\ln(1-y)+\frac{1+y^2}{1-y}\,\ln y\right],$$

$$y_{\min}\leqslant y\leqslant 1+m_e^2/m_\pi^2, \tag{1}$$

where $y=2\varepsilon_e/m_\pi$ is the positron energy fraction, ε_e is the positron energy (here and below we have in mind the rest frame of the pion), $L=\ln(m_\pi/m_e)=5.6$ is the ''large logarithm'', and m_π and m_e are the masses of the pion and positron. The quantity

$$\Gamma_0=\frac{G^2|V_{ud}|^2}{8\pi}\,f_\pi^2 m_e^2 m_\pi\left(1-\frac{m_e^2}{m_\pi^2}\right)^2=2.53\cdot 10^{-14}\ \text{MeV}, \tag{2}$$

is the total width of π_{e2} decay, calculated in the Born approximation.

We will now calculate the photon spectrum. Consider first the emission of a soft real photon. The corresponding contribution to the total width may be obtained by the standard integration of the differential widths:

$$\frac{\mathbf{d}\Gamma^{\text{soft}}}{\Gamma_0}=-\frac{\alpha}{4\pi^2}\int\frac{\mathbf{d}^3k}{\omega}\left(\frac{P}{Pk}-\frac{p_e}{p_e k}\right)^2\Bigg|_{\omega\leqslant\Delta\varepsilon\ll m_\pi/2}, \tag{3}$$

where P, p_e, and k are the four-momenta of the pion, positron, and photon, respectively, $P^2=m_\pi^2$, $p_e^2=m_e^2$, $k^2=\lambda^2$, and λ is the photon mass. The result has the form

$$\frac{\Gamma^{\text{soft}}}{\Gamma_0}=\frac{\alpha}{\pi}\left[-b(\sigma)\ln\frac{2\Delta\varepsilon}{\lambda}+1-\frac{1+\sigma}{2(1-\sigma)}\ln\sigma-\frac{1+\sigma}{4(1-\sigma)}\ln^2\sigma\right.$$
$$\left.-\frac{1+\sigma}{1-\sigma}\,\mathrm{Li}_2(1-\sigma)\right], \tag{4}$$

where

$$b(\sigma)=\frac{1+\sigma}{1-\sigma}\ln\sigma+2,\quad \sigma=\frac{m_e^2}{m_\pi^2},\quad \mathrm{Li}_2(x)=-\int_0^x\frac{\mathbf{d}t}{t}\ln(1-t). \tag{5}$$

Consider now the hard photon emission process

$$\pi^+(P)\to e^+(p_e)+\nu_e(p_\nu)+\gamma(k). \tag{6}$$

The standard procedure of final-states summing of the squared modulus of its matrix element and integration over the neutrino phase volume leads to the spectral distribution over the photon energy fraction $x=2k^0/m_\pi$:

$$\frac{\mathbf{d}\Gamma}{\Gamma_0\mathbf{d}x}=\frac{\alpha}{2\pi}\frac{x(1-x-\sigma)}{(1-\sigma)^2}\left[-\frac{4(1-\sigma)}{x^2}-\frac{1}{1-x}+\frac{1}{x(1-x-\sigma)}\left(\frac{1}{x}\,(1+(1-x)^2)\right.\right.$$
$$\left.\left.+2\sigma-2\frac{\sigma^2}{x}\right)\ln\frac{1-x}{\sigma}\right]. \tag{7}$$

Further integration of this spectrum give the result

$$\int_{x_{\min}}^{1-\sigma}\frac{\mathbf{d}\Gamma}{\Gamma_0\mathbf{d}x}\,\mathbf{d}x=\frac{\alpha}{2\pi}\left[-2b(\sigma)\ln\frac{1-\sigma}{x_{\min}}-2\frac{1+\sigma}{1-\sigma}\,\mathrm{Li}_2(1-\sigma)+\frac{3(1-2\sigma)}{2(1-\sigma)^2}\ln\sigma\right.$$
$$\left.+\frac{19-25\sigma}{4(1-\sigma)}\right],\quad x_{\min}=\frac{2k^0_{\min}}{m_\pi}. \tag{8}$$

Putting $k^0_{\min}=\Delta\varepsilon$ in this formula and adding the soft photon contribution, we obtain (in agreement with Kinoshita's 1959 result) the contribution to the width from the inner bremsstrahlung of a point-like pion:

$$\frac{\Gamma_{IB}}{\Gamma_0}=\frac{\alpha}{\pi}\left\{b(\sigma)\left[\ln\frac{\lambda}{m_\pi}-\ln(1-\sigma)-\frac{1}{4}\ln\sigma+\frac{3}{4}\right]-2\frac{1+\sigma}{1-\sigma}\,\mathrm{Li}_2(1-\sigma)\right.$$
$$\left.-\frac{\sigma(10-7\sigma)}{4(1-\sigma)^2}\ln\sigma+\frac{15-21\sigma}{8(1-\sigma)}\right\}. \tag{9}$$

Now return to the positron spectrum. The contributions to it containing the large logarithm L may be associated with the known kernel of the Altarelli–Parisi–Lipatov evolution equation (see Ref. 2):

$$P^{(1)}(y)=\lim_{\Delta\to0}\left[\frac{1+y^2}{1-y}\,\theta(1-y-\Delta)+\left(\frac{3}{2}+2\ln\Delta\right)\delta(1-y)\right]=\left(\frac{1+y^2}{1-y}\right)_+. \tag{10}$$

Using the factorization theorem, we may generalize this spectrum to include the leading logarithmic terms in all orders of perturbation theory. This may be done in terms of

structure functions $D(y,\sigma)$ (Ref. 2). In the case of the photon spectrum the function $D(1-x,\sigma)$ appears. The function $D(y,\sigma)$ describes the probability of finding a positron with energy fraction y inside the initial positron. It may be present in the form of a sum of non-singlet and singlet contributions, $D=D^{\gamma}+D^{e^+e^-}$. Iteration of the evolution equations gives

$$D(y,\sigma)=\delta(1-y)+P^{(1)}(y)\,\gamma+\frac{1}{2}\,(P^{(2)}(y)+P^{e^+e^-}(y))\,\gamma^2+\ldots, \tag{11}$$

where

$$\gamma=-3\ln\left(1-\frac{\alpha}{3\pi}\,(L-1)\right),$$

$$P^{(2)}(y)=\int_y^1\frac{\mathbf{d}t}{t}\,P^{(1)}(t)P^{(1)}\left(\frac{y}{t}\right)=\lim_{\Delta\to 0}\left\{\left[\left(2\ln\Delta+\frac{3}{2}\right)^2-\frac{2\pi^2}{3}\right]\delta(1-y)\right.$$
$$+2\left[\frac{1+y^2}{1-y}\left(2\ln(1-y)-\ln y+\frac{3}{2}\right)\right.$$
$$\left.\left.+\frac{1}{2}\,(1+y)\ln y-1+y\right]\theta(1-y-\Delta)\right\},$$

$$P^{e^+e^-}(y)=\frac{2}{3}\,P^{(1)}(y)+\frac{(1-y)}{3y}\,(4+7y+4y^2)+2(1+y)\ln y. \tag{12}$$

It is convenient to use the smoothed form of them:

$$D^{\gamma}(y)=\frac{1}{2}\,b(1-y)^{(1/2)b-1}\left[1+\frac{3}{2}\,b-\frac{1}{48}\,b^2\left(\frac{2}{3}\,L+\pi^2-\frac{47}{8}\right)\right]-\frac{1}{4}\,b(1+y)$$
$$+\frac{1}{32}\,b^2\left[4(1+y)\ln\frac{1}{1-y}+\frac{1+3y^2}{1-y}\ln\frac{1}{y}-5-y\right]+\mathcal{O}(b^3),$$

$$D^{e^+e^-}(y)=\frac{1}{3}\left(\frac{\alpha}{\pi}\left(L-\ln(1-y)-\frac{5}{6}\right)\right)^2(1-y)^{(1/2)b-1}\left(1+y^2+\frac{1}{3}\,b\left(L-\ln(1-y)\right.\right.$$
$$\left.\left.-\frac{5}{6}\right)\right)+\frac{1}{96}\,b^2\left[\frac{1-y}{y}\,(4+7y+4y^2)+6(1+y)\ln y\right]+\mathcal{O}(b^3),$$

$$b=\frac{4\alpha}{\pi}\,(L-1). \tag{13}$$

The expressions for spectra are as follows:

$$\frac{\mathbf{d}\Gamma}{\Gamma_0\mathbf{d}y}=D(y,\sigma)\left[1+\frac{\alpha}{\pi}\,K_e(y)\right],$$

$$K_e(y)=-1+y-\frac{1-y}{2}\ln(1-y)+\frac{1+y^2}{1-y}\ln y,\quad y=\frac{2\varepsilon_e}{m_{\pi}},$$

$$\frac{\mathbf{d}\Gamma}{\Gamma_0 \mathbf{d}x} = D(1-x,\sigma)\left[1+\frac{\alpha}{\pi}K_\gamma(x)\right];$$

$$K_\gamma(x) = x + \frac{1+(1-x)^2}{x}\ln(1-x), \quad x = \frac{2\omega}{m_\pi}. \tag{14}$$

Let us discuss the contribution of the inelastic processes considered above to the ratio of the widths of the positron and muon modes of pion decay, $R_{\pi l2}$:

$$R_{\pi l2} = \frac{\Gamma(\pi \to e\nu) + \Gamma(\pi \to e\nu\gamma)}{\Gamma(\pi \to \mu\nu) + \Gamma(\pi \to \mu\nu\gamma)}. \tag{15}$$

Close attention was paid to this quantity some years ago,[3,4] but the corrections for emission processes in higher orders of perturbation theory were not taken into account. Keeping in mind that the quantity $P^{(1)}(y)$ has the property

$$\int_0^1 \mathbf{d}y \; P^{(1)}(y) = 0, \tag{16}$$

we make the important observation that as long as an experiment is proceeding in such a way that no cuts are imposed on the positron energy, then no large logarithmic contributions appear. However, if the cuts are such that the y integration is restricted or convoluted with a y-dependent function, some terms proportional to the large logarithm L will remain. We now suggest that there exists some minimum energy ε_{th} for detection of the positron. An additional contribution (not considered in Ref. 4) appears:

$$\frac{\Delta R}{R_0} = -\frac{\alpha}{\pi}\int_0^{x_{\text{th}}} \mathbf{d}x \; \frac{1+x^2}{1-x}(L-1) + \frac{\alpha}{\pi}\int_{x_{\text{th}}}^1 \mathbf{d}x \; D(x,\sigma)K_e(x), \quad x_{\text{th}} = \frac{2\varepsilon_{\text{th}}}{m_\pi}, \tag{17}$$

where

$$R_0 = \frac{m_e^2}{m_\mu^2}\frac{(1-m_e^2/m_\pi^2)^2}{(1-m_\mu^2/m_\pi^2)^2} = 1.28347\cdot 10^{-4}. \tag{18}$$

For typical values $x_{\text{th}} = 0.1$ this additional contribution will have a magnitude of order 10^{-3} and should be taken into account in calculations for accuracy at the 0.1% level.

The author is grateful to the Russian Fund for Fundamental Research for Grant 96-02-17512. He is also thankful to V. Gordeev and A. Arbuzov for discussions and help.

[1] S. M. Berman, Phys. Rev. Lett. **1**, 468 (1958); T. Kinoshita, Phys. Rev. Lett. **2**, 477 (1959).
[2] E. A. Kuraev and V. S. Fadin, Sov. J. Nucl. Phys. **41**, 466 (1985).
[3] D. Bryman, Comments Nucl. Part. Phys. **21**, 101 (1993).
[4] W. Marciano and A. Sirlin, Phys. Rev. Lett. **71**, 3629 (1993).

Published in English in the original Russian journal. Edited by Steve Torstveit.

On the possibility of measuring the degree of transverse polarization of a proton beam by means of elastic *pe* scattering

I. V. Glavanakov, Yu. F. Krechetov,[a)] G. M. Radutskiĭ, and A. N. Tabachenko
Scientific-Research Institute of Nuclear Physics, 634050 Tomsk, Russia

(Submitted 3 December 1996)
Pis'ma Zh. Éksp. Teor. Fiz. **65**, No. 2, 123–127 (25 January 1997)

The analyzing power of the elastic scattering of high-energy polarized protons by polarized electrons for the polarimetry of proton beams is calculated. It is shown that this process can be used to measure the degree of transverse polarization of a beam at energies all the way up to those at LHC. © *1997 American Institute of Physics.*
[S0021-3640(97)00202-8]

PACS numbers: 12.20.Ds, 13.60.Fz

Measurements of spin effects in proton–proton scattering are being proposed for increasingly higher energies.[1,2] In such experiments it is necessary to know the degree of polarization of the proton beam. One of the main criteria which determine the reaction to be used as a proton polarization analyzer is that there be no large theoretical uncertainties in models for the amplitude of the process. We propose to use for this purpose the elastic scattering of protons by electrons. The one-photon approximation, in which the amplitude uncertainties are due solely to the electromagnetic form factors of the proton and which agree well with existing experimental data, can be used for calculations in the kinematic range of interest.

We showed in a previous work that the longitudinal polarization of protons with energy above 15 GeV and the transverse polarization at proton energy $\simeq 25$ GeV can be measured by means of the elastic scattering of polarized protons by polarized electrons.[3,4] The possible variants of the polarized electronic target were analyzed.[5] In solid-state targets with a relatively low degree of polarization of the electrons (e.g., in Permendur, where the degree of polarization is about 7%), as a result of multiple Coulomb scattering, the beam breaks up during the acquisition of the statistical sample. Moreover, solid-state and gaseous targets give a high hadronic background. It is preferable to use a beam of free electrons for the target.

To describe the elastic scattering of protons by electrons, we shall employ the spiral-amplitudes formalism (the notation is similar to that adopted for elastic *pp* scattering[6]). In the one-photon approximation we have

$$\varphi_1=\langle++|A|++\rangle=F_1(t)\left[\frac{s-M^2-m^2}{t}+\frac{s(M^2+m^2)-(M^2-m^2)^2}{4q^2s}\right]-\kappa_pF_2(t),$$

$$\varphi_2=\langle++|A|--\rangle=F_1(t)\frac{Mm}{2q^2}-\frac{m}{2M}\kappa_pF_2(t),$$

$$\varphi_3=\langle+-|A|+-\rangle=F_1(t)\frac{s-M^2-m^2}{t}\left(1+\frac{t}{4q^2}\right),$$

$$\varphi_4=\langle+-|A|-+\rangle=-\varphi_2,$$

$$\varphi_5=\langle++|A|+-\rangle=-F_1(t)\frac{m}{4q^2}\frac{s+M^2-m^2}{s}\sqrt{-\frac{s}{t}(4q^2+t)},$$

$$\varphi_6=\langle++|A|-+\rangle=\left[F_1(t)\frac{M}{4q^2}\frac{s-M^2+m^2}{s}-\frac{\kappa_p}{2M}F_2(t)\right]\sqrt{-\frac{s}{t}(4q^2+t)}.$$

Here s, t, and q^2 are the squares of the total energy, the 4-momentum transfer, and the 3-momentum in the center-of-momentum frame, $F_1(t)$ and $F_2(t)$ are proton form factors, $\kappa_p=1.793$ is the anomalous magnetic moment of the proton, and M and m are the proton and electron masses. The amplitudes φ_i are normalized so that[7]

$$\frac{d\sigma}{dt}=\frac{\pi\alpha^2}{2q^2s}[\varphi_1^2+\varphi_3^2+2(\varphi_2^2+\varphi_5^2+\varphi_6^2)]\equiv\frac{\pi\alpha^2}{2q^2s}\sum, \quad A_{LL}\sum=\varphi_1^2-\varphi_3^2,$$

$$A_{NN}\sum=4\frac{Mm}{t}F_1(t)(\varphi_1-\varphi_3), \quad A_{SS}\sum=2\varphi_2(\varphi_1-\varphi_3),$$

$$A_{SL}\sum=-2\varphi_6(\varphi_1-\varphi_3), \quad A_{LS}\sum=2\varphi_5(\varphi_1-\varphi_3).$$

The two-spin asymmetries A_{IJ} are defined in a reference frame attached to each particle so that the unit vector $\hat{N}$ is oriented in a direction normal to the scattering plane, $\hat{L}$ is in the direction of motion, and $\hat{S}=\hat{N}\times\hat{L}$ lies in the scattering plane. One can see from these formulas that all the two-spin asymmetries are proportional to the difference

$$\varphi_1-\varphi_3=-[F_1(t)+\kappa_pF_2(t)],$$

which depends only on t. For maximum $|t|=4q^2$ the asymmetry A_{LL} is close to 1, $A_{NN}\simeq A_{SS}$, but, as calculations showed, A_{SS} decreases rapidly with $|t|$. It is also evident that A_{LS} is always appreciably less than A_{SL}.

The transverse polarization of the proton beam can be determined by measuring the asymmetry of the angular distribution of the electrons, which depends on A_{NN}, A_{SS}, and A_{SL}. The behavior of A_{NN} and A_{SL} as a function of the initial proton momentum and the electron recoil angle is displayed in Figs. 1 and 2. Form-factor scaling, $(1+\kappa_p)G_E=G_M$, was assumed in the calculations, so that the asymmetry does not depend on the form factors. The predicted values of these asymmetries as well as the differential cross section of the reaction (Fig. 3) are quite large, so that there is hope of obtaining reliable information about the polarization of the beam over a wide energy

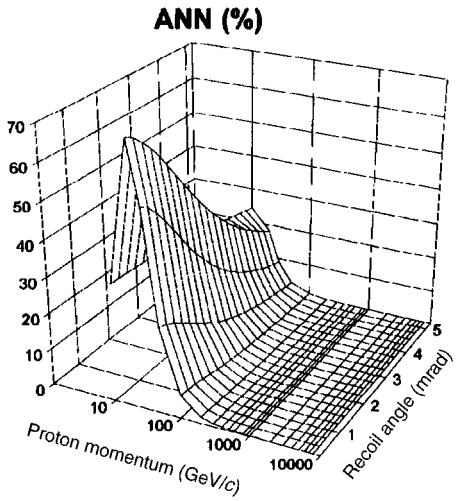

FIG. 1. Two-spin asymmetry A_{NN} versus proton momentum and electron recoil angle.

range. Furthermore, even for 8 TeV protons (LHC) s is small (about 9 GeV^2), so that the background from the inelastic scattering is relatively small, and it is virtually absent for protons with energy less than 300 GeV.

The two-spin asymmetries of the scattering of transversely polarized protons by polarized electrons at rest are large for proton momenta less than 100 GeV/c. Specifically, the asymmetry A_{NN} is maximum for initial proton momentum of about 20 GeV ($\sim$70%, Fig. 1), which corresponds to a squared total energy in the center-of-momentum

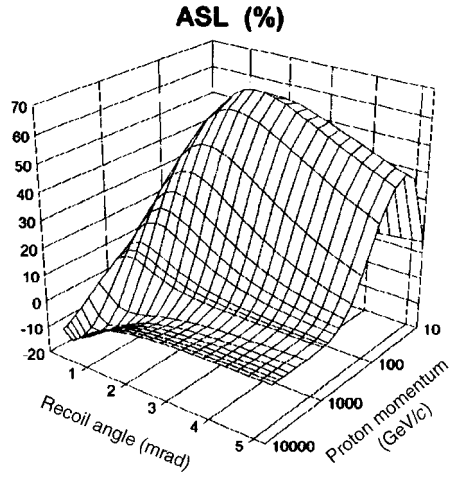

FIG. 2. Two-spin asymmetry A_{SL} versus proton momentum and electron recoil angle.

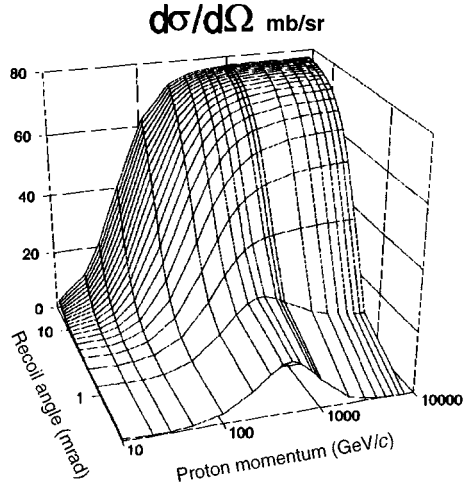

FIG. 3. Differential cross section versus proton momentum and electron recoil angle.

frame $s_0 \simeq 0.9$ GeV^2. As the proton momentum increases, s increases and the asymmetry decreases, which makes it difficult to measure the polarization in the TeV energy range.

We propose a new method of polarimetry of high-energy protons. The heart of the method is the use of a target consisting of a beam of polarized electrons accelerated in the direction of motion of the proton (''anticollider'' scattering). This makes it possible to find for any proton momentum the electron momentum for which $s = s_0$ and so the maximum asymmetry will be observed. As the electron momentum increases, s at first decreases from the value $s' = m^2 + M^2 + 2E_p m$ to the minimum value $(m+M)^2$, at which point the relative velocity of the electron and proton equals zero, and then increases to $s'' = m^2 + M^2 + 2(E_p E_e - P_p P_e)$ (see Fig. 4). Here E_e (P_e) and E_p (P_p) are the electron and proton energies (momenta). If $s_0 < s'$, s'', then for any proton momentum there exists

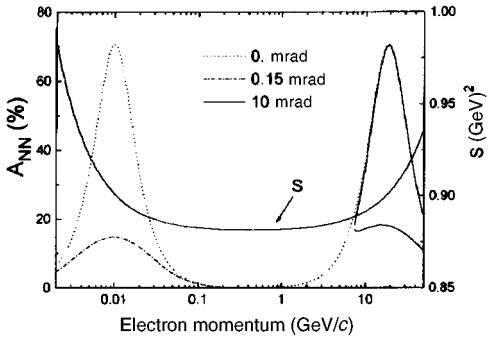

FIG. 4. Two-spin asymmetry A_{NN} and squared total energy s in the center-of-momentum frame versus the initial electron momentum for a proton momentum of 800 GeV/c.

a pair of values of the electron momentum (which differ by an order of magnitude) for which the asymmetry will be maximum:

$$P_e^{\pm} = \frac{m}{M^2}(E_0 P_p \pm P_0 E_p),$$

where $E_0(P_0)$ is the proton energy (momentum) corresponding to maximum asymmetry for scattering by electrons at rest. These two values of the momentum correspond to higher and lower electron velocity compared with the proton velocity. If $s_0 > s'$, i.e., $E_p < E_0$, the maximum asymmetry will be reached only for one value of the momentum of the electron beam, P_e^+.

As an illustration, Fig. 4 shows A_{NN} as a function of the initial electron momentum for an 800 GeV/c proton beam. Two branches of the curve are shown for an electron recoil angle of 10 mrad. These branches are due to the double-valued nature of the solution of the kinematic equations. The relative directions of motion of the center-of-momentum frame and the momentum of the scattered electron in the center-of-momentum frame near the two maxima are opposite, so that the angular distributions of the electrons in the kinematic region of these maxima are substantially different. As one can see from the figure, the angular distribution in the first maximum is two orders of magnitude narrower than in the second maximum.

The great advantage of the ''anticollider'' variant of the *pe* polarimeter is that the total energy at which measurements of A_{NN} are to be performed corresponds to the scattering of an electron with an energy of only[b)] about 14 MeV by a proton at rest. The absence of background processes simplifies the measuring apparatus and lowers its cost. For the same reason, to make a complete kinematic determination of ''anticollider'' *pe* scattering events it is sufficient to measure the energy and direction of an electron or proton, and one of the kinematic quantities can be measured with a low accuracy sufficient for identifying (when necessary) events associated with the double-valued nature of the solution of the kinematic equations. The calculations showed that the region of the second maximum, where, over a relatively wide range of angles of emergence of the electron, the asymmetry is large and is virtually independent of angle, may be attractive for HERA type colliders (in the *ep* variant). In this case, the proton propagates practically on an equilibrium orbit with energy greater than the initial energy; this can probably be used to identify elastic scattering events.

Similar arguments can be repeated for the asymmetry A_{SL} in the TeV range.

We thank S. B. Nurushev and A. P. Potylitsyn for their interest in this work and for helpful discussions.

[a)]e-mail: krechetov@tsinph.tomsk.su

[b)]Hence it follows that the contribution of two-phonon exchange is very small.[8]

[1]RHIC Spin Coll., Proposal on Spin Physics using the RHIC Polarized Collider, August 1992.
[2]W.-D. Nowak, Preprint DESY 96-095.
[3]S. B. Nurushev, A. P. Potylitsin, G. M. Radutsky *et al.*, in *Fifth Workshop on High Energy Spin Physics*, Protvino (1994), p. 311.

[4] S. B. Nurushev, A. P. Potylitsin, G. M. Radutsky *et al.*, in *Proceedings of the Eleventh International Symposium on High Energy Spin Physics*, Bloomington (1994), p. 192.
[5] I. V. Glavanakov, Yu. F. Krechetov, A. P. Potylitsin *et al.*, in *Sixth Workshop on High Energy Spin Physics*, Protvino (1996), p. 187 (to be published in Nucl. Instrum. Methods A (1996)).
[6] M. L. Goldberger, M. T. Grisaru, S. W. MacDowell, and D. Y. Wang, Phys. Rev. **120**, 2250 (1960).
[7] N. H. Buttimore, E. Gotsman, and E. Leader, Phys. Rev. D **18**, 694 (1978).
[8] S. D. Drell and S. Fubini, Phys. Rev. **113**, 741 (1959); J. Arafune and Y. Shimizu, Phys. Rev. D **1**, 3094 (1970).

Translated by M. E. Alferieff

Effective quark Lagrangian in the instanton vacuum with nonzero modes included

B. O. Kerbikov, D. S. Kuzmenko, and Yu. A. Simonov
Institute of Theoretical and Experimental Physics, 117259 Moscow, Russia

(Submitted 5 September 1996; resubmitted 3 December 1996)
Pis'ma Zh. Éksp. Teor. Fiz. **65**, No. 2, 128–132 (25 January 1997)

A new approach to the effective theory of quarks in the instanton vacuum is presented. Exact equations for the quark propagator and Lagrangian are derived which contain contributions of all quark modes with known coefficients. The resulting effective Lagrangian differs from the standard one and resembles that of the Nambu–Jona-Lasinio model. © *1997 American Institute of Physics.*
[S0021-3640(97)00302-2]

PACS numbers: 11.10.Ef, 14.65.−q, 11.15.−q, 02.30.Jr

1. The recent lattice data[1] provided evidence that instantons may be responsible for nonperturbative behavior of $q\bar{q}$ correlators,[2] which makes the study of the quark dynamics in the instantonic vacuum[3–5] an important and fundamental problem.

To date practically all papers on the subject have relied upon the use of the so-called zero-mode approximation (ZMA), which amounts to including only the zero quark mode in a single-instanton fermion propagator.[3] Correspondingly an ansatz for the partition function and effective quark Lagrangian (EQL) containing zero modes only have been proposed[5] and are widely used in the literature.[6,7]

The purpose of this letter is to give a complete normal-mode expansion of the EQL and of the quark propagator. Keeping only zero-mode coefficients in this expansion, one retrieves the ansatz of Ref. 5 for the EQL. Naively one would expect that this choice of the coefficients would yield the dominant contribution to the physical quantities and thus justify the ZMA. However, the exact calculation of the EQL presented below does not show this dominance. More intricate is the analysis of the quark propagator S in the instanton–anti-instanton vacuum. Here the zero-mode term survives but higher modes enter with coefficients of the same order. A similar feature can be seen in the quark partition function $\langle \det S^{-1} \rangle$, where the average $\langle ... \rangle$ is defined below. Thus a new quark dynamics associated with nonzero modes emerges. The main features of this dynamics are outlined below.

2. For clarity of discussion consider an ideal instanton gas with the superposition ansatz[8–10] and with zero net topological charge, i.e., equal numbers of instantons and anti-instantons, $N_+ = N_- = N/2$:

$$A_\mu(x) = \sum_{i=1}^{N} A_\mu^{(i)}(x - R_i), \tag{1}$$

$$gA_\mu^{(i)}=\frac{\overline{\eta}_{a\mu\nu}(x-R_i)_\nu\rho^2\Omega_i^+\tau_a\Omega_i}{(x-R_i)^2[(x-R_i)^2+\rho^2]}, \tag{2}$$

where Ω_i, R_i, and ρ are the color orientation, position, and scale size of the ith instanton.

The EQL is obtained from the Euclidean partition function after averaging over $\{\Omega_i, R_i\}$:

$$Z=\int D\psi D\psi^+ e^{-\int dx\psi^+ S^{-1}\psi}\prod_{i=1}^{N}\frac{dR_i}{V}\,d\Omega_i=\int D\psi D\psi^+ e^{-L_{\rm eff}}, \tag{3}$$

where we have introduced the following definitions:

$$S_0^{-1}=-i\hat{\partial}-im_f,\quad S_i^{-1}=-i\hat{\partial}-g\hat{A}^{(i)}-im_f,\quad S^{-1}=-i\hat{\partial}-g\hat{A}-im_f. \tag{4}$$

Next we introduce the standard set of eigenfunctions $\{u_n^i\}$, $n=0,1,2,...$,

$$(-i\hat{\partial}-g\hat{A}^{(i)})|u_n^i\rangle=\lambda_n|u_n^i\rangle. \tag{5}$$

Then S^{-1} given by (4) has a formal representation as a sum over normal modes,

$$S^{-1}=S_0^{-1}+\sum_{i,m,n}S_0^{-1}|u_m^i\rangle\varepsilon_{mn}^i\langle u_n^i|S_0^{-1}, \tag{6}$$

where $\hat{\varepsilon}$ can be represented either as

$$\varepsilon_{mn}^i=-\langle u_m^i|(S_i-S_0)[1+S_0^{-1}(S_i-S_0)]^{-1}|u_n^i\rangle, \tag{7}$$

or simply as

$$\varepsilon_{mn}^i=-g\langle u_m^i|S_0\hat{A}^{(i)}S_0|u_n^i\rangle. \tag{8}$$

Performing the averaging in Eq. (3) with the help of a cumulant or cluster expansion, one obtains $L_{\rm eff}$ in the form

$$L_{\rm eff}=\int dx\psi^+S_0^{-1}\psi+\sum_{n=2}^{\infty}(-1)^{n-1}\left(\frac{2V}{N}\right)^{n-1}\sum_{fmm'}\int d\Gamma_n\,\det{}_{k,l}^{(n)}J_{kl}, \tag{9}$$

where

$$d\Gamma_n=\prod_{j=1}^{n}\frac{dp_j}{(2\pi)^4}\frac{dp_j'}{(2\pi)^4}(2\pi)^4\delta\left(\sum_j(p_j-p_j')\right), \tag{10}$$

$$J_{kl}=(\psi^{f_k}(p_k))^+M_{m_km_l'}^{f_kf_l}(p_k,p_l')\psi^{f_l}(p_l'), \tag{11}$$

and as in Refs. 5 and 6 we have introduced the vertices

$$M_{mm'}^{gr}(p,p')=\frac{N}{2VN_c}(\hat{p}-im_g)\varphi_m(p)\varepsilon_{mm'}^i\varphi_{m'}^+(p')(\hat{p}'-im_r), \tag{12}$$

with $\varphi_m(p)$ being the form factor of u_m^i in momentum space.

The summation in Eq. (9) starts from $n=2$, since the $n=1$ term drops out as a result of integration over color orientations.

The EQL in Eq. (9) is a sum of $n\times n$ determinants. If one confines oneself to the ZMA, i.e., puts ε^i_{00} finite and $\varepsilon^i_{m>0,n>0}$ equal to zero, the sum runs only over $n\leqslant N_f$. This restriction is due to the Grassmannian nature of J_{kl}. Thus even in the ZMA one obtains, e.g., for $N_f=3$, three 2×2 determinants and one 3×3 determinant. Only the last of these is present in the ansatz of Ref. 5, with the identification $\varepsilon^i_{00}\equiv\varepsilon$, $M_{00}\equiv M$. Therefore our results are in contrast to the common lore according to which for a given number of flavors N_f, the only vertex appearing in the chiral limit contains $2N_f$ quark operators. We can reproduce this result for $N_f=2$ if only ε^i_{00} is kept nonzero, while for $N_f=3$ this conjecture does not suffice and we get additional $4q$ terms.

Consider now ε^i_{00} using (8). In the chiral limit the operator $S_0\hat{A}^{(i)}S_0$ is chirally odd, while the instanton zero mode has definite chirality, and therefore ε^i_{00} vanishes, and for $m_f\neq0$ one has

$$\varepsilon^i_{00}=O(m_f),\quad m_f\to0. \tag{13}$$

At the same time the nonzero modes u^i_{mn} do not have definite chirality, and hence the matrix elements ε^i_{mn} do not vanish as $m_f\to0$. Thus the ZMA in the naive sense of dominance of the zero-mode terms in the EQL is not supported by our calculations. In the next section we discuss what it means in terms of the quark propagator.

3. We now turn to the quark propagator, expressing it again in terms of ε^i_{mn}. Inverting (6), one finds

$$S=S_0-\sum_{ijmn}|u^i_m\rangle\left(\frac{1}{\hat{\varepsilon}^{-1}+\hat{V}}\right)^{ij}_{mn}\langle u^j_n|, \tag{14}$$

where $(\hat{\varepsilon})^{ij}_{mn}=\delta_{ij}\varepsilon^i_{mn}$, and

$$(\hat{V})^{ij}_{mn}=\langle u^i_m|S_0^{-1}|u^j_n\rangle. \tag{15}$$

Note that the summation in (14) extends over different instantons and hence over u^i_0 and u^j_0 of different chiralities. Equation (14) is to be compared to the following expression common to most papers on the subject[3,5,6]

$$S=S_0-\sum_{i,j}|u^i_0\rangle\left(\frac{1}{2im+V}\right)^{ij}_{00}\langle u^j_0|, \tag{16}$$

which contains only zero-mode contributions. To derive (16) one starts with the following approximation for the quark propagator in a single-instanton field:[3,5]

$$S_i=(-i\hat{\partial})^{-1}+\frac{|u^i_0\rangle\langle u^i_0|}{-im}. \tag{17}$$

Introducing this ansatz into expression (7) for ε^i_{mn}, we get

$$\varepsilon^i_{00}=\frac{1}{2im},\quad \varepsilon^i_{m>0,n>0}=0. \tag{18}$$

Using this form of $\hat{\varepsilon}$ in Eq. (14), one recovers the standard ZMA (16). Now, comparing Eq. (18) to (13), we conclude that ansatz (17) is unjustified. Actually, when ε^i_{00} vanishes

in the chiral limit in accordance with (13), the propagator (14) still contains terms $|u_0^i\rangle\langle u_0^j|$, but with coefficients depending upon higher-mode contributions V_{mn}^{ij}. This can be seen by expanding Eq. (14) in a series in powers of ε, i.e.,

$$S=S_0-\sum_{i,j,m,n}|u_m^i\rangle(\hat{\varepsilon}-\hat{\varepsilon}\hat{V}\hat{\varepsilon}+\hat{\varepsilon}\hat{V}\hat{\varepsilon}\hat{V}\hat{\varepsilon}-\ldots)_{mn}^{ij}\langle u_n^j|. \tag{19}$$

If one neglects nonzero modes in V_{mn} in Eq. (19), then the coefficient of $|u_0^i\rangle\langle u_0^j|$ automatically vanishes. To make contact with popular instantonic technique,[3,5,6] where only zero modes are kept in the quark wave functions of the instantons I and anti-instantons I, we rearrange the series for the quark propagator and partition function, using the relation $\hat{\varepsilon}\hat{V}=S_0\hat{A}$, and separate out the terms containing the overlap of II zero modes.

In the standard ZMA these terms are assumed to be dominant, while the overlaps of nonzero modes are neglected. Our expression (19) includes both types of contributions and does not show zero-mode dominance. Therefore we propose to study the new EQL derived above and calculate physical quantities like the chiral quark mass and chiral condensate in order to estimate the contribution of nonzero modes.

It is worth noting that the consistency of the approximation (17) was questioned in Ref. 9 in connection with the calculation of the two-point correlation function. It was shown in Ref. 9 that it is absolutely necessary to keep the terms of order $\sim m$ in S_i. However, since for massive fermions the single instanton propagator S_i is not explicitly known, the effects of the higher modes and finite mass have been investigated only numerically.[11]

Finally, let us examine the effect of nonzero modes in the quark partition function, which is obtained from Eq. (3) by integrating first over quark fields. Using Eq. (6) for S^{-1}, one easily obtains

$$Z/Z_0=\prod_{f=1}^{N_f}\det(1+\hat{\varepsilon}\hat{V}), \tag{20}$$

where $\hat{\varepsilon}$ and $\hat{V}$ are the same matrices as in Eqs. (14) and (15). We may now repeat the arguments presented after Eq. (19) to demonstrate the presence of nonzero modes and the absence of zero-mode dominance.

4. One may wonder why the ZMA (i.e., keeping only zero modes in the EQL) might be invalid even though phenomenologically it seems to be giving reasonable results.[5–6,12] One of the reasons might be that $\varepsilon_{00}^i\equiv\varepsilon$ has been treated as a parameter connected to the properties of the instanton vacuum via the relation $\varepsilon\sim(N_cV/N\rho^2)^{1/2}$, while the properties of the vacuum have been in turn adjusted to the correct value of the gluon condensate.

Our results are at first sight in contradiction to the Banks–Casher relation[13] which connects the chiral condensate with the density of global (quasi) zero modes. The standard picture suggests that the latter originate from individual zero modes, and hence would disappear as soon as (13) holds. However here the standard picture may fail. An insight into its possible failure is provided by quantum mechanics of collective levels in N potential wells in 4D. If each of the wells has one loosely bound level and a continuum (equivalent to a zero mode and nonzero modes), then the approximation of keeping only

the bound-state poles in the Green's functions of each well is known to give an inadequate description of collective bound states.[14] More than that, the pole approximation is a poor one even for the Green's function of an individual well, and instead the so-called unitary pole approximation has to be used.[15]

5. To summarize, we have outlined a new approach to the effective theory of quarks in the instanton vacuum. Our EQL is similar to that of Nambu and Jona-Lasinio,[16] namely it starts from a $4q$ term which might play an important role in phenomenology. Analogy to the NJL model calls for construction of a gap equation yielding the chiral quark mass and quark condensate. Also, the bosonization procedure has to be performed, yielding the effective chiral Lagrangian for the Nambu–Goldstone modes. Finally, the low-density limit deserves a special discussion. This program is in progress now and will be reported elsewhere.

The authors are grateful to S. V. Bashinsky, Yu. M. Makeenko, V. A. Novikov, V. A. Rubakov, and A. V. Smilga for helpful discussions. This study was supported by INTAS Grant 94-2851 and by the Russian Fund for Fundamental Research, Grant 96-02-19184a.

[1] M. C. Chu, J. M. Grandy, S. Huang, and J. W. Negele, Phys. Rev. Lett. **70**, 225 (1993); Phys. Rev. D **49**, 6039 (1994).
[2] E. V. Shuryak, Rev. Mod. Phys. **65**, 1 (1993).
[3] D. Diakonov and V. Petrov, Nucl. Phys. B **272**, 457 (1986).
[4] E. V. Shuryak, Nucl. Phys. B **302**, 559, 574, 599 (1988).
[5] D. Diakonov and V. Petrov, Preprint LNPI-1153 (1986); D. Diakonov and V. Petrov, in *Quark Cluster Dynamics, Lecture Notes in Physics*, Springer-Verlag, 1992, p. 288.
[6] M. A. Nowak, J. J. M. Verbaarschot, and I. Zahed, Phys. Lett. B **228**, 251 (1989); Nucl. Phys. B **324**, 1 (1989).
[7] Yu. A. Simonov, Yad. Fiz. **57**, 1491 (1994) [Phys. At. Nucl. **57**, 1418 (1994)].
[8] C. Callan, R. Dashen, and D. Gross, Phys. Rev. D **17**, 2717 (1978).
[9] N. Andrei and D. J. Gross, Phys. Rev. D **18**, 468 (1978).
[10] H. Levine and L. G. Yaffe, Phys. Rev. D **19**, 1225 (1979).
[11] E. V. Shuryak and J. J. M. Verbaarschot, Nucl. Phys. B **410**, 37 (1993).
[12] T. Wettig, A. Schäfer, and H. A. Weidenmüller, Phys. Lett. B **367**, 28 (1996).
[13] T. Banks and A. Casher, Nucl. Phys. B **169**, 103 (1980).
[14] A. I. Baz', Ya. B. Zeldovich, and A. M. Perelomov, *Scattering, Reactions and Decays in Nonrelativistic Quantum Mechanics*, Moscow, Nauka, 1971; B. Sakita, *Quantum Theory of Many-Variable Systems and Fields*, World Scientific, 1985.
[15] C. Lovelace, Phys. Rev. **135**, B122 (1964).
[16] Y. Nambu and G. Jona-Lasinio, Phys. Rev. **122**, 345 (1961).

Published in English in the original Russian journal. Edited by Steve Torstveit.

Wilson area law in a gas of Abelian monopoles

B. V. Martem'yanov and S. V. Molodtsov
Institute of Theoretical and Experimental Physics, 117259 Moscow, Russia

(Submitted 1 October 1996; resubmitted 5 December 1996)
Pis'ma Zh. Éksp. Teor. Fiz. **65**, No. 2, 133–138 (25 January 1997)

A gas of Abelian monopoles is studied taking account of the interaction of the particles. The Wilson average, for which the law of areas is obtained with allowance for Debye screening, is calculated, with a ''tension'' coefficient proportional to the monopole density. © *1997 American Institute of Physics.* [S0021-3640(97)00402-7]

PACS numbers: 12.38.Aw, 11.30.Rd, 14.80.Hv

The pressing need for a realistic model of the quantum chromodynamics (QCD) vacuum with the properties of chiral symmetry breaking (CSB) and confinement (Wilson area law) was noted in a recent review.[1] The model studied in greatest detail — an instanton gas (liquid)[2] — exhibits the CSB property but does not give confinement.[3] The dyon gas model[4] proposed several years ago is most promising with respect to confinement and exhibits the CSB property at the same time. Estimates have demonstrated the possibility of the area law for Wilson loops in a gas of dyons (monopoles). The first quantitative results for a gas of dyons (Abelian monopoles) were obtained recently neglecting the interaction of the particles.[5,6] It was shown that in a gas of dyons with characteristic size r_{dyon} much less than the loop size r (point-dyon limit) ''superconfinement'' holds for the space-like Wilson loop — the tension is proportional to the size of the loop, specifically, for a circle of radius r,

$$\langle W\rangle = \exp(-\sigma r^2), \quad \sigma = C\ nr, \tag{1}$$

where n is the density of the dyon gas in three-dimensional space, $C = 9.846\ldots$ is a constant extracted from the numerical calculations and approximately equal to π^2. Formula (1) is valid for quasistatic charges, when the fields generated by the particles are taken without allowance for retardation caused by displacements of the particles in three-dimensional space. Allowance for motion decreases the constant C (Ref. 6). Furthermore, C changes for multidyonic configurations studied in a container of large but finite size $L \gg r$. It has been noted that allowance for interaction, in particular, the screening of the field of a charge in a gas, can yield the correction to formula (1) of interest to us, i.e., it can lead to the Wilson area law (confinement of space-like loops).

The present letter discusses the effect of the interaction of Abelian monopoles (screening) on the ''confining'' properties of a gas. Furthermore, it is shown on the basis of an explicit calculation of the two-particle correlation function that it is important to take multiparticle correlation functions into account in the present model.

SPACE-LIKE WILSON LOOP FOR A NEUTRAL GAS OF MONOPOLES WITH INTERACTION

By definition, the observed Wilson loop for a gas of monopoles is given by the limit of the time-average partial contribution $W(C,\ t)$ as $T\to\infty$ for an instantaneous arrangement of the charges

$$\langle W(C)\rangle = \lim_{T\to\infty}\frac{\int_0^T dt W(C,t)}{T}, \tag{2}$$

where

$$W(C,t)=\exp\left(i\frac{g}{2}\ \oint_C A_\mu(x)dx_\mu\right),$$

and C is the Wilson contour. Applying the ergodic hypothesis, we rewrite the definition (2) for a N-particle gas in terms of the particle distribution function $F_N(x_1, \ldots, x_N)$:

$$\langle W(C)\rangle = \frac{\int dx_1 \ldots dx_N W_N(x_1, \ldots, x_N)F_N(x_1, \ldots, x_N)}{\int dx_1 \ldots dx_N F_N(x_1, \ldots, x_N)}. \tag{3}$$

As was shown in Refs. 5 and 6, superconfinement (1) holds for noninteracting particles. In a gas of particles with long-range interaction, however, a correlated arrangement of the charges must be considered — each particle is surrounded by a cloud of oppositely charged particles which screens the particle. In the simplest case of a rarefied (nondegenerate) gas the Debye screening is described, with adequate accuracy, as a function of the thermodynamic parameters by the Debye radius $D=(\Theta/e^2n)^{1/2}$, where e is the particle charge and Θ is the gas temperature.

For an Abelian monopole (point dyon) we have the following magnetic fields: with no screening

$$\mathbf{B}=-\frac{1}{g}\nabla\left(\frac{1}{|\mathbf{x}|}\right), \tag{4}$$

and with Debye screening

$$\mathbf{B}=-\frac{1}{g}\nabla\left(\frac{e^{-|\mathbf{x}|/D}}{|\mathbf{x}|}\right); \tag{5}$$

in formula (2) a singular Dirac potential, for example, of the following form, is used:

$$\mathbf{A}_D=\frac{1}{g}\frac{\mathbf{e}_\varphi}{\rho}\frac{z}{[\rho^2+z^2]^{1/2}},$$

where ρ is the distance from the Dirac string and $\mathbf{e}_\varphi$ is the azimuthal unit vector.

Besides screening, the interaction influences the form of the distribution function, to find which for a rarefied gas only the two-particle correlation functions need be taken into account. Specifically, for a neutral monopole–antimonopole gas averages of the following form are calculated in formula (3):

$$\int d\mathbf{x}_i d\mathbf{x}_j \left\{ \sum_{i,j=1}^{N_+} W_1^+(\mathbf{x}_i) W_1^+(\mathbf{x}_j) F_{ij}^{++} + \sum_{i=1}^{N_+} \sum_{j=1}^{N_-} W_1^+(\mathbf{x}_i) W_1^-(\mathbf{x}_j) F_{ij}^{+-} + \dots \right\},$$

where $N_+ = N_- = N$ is the number of monopoles (antimonopoles). Since the fields commute in the present model, the Wilson loop decomposes into a product of one-particle contributions $W_2(x_1, x_2) = W_1(x_1) W_1(x_2)$. The two-particle function is well known in the limit $\varepsilon = v/D^3 \ll 1$ (where $v = V/N$ is the specific volume):

$$F_1 = 1, \quad F_2 = 1 - \varepsilon e_1 e_2 \frac{e^{-|x_1 - x_2|/D}}{|x_1 - x_2|/D}; \tag{6}$$

where e_1 and e_2 are the particle charges and a cutoff is introduced at small distances so as to avoid nonphysical negative values in the case of repulsion.

So, for $N \gg 1$ we have instead of formula (3)

$$\langle W \rangle = \left[\int \frac{dx_1 dx_2}{2} \{ W_1^+ W_2^+ F_{12}^{++} + W_1^+ W_2^- F_{12}^{+-} \} \right]^N, \tag{7}$$

and the fluxes of the magnetic field through the contour for a monopole and antimonopole are taken with the Debye screening (5).

To see which effect — Debye screening or the change in the distribution function — makes the larger contribution to the answer, we shall examine them separately. First, we study the effect of a change in the distribution function on ''superconfinement.'' For a singular Dirac potential the flux of the magnetic field is expressed in terms of the solid angle Φ within which the contour is visible from the location of the charge. Then the real part of formula (7) has the form

$$\langle W \rangle = \left[\int \frac{dx_1 dx_2}{2} \left\{ \cos\left(\frac{\Phi_1}{2} + \frac{\Phi_2}{2} \right) \left(1 - \frac{\varepsilon}{g^2} \frac{e^{-r_{12}/D}}{r_{12}/D} \right) + \right. \right.$$
$$\left. \left. + \cos\left(\frac{\Phi_1}{2} - \frac{\Phi_2}{2} \right) \left(1 + \frac{\varepsilon}{g^2} \frac{e^{-r_{12}/D}}{r_{12}/D} \right) \right\} \right]^N. \tag{8}$$

With no interaction[5,6]

$$\langle W_1 \rangle = \langle \cos(\Phi/2) \rangle \to 1 - C \frac{r^3}{V}, \tag{9}$$

and in a gas

$$\langle W \rangle \to \left(1 - C \frac{r^3}{V} \right)^N,$$

where in the limits $N \to \infty$, $V \to \infty$, and $N/V = n$ one has

$$\langle W \rangle \to \exp(-Cnr^3).$$

One can see from formula (8) that the most significant part, which is given by a product with $\cos(\Phi/2)$, is not affected by a change of the distribution function. The contributions of the monopole–monopole and monopole–antimonopole pairs compensate one another.

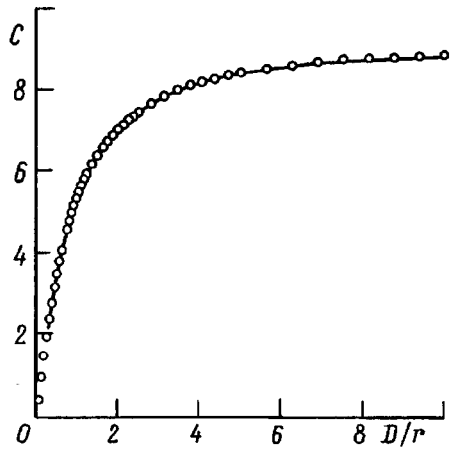

FIG. 1. Coefficient C as a function of the Debye radius D. The circles show the computational results obtained with a step $h/r=6.25\cdot 10^{-2}$; the solid curve, those for $h/r=2.5\cdot 10^{-1}$.

This is also confirmed by a numerical calculation both with ($F_{\rm reg}$) and without (F_2) a cutoff of the distribution function at short distances. The coefficient C in formula (9) does not change much:

$$C=9.115\ (F_2=F_1=1),\quad C'=9.011\ (F_2=F_{\rm reg}),\quad C''=8.269(F_2),$$

(the dimensions of the box containing the gas are: $L/r=3.625$, $D/r=0.1$, $\varepsilon=0.1$). A numerical calculation shows that compensation occurs over a wide range of values of the parameters D and ε, i.e., to within 10% the distribution function can be assumed to be free, $F_2=1$.

The effect of allowing for Debye screening directly in W is shown in Fig. 1, which displays the coefficient C as a function of the Debye radius D (the magnetic flux is determined with the aid of the expression (5) and the flux is integrated over the minimum surface spanned by the contour). One can see that for $D\ll r$ the coefficient C is a linear function of D:

$$C=C_D\frac{D}{r}.$$

The following value was obtained for the coefficient C_D from a numerical calculation with a very small integration step:

$$C_D=7.9\ldots .$$

Hence we obtain confinement for a space-like Wilson loop in a gas of monopoles with Debye screening:

$$\langle W\rangle\to\exp(-\sigma r^2),\quad \sigma=C_D nD.$$

CORRELATION FUNCTION FOR MONOPOLES

Expanding $\cos(\Phi/2)$ in a series in powers of Φ, we shall now relate the Wilson average with the correlation functions of the fields. The first significant contribution is given by the expansion

$$\langle\cos(\Phi/2)\rangle = 1 - \langle\Phi^2\rangle/8 + \ldots, \quad \langle\Phi^2\rangle = \int_{S\times S} d\sigma_1 d\sigma_2 \langle B_3(x_1) B_3(x_2)\rangle,$$

where the integration extends over the surface S of a circle lying in the x,y plane and $d\sigma$ is an element of the surface.

For a monopole, the intensities B_i are of the Coulomb form. The correlation function of such fields can be calculated exactly:

$$\int \frac{d\mathbf{x}}{V} B_i(\mathbf{x}-\mathbf{x}_1) B_j(\mathbf{x}-\mathbf{x}_2) = \frac{4\pi}{V|\mathbf{x}_1-\mathbf{x}_2|} \frac{1}{2}(\delta_{ij} - n_i n_j), \quad n = \frac{\mathbf{x}_1-\mathbf{x}_2}{|\mathbf{x}_1-\mathbf{x}_2|}. \tag{10}$$

The integral of the correlation function can also be calculated exactly:

$$\int_{S\times S} d\sigma_1 d\sigma_2 \frac{1}{|\mathbf{x}_1-\mathbf{x}_2|} = \frac{16\pi}{3} r^3. \tag{11}$$

Therefore we have for the Wilson average the approximate result

$$\langle W\rangle = \langle\cos(\Phi/2)\rangle \approx 1 - \frac{4\pi^2}{3}\frac{r^3}{V}, \tag{12}$$

or $C \approx 4\pi^2/3$, which agrees to within 30% with the complete answer for C.

The correlation function can also be calculated exactly in the case of screened fields (5):

$$\int \frac{d\mathbf{x}}{V} B_i(\mathbf{x}-\mathbf{x}_1) B_j(\mathbf{x}-\mathbf{x}_2) = \frac{4\pi e^{-|\mathbf{x}_1-\mathbf{x}_2|/D}}{V|\mathbf{x}_1-\mathbf{x}_2|} \left\{ \frac{1}{2}(\delta_{ij} - n_i n_j) - \frac{|\mathbf{x}_1-\mathbf{x}_2|}{2D} n_i n_j \right\}. \tag{13}$$

The integral

$$I = \int_{S\times S} d\sigma_1 d\sigma_2 \frac{e^{-|\mathbf{x}_1-\mathbf{x}_2|/D}}{|\mathbf{x}_1-\mathbf{x}_2|}$$

can be estimated for $D \ll r$ as

$$I = 2\pi^2 D r^2.$$

We obtain for the Wilson average

$$\langle W\rangle = \langle\cos(\Phi/2)\rangle \approx 1 - \frac{\pi^3}{2}\frac{Dr^2}{V}, \tag{14}$$

and for a gas we have, accordingly,

$$\langle W\rangle \approx \exp\left(-\frac{\pi^3}{2} D n r^2\right).$$

The estimate obtained for $C_D = \pi^3/2 \approx 15$ is substantially different from the total value. This shows that multiparticle correlation functions play an important role in the present model.

As was mentioned at the beginning of this letter, the results for a gas of monopoles are largely identical to the results for a gas of point dyons. If an analogy with screening in a gas of monopoles proves to be possible, then the required confinement property will be obtained for the dyon gas.

We have calculated the Wilson loop for a gas of interacting monopoles (dyons). Debye screening leads to the law of areas for the Wilson average. A direct calculation agrees with the approximate analytical calculation by the method of correlation functions. It has been shown that it is important to allow for multiparticle correlation functions in this problem.

This work is supported by Russian Fund for Fundamental Research (Grant 95-02-05436) and the German Scientific Research Society (Grant 96-02-00088a).

[1] Yu. A. Simonov, Usp. Fiz. Nauk **166**, 337 (1996).
[2] C. G. Callan, R. Dashen, and D. J. Gross, Phys. Rev. D **17**, 2717 (1978); E. V. Shuryak, Nucl. Phys. B **203**, 93, 116, 140 (1982); D. I. Diakonov and V. Yu. Petrov, Nucl. Phys. B **245**, 259 (1984).
[3] C. G. Callan, R. Dashen, and D. J. Gross, Phys. Lett. B **66**, 375 (1977); D. I. Diakonov, V. Yu. Petrov, and P. V. Pobylitsa, Phys. Lett. B **226**, 471 (1989); E. V. Shuryak, Nucl. Phys. B **328**, 85, 102 (1980).
[4] Yu. A. Simonov, Yad. Fiz. **42**, 557 (1985) [Sov. J. Nucl. Phys. **43**, 352 (1985)]; J. Smit and A. van der Sijs, Nucl. Phys. B **335**, 603 (1991).
[5] B. V. Martem'yanov and S. V. Molodtsov, Yad. Fiz. **59**, 776 (1996).
[6] A. I. Veselov, B. V. Martem'yanov, S. V. Molodtsov, and Yu. A. Simonov, Yad. Fiz. (1996) (in press).

Translated by M. E. Alferieff

Search for flavor lepton number violation in slepton decays at LHC

N. V. Krasnikov
Institute for Nuclear Research, Russian Academy of Sciences, 117312 Moscow, Russia

(Submitted 6 December 1996)
Pis'ma Zh. Éksp. Teor. Fiz. **65**, No. 2, 139–144 (25 January 1997)

We show that in supersymmetric models with explicit flavor lepton number violation due to soft supersymmetry breaking mass terms there could be detectable flavor lepton number violation in slepton decays. We estimate the potential for discovery of lepton flavor number violation in slepton decays at LHC. © *1997 American Institute of Physics.* [S0021-3640(97)00502-1]

PACS numbers: 12.60.−i, 11.30.Hv

Supersymmetric electroweak models offer the simplest solution of the gauge hierarchy problem.[1–4] In real life supersymmetry has to be broken, and the masses of superparticles must be lighter than $O(1)$ TeV.[4] For the supersymmetric extension of the Weinberg–Salam model, soft supersymmetry breaking terms usually consist of the gaugino mass terms, squark and slepton mass terms with the same mass at Planck scale, and trilinear soft scalar terms proportional to the superpotential.[4] For such ''standard'' supersymmetry breaking terms the lepton flavor number is conserved in the supersymmetric extension of the Weinberg–Salam model. In general, however, the squark and slepton soft supersymmetry breaking mass terms are not diagonal due to many causes (Refs. 5–15; allowance for stringlike or GUT interactions, a nontrivial hidden sector, etc.), and flavor lepton number is explicitly broken. As a consequence such models predict flavor lepton number violation in μ and τ decays.[5–13] In our previous papers[16–18] we proposed to look for flavor lepton number violation in slepton decays at LEP2 and NLC.

In this paper we investigate the potential for discovery of flavor lepton number violation in slepton decays at LHC. We find that at LHC it would be possible to discover lepton number violation in slepton decays for slepton masses up to 300 GeV, provided that the mixing between sleptons is close to the maximal one.

In supersymmetric extensions of the Weinberg–Salam model, supersymmetry is softly broken at some high-energy scale $M_{\rm GUT}$ by generic soft terms:

$$
\begin{aligned}
-L_{\rm soft} = {} & m_{3/2}(A^u_{ij}\tilde{u}^j_R\tilde{q}^{\,i}_L H_u + A^d_{ij}\tilde{d}^j_R\tilde{q}^{\,i}_L H_d + A^l_{ij}\tilde{e}_R\tilde{l}_L H_d + \text{h.c.}) + (m^2_q)_{ij}\tilde{q}^{\,i}_L(\tilde{q}^{\,i}_L)^+ \\
& + (m^2_u)_{ij}\tilde{u}^{\,i}_R(\tilde{u}^{\,j}_R)^+ + (m^2_d)_{ij}\,\tilde{d}^{\,i}_R(\tilde{d}^j_R)^+ + (m^2_l)_{ij}\tilde{l}^{\,i}_L(\tilde{l}^{\,j}_L)^+ + (m^2_e)_{ij}\tilde{e}^{\,i}_R(\tilde{e}^{\,j}_R)^+ \\
& + m^2_1 H_u H^+_u + m^2_2 H_d H^+_d + \left(B m^2_{3/2} H_u H_d + \frac{1}{2} m_a(\lambda\lambda)_a + \text{h.c.} \right), \qquad (1)
\end{aligned}
$$

where i,j,a are summed over 1, 2, 3 and $\tilde{q}_L$, $\tilde{u}_R$, $\tilde{d}_R$ denote the left- (right-)handed

squarks, $\tilde{l}_L$, $\tilde{e}_R$ the left- (right-)handed sleptons, and H_u, H_d the two Higgs doublets; m_a are the three gaugino masses of $SU(3)$, $SU(2)$, and $U(1)$, respectively. In most analyses the mass terms are assumed to be diagonal at the $M_{\rm GUT}$ scale, and the gaugino and trilinear mass terms are also assumed universal at the $M_{\rm GUT}$ scale. The renormalization group equations for soft parameters[19] enable one to connect the high-energy scale with the observable electroweak scale. The standard consequence of such analyses is that the right-handed sleptons $\tilde{e}_R$, $\tilde{\mu}_R$, and $\tilde{\tau}_R$ are the lightest particles among the squarks and sleptons. In the approximation wherein one neglects the lepton Yukawa coupling constants they are degenerate in mass.

In our analysis we assume that the lightest stable particle is the gaugino corresponding to the $U(1)$ gauge group, which is now a more or less standard assumption.[20] As has been discussed in many papers,[5–15] in general we can expect nonzero off-diagonal soft supersymmetry breaking terms in Lagrangian (1) which lead to additional contributions for flavor-changing neutral currents and to flavor lepton number violation. From the nonobservation of $\mu\to e+\gamma$ decay ($Br(\mu\to e+\gamma)\leqslant 5\cdot 10^{-11}$; Ref. 21) one can find that[5–19]

$$\frac{(\Delta m^2{}_e\mu)_{RR}}{M^2_{av}}\equiv(\delta_{e\mu})_{RR}\leqslant 2k\cdot 10^{-1}M^2_{av}/(1\,\mathrm{TeV})^2, \tag{2}$$

where $k=O(1)$. For $m_{\tilde{e}_R}=70$ GeV we find that $(\delta_{e\mu})_{RR}\leqslant 10^{-3}$. The analogous bounds inferred from the nonobservation of $\tau\to e\gamma$ and $\tau\to\mu\gamma$ decays are not very stringent.[5–23]

The mass term for the right-handed sleptons $\tilde{e}_R$ and $\tilde{\mu}_R$ has the form

$$-\delta L=m_1^2\tilde{e}^{\,+}_R\tilde{e}_R+m_2^2\tilde{\mu}^{\,+}_R\tilde{\mu}_R+m_{12}^2(\tilde{e}^{\,+}_R\tilde{\mu}_R+\tilde{\mu}^{\,+}_R\tilde{e}_R). \tag{3}$$

After the diagonalization of the mass term (3) we find that the eigenstates of the mass term (3) are

$$\tilde{e}'_R=\tilde{e}_R\cos(\phi)+\tilde{\mu}_R\sin(\phi), \tag{4}$$

$$\tilde{\mu}'_R=\tilde{\mu}_R\cos(\phi)-\tilde{e}'_R\sin(\phi) \tag{5}$$

with the masses

$$M^2_{1,2}=(1/2)[(m_1^2+m_2^2)\pm((m_1^2-m_2^2)^2+4(m_{12}^2)^2)^{1/2}], \tag{6}$$

which practically coincide for small values of $m_1^2-m_2^2$ and m_{12}^2. Here the mixing angle ϕ is determined by the formula

$$\tan(2\phi)=2m_{12}^2(m_1^2-m_2^2)^{-1}. \tag{7}$$

The crucial point is that even for a small mixing parameter m_{12}^2, on account of the smallness of the difference $m_1^2-m_2^2$ the mixing angle ϕ is in general not small (at present state of art it is impossible to calculate the mixing angle ϕ reliably). For the most probable case when the lightest stable superparticle is the superpartner of the $U(1)$ gauge boson plus some small mixing with other gauginos and higgsinos, the sleptons $\tilde{\mu}_R$ and $\tilde{e}_R$ decay mainly into the leptons μ_R and e_R plus the $U(1)$ gaugino λ. The corresponding term in the Lagrangian responsible for slepton decays is

$$L_1=\frac{2g_1}{\sqrt{2}}(\overline{e_R}\lambda_L\tilde{e}_R+\overline{\mu_R}\lambda_L\tilde{\mu}_R+\text{h.c.}), \tag{8}$$

where $g_1^2\approx 0.13$. For the case when mixing is absent the decay width of the slepton into a lepton and LSP is given by the formula

$$\Gamma=\frac{g_1^2}{8\pi}M_{sl}\Delta_f\approx 5\cdot 10^{-3}M_{sl}\Delta_f, \tag{9}$$

$$\Delta_f=\left(1-\frac{M_{LSP}^2}{M_{sl}^2}\right)^2, \tag{10}$$

where M_{sl} and M_{LSP} are the masses of slepton and the lightest superparticle (U(1)-gaugino), respectively. For the case of nonzero mixing we find that the Lagrangian (11) in terms of slepton eigenstates reads

$$L_1=\frac{2g_1}{\sqrt{2}}[\overline{e_R}\lambda_L(\tilde{e}'_R\cos(\phi)-\tilde{\mu}'_R\sin(\phi))+\overline{\mu_R}\lambda_L(\tilde{\mu}'_R\cos(\phi)$$
$$+\tilde{e}'_R\sin(\phi))+\text{h.c.}]. \tag{11}$$

At LEP2 and NLC, in neglect of slepton mixing, $\tilde{\mu}_R$ and $\tilde{\tau}_R$ slepton pair production occurs[22] via annihilation graphs involving a photon and a Z^0 boson and leads to the production of $\tilde{\mu}_R^+\tilde{\mu}_R^-$ and $\tilde{\tau}_R^+\tilde{\tau}_R^-$ pairs. For the production of right-handed selectrons, in addition to the annihilation graphs we also have contributions from the t-channel exchange of the neutralino.[23]

Allowance for nonzero smuon–selectron mixing leads to the following formulas for the cross sections for LEP2 and NLC:

$$\sigma(e^+e^-\to e^+e^-+LSP+LSP)=k[(A+B\cos^2(\phi))^2\cos^4(\phi)$$
$$+(A+B\sin^2(\phi))^2\sin^4(\phi)+B^2\sin^4(2\phi)/8], \tag{12}$$

$$\sigma(e^+e^-\to\mu^+\mu^-+LSP+LSP)=k[(A+B\cos^2(\phi))^2\sin^4(\phi)$$
$$+(A+B\sin^2(\phi))^2\cos^4(\phi)+B^2\sin^4(2\phi)/8], \tag{13}$$

$$\sigma(e^+e^-\to\mu^\pm+e^\mp+LSP+LSP)=\frac{k\sin^2(2\phi)}{4}[(A+B\cos^2(\phi))^2$$
$$+(A+B\sin^2(\phi))^2+B^2(\cos^4(\phi)+\sin^4(\phi))]. \tag{14}$$

Here A is the amplitude of s exchange, B is the amplitude of t exchange, and k is the normalization factor. The corresponding formulas for A, B, and k are found in Ref. 23. The reaction (14) proceeds with violation of flavor lepton number.

It should be noted that formulas (12)–(14) are valid only in the approximation of a narrow slepton decay width:

$$2\Gamma m_{\tilde{e}_R}\leqslant|m_{\tilde{\mu}_R}^2-m_{\tilde{e}_R}^2|. \tag{15}$$

For the case when the inequality (15) does not hold, effects due to the finite decay width are important and decrease the cross section for violation of flavor lepton number. The cross section for the reaction $e^+e^-\to e^+\mu^-+LSP+LSP$ is proportional to

$$\sigma\sim\sin^2(\phi)\cos^2(\phi)\int|D(p_1,m_{\tilde{e}},\Gamma)D(p_2,m_{\tilde{e}},\Gamma)$$
$$-D(p_1,m_{\tilde{\mu}},\Gamma)D(p_2,m_{\tilde{\mu}},\Gamma)|^2dp_1^2dp_2^2, \tag{16}$$

where

$$D(p,m,\Gamma)=\frac{1}{p^2-m^2-i\Gamma m} \tag{17}$$

and $\Gamma_{\tilde{e}}\approx\Gamma_{\tilde{\mu}}=\Gamma$. The approximation (12)–(14) corresponds to neglect of the interference terms in (16) and is valid if inequality (15) holds. For smaller slepton mass differences it is very important to take into account the interference terms in (16).[18,25] The integral (16) is approximately equal to

$$\sigma\sim\sin^2(\phi)\cos^2(\phi)\frac{2\pi^2}{b^2}\left(1-\frac{b^2\left(b^2-\frac{a^2}{4}\right)}{\left(b^2+\frac{a^2}{4}\right)^2}\right), \tag{18}$$

where $a=m^2_{\tilde{e}_R}-m^2_{\tilde{\mu}_R}$, $b=\Gamma[(m_{\tilde{e}_R}+m_{\tilde{\mu}_R})/2]$. Taking the interference effects into account leads to a decrease of the cross section (14) by factors of 1, 0.82, 0.52, and 0.17 for $|m^2_{\tilde{e}}-m^2_{\tilde{\mu}}|=2\Gamma m_{\tilde{e}}$, $1.5\Gamma m_{\tilde{e}}$, $\Gamma m_{\tilde{e}}$, and $0.5\Gamma m_{\tilde{e}}$, respectively.

Consider now the possibility for discovery of lepton number violation in slepton decays at LHC. The possibility of discovering sleptons at LHC has been discussed in Refs. 26–28. Here we shall use the results of Ref. 28, where concrete estimates were made for the CMS detector. To be specific, let us consider two points from Ref. 28:

Point A: $m(\tilde{l}_L)=314$ GeV, $m(\tilde{l}_R)=192$ GeV, $m(\tilde{\nu})=308$ GeV, $m(\tilde{\chi}^0_1)=181$ GeV, $m(\tilde{\chi}^0_2)=358$ GeV, $m(\tilde{g})=1036$ GeV, $m(\tilde{q})=905$ GeV, $\tan(\beta)=2$, $\mathrm{sign}(\mu)=-$.

Point B: $m(\tilde{l}_L)=112$ GeV, $m(\tilde{l}_R)=98$ GeV, $m(\tilde{\nu})=93$ GeV, $m(\tilde{\chi}^0_1)=39$ GeV, $m(\tilde{\chi}^0_2)=87$ GeV, $m(\tilde{g})=254$ GeV, $m(\tilde{q})=234$ GeV, $\tan(\beta)=2$, $\mathrm{sign}(\mu)=-$.

For point A the following cuts have been used: $p^l_T\geqslant 50$ GeV, $Isol\leqslant 0.1$, $|\eta|\leqslant 2.5$, $E^{\mathrm{miss}}_T\geqslant 120$ GeV, $\Delta\phi(E^{\mathrm{miss}}_T,ll)\geqslant 150°$, jet veto — no jets with $E^{\mathrm{jet}}_T\geqslant 30$ GeV in $|\eta|\leqslant 4.5$, Z-mass cut — $M_Z\pm 5$ GeV excluded, $\Delta\phi(l^+l^-)\leqslant 130°$. With such cuts for a total luminosity $L_t=10^5$ pb^{-1}, 91 events $e^+e^-+\mu^+\mu^-$ resulting from slepton decays have been found. The standard WS model background comes from WW, tt, Wtb, WZ, and $\overline{\tau\tau}$ and gives 105 events. No SUSY background has been found. The significance for slepton discovery at point A is 6.5. Using these results it is trivial to estimate the prospects for the discovery of flavor violation in slepton decays. Consider the most optimistic case of maximal slepton mixings and neglect of the effects of destructive interference. For the case of maximal selectron–smuon mixing, the number of signal events coming from slepton decays is $N_{\mathrm{sig}}(e^+e^-)=N_{\mathrm{sig}}(\mu^+\mu^-)=N_{\mathrm{sig}}(\mu^\pm e^\mp)=23$. The number of background events is $N_{\mathrm{back}}(e^+e^-)=N_{\mathrm{back}}(\mu^+\mu^-)=N_{\mathrm{back}}(e^\pm\mu^\mp)=53$. The signifi-

cance $S=$ Sleptons/$\sqrt{\text{Background + Sleptons}}$ is 5.2 for all dilepton modes. For the case of maximal smuon–selectron mixing we have the same number of e^+e^-, $\mu^+\mu^-$, and $e^\pm\mu^\mp$ signal events, whereas in the absence of mixing we do not have $e^\pm\mu^\mp$ events. For the case of the maximal stau–smuon mixing we expect 23 $\mu^+\mu^-$ signal events, 46 e^+e^- signal events, and 2 $\mu^\pm e^\mp$ signal events, while the background is the same as for the case of maximal smuon–selectron mixing. The significance is: 4.6(e^+e^- mode), 2.6 ($\mu^+\mu^-$ mode), 5.2($e^+e^-+\mu^+\mu^-$ mode). The case of selectron–stau mixing is similar to that of smuon–stau mixing, the only difference being the interchange $e\to\mu$, $\mu\to e$. For the case of maximal selectron–smuon–stau mixing we expect 46 $e^+e^-+\mu^+\mu^-+e^\pm\mu^\mp$ signal events, and the significance is 2.8.

For point B the cuts are similar to the point A, except $p_T^l\geqslant 20$ GeV, $E_T^{\text{miss}}\geqslant 50$ GeV, $\Delta\phi(E_T^{\text{miss}},ll)\geqslant 160°$. For a total luminosity $L_{\text{tot}}=10^4$ pb^{-1} the number of $e^+e^-+\mu^+\mu^-$ events resulting from direct slepton production has been found to be 323. The number of background events have been estimated equal to 989(standard model background) + 108(SUSY background)= 1092. The significance is 8.6. Our analysis for the point B is similar to the corresponding analysis for the point A. For the case of maximal selectron–smuon mixing we have found that the significance for all delepton modes is 6.4. For the case of the maximal smuon–stau mixing the significance for the $e^+e^-+\mu^+\mu^-$ mode is 6.6. The same significance obtains for the case of maximal selectron–stau mixing. For the case of maximal selectron–smuon–stau mixing the significance for the $e^+e^-+\mu^+\mu^-+e^\pm\mu^\mp$ mode is 3.0. For a total luminosity $L_{\text{tot}}=10^5$ pb^{-1} the significance is increased by factor ≈ 3.1. It is interesting to mention that at LHC the main mechanism of slepton pair production is the Drell–Yan mechanism, and, as a consequence, for equal smuon and selectron masses the corresponding cross sections and the number of e^+e^- and $\mu^+\mu^-$ signal events coincide. The corresponding cross sections depend rather strongly on the slepton masses. If the smuon and selectron masses differ by 20 percent, the corresponding cross sections and, hence, the number of e^+e^- and $\mu^+\mu^-$ signal events will differ by factor of ≈ 2, which, as has been demonstrated for the example of points A and B, is detectable at LHC. However, the effect of a 20-percent smuon and selectron mass difference will imitate the effect of selectron–stau or smuon–stau mixing. So the situation could be rather complicated. At any rate, by measurement of the difference in $\mu^+\mu^-$ and e^+e^- events it would be possible to measure the difference of smuon and selectron masses with an accuracy of ≈ 20 percent, which is very important because in MSSM the smuon and selectron masses practically coincide for both right-handed and left-handed sleptons.

Let us state the main result of this paper: in the supersymmetric extension of the standard Weinberg–Salam model there could be soft supersymmetry breaking terms responsible for flavor lepton number violation and slepton mixing. At LHC it would be possible to discover flavor lepton number violation in slepton decays for sleptons lighter than 300 GeV provided that the mixing among sleptons is close to maximal. For the case of unequal smuon and selectron masses the number of e^+e^- and $\mu^+\mu^-$ events will be different, an effect which imitates that of stau–smuon or stau–selectron mixing. At any rate, the observation (or nonobservation) of the ($\mu^+\mu^-$–e^+e^-) difference will allow one to conclude that the smuon and selectron masses differ (agree) at least to an accuracy of 20 percent or to draw a conclusion as to the discovery of slepton mixing. Unfortunately

it is rather difficult to distinguish between these two possibilities. For the case of nonzero smuon–selectron mixing the number of $\mu^+\mu^-$ and e^+e^- events is predicted to be the same, and, moreover, for the case of maximal smuon–selectron mixing the numbers of μ^+e^- and μ^-e^+ events coincide with the numbers of $\mu^+\mu^-$ and e^+e^- events. Of course, it is clear that the prospects for discovery of flavor lepton number violation are the most promising at NLC or the $\mu^+\mu^-$ collider, but unfortunately now those prospects are too far from reality.

I thank the CERN TH Department for hospitality during my stay at CERN, where this paper was completed. I am indebted to the staff of the INR theoretical department for discussions and critical comments. I am indebted to L. Rurua for very helpful discussions.

[1] S. Dimopoulos and S. Raby, Nucl. Phys. B **192**, 353 (1981).
[2] E. Witten, Nucl. Phys. B **185**, 513 (1981).
[3] S. Dimopoulos, S. Raby, and F. Wilczek, Phys. Rev. D **24**, 1681 (1981).
[4] For reviews and references, see H. P. Nilles, Phys. Rep. **110**, 3 (1984).
[5] F. Gabbiani and A. Masiero, Nucl. Phys. B **322**, 235 (1989).
[6] J. Hagelin, S. Kelley, and T. Tanaka, Nucl. Phys. B **415**, 293 (1994).
[7] F. Barzumanti and A. Masiero, Phys. Rev. Lett. **57**, 961 (1986).
[8] G. K. Leontaris, K. Tamvakis, and J. D. Vergados, Phys. Lett. B **171**, 412 (1986).
[9] I. Antoniadis, J. Ellis, J. S. Hagelin, and D. V. Nanopoulos, Phys. Lett. B **231**, 65 (1989).
[10] S. Kelley, J. L. Lopez, D. V. Nanopoulos, and H. Pois, Nucl. Phys. B **358**, 27 (1991).
[11] L. Ibanez and D. Lust, Nucl. Phys. B **382**, 305 (1992).
[12] V. Kaplunovsky and J. Louis, Phys. Lett. B **306**, 269 (1993).
[13] R. Barbieri and L. J. Hall, Phys. Lett. B **338**, 212 (1995).
[14] D. Choudhury *et al.*, Phys. Lett. B **342**, 180 (1995).
[15] N. V. Krasnikov, Mod. Phys. Lett. A **9**, 2825 (1994).
[16] N. V. Krasnikov, Mod. Phys. Lett. A **9**, 791 (1994).
[17] N. V. Krasnikov, Preprint INR-927-95, hep-ph/9511464.
[18] N. V. Krasnikov, to be published in Phys. Lett. B.
[19] L. E. Ibanez and C. Lopez, Nucl. Phys. B **233**, 511 (1984).
[20] For reviews, see: H. P. Nilles, Phys. Rep. **110**, 1 (1984); G. G. Ross, *Grand Unified Theories*, Benjamin, New York, 1984; R. N. Mohapatra, *Unification and Supersymmetry*, Springer, New York, 1992.
[21] Particle Data Group, ''Review of particle properties,'' Phys. Rev. D **50**, 1173 (1994).
[22] Y. Nir and N. Seiberg, Phys. Lett. B **309**, 340 (1993).
[23] M. Chen, C. Dionisi, M. Martinez, and X. Tata, Phys. Rep. **159**, 201 (1988).
[24] H. Baer *et al.*, ''Low energy supersymmetry phenomenology,'' CERN-PRE/94-45.
[25] Nima Arkani-Hamed, Hsin-Chia Cheng, J. L. Feng, and L. J. Hall, Phys. Rev. Lett. **77**, 1937 (1996).
[26] F. del Agulia and Ll. Ametller, Phys. Lett. B **261**, 326 (1991).
[27] H. Baer, C. Chen, F. Paige, and X. Tata, Phys. Rev. D **49**, 3283 (1994).
[28] D. Denegri, L. Rurua, and N. Stepanov, ''Detection of sleptons and instrumental requirements in CMS,'' CMS Technical Note TN/96-059, October 1996.

Published in English in the original Russian journal. Edited by Steve Torstveit.

Mechanism of stratification of turbulent heat transfer in a sound field in the presence of rotational anisotropy of the flow

V. N. Zaĭkovskiĭ and V. M. Trofimov
Institute of Theoretical and Applied Mechanics, Siberian Branch of the Russian Academy of Sciences, 630090 Novosibirsk, Russia

(Submitted 4 December 1996)
Pis'ma Zh. Éksp. Teor. Fiz. **65**, No. 2, 145–149 (25 January 1997)

It is established that the stratification of the heat transfer intensity coefficients into n discrete levels, as discovered previously in the turbulent flow accompanying rotation of a supersonic flow, is described by the formula $\alpha_n^2/\alpha_1^2=2^{n-1}$, $n=1, 2, 3, \ldots$. It is found that the ratio of the measured amplitudes of the discrete components of the pressure-pulsation spectrum is of a similar form and corresponds to the pressure field from multipole sources. As expected, similarly to the case of acoustic paramagnetic resonance, the selection of discrete frequencies of intense acoustic radiation from the external flow occurs under the influence of resonances with the radiation of multipoles of turbulent vortices oriented in the rotational anisotropy field. © *1997 American Institute of Physics.* [S0021-3640(97)00602-6]

PACS numbers: 47.55.Hd, 47.27.Te, 47.32.−y

It was predicted theoretically,[1] two years ago and experimentally observed[2] a year later that the asymmetry of the molecules of a gas and/or the corresponding excitation of their rotational degrees of freedom have at least a strong influence on the transition to turbulence in gas flows. A quantum mechanism is proposed as a possible path leading to asymmetry (in the case of spherically symmetric intermolecular interaction potentials).[1] The introduction of asymmetry into the phenomenology of developed turbulence[3] makes it possible to describe the turbulence as an active system with diffusion, capable of generating internal structure.[4] Acoustic interactions with developed turbulence under conditions of strong rotational anisotropy (losses of reflection symmetry) of the flow are of special interest, since the effect of the acoustics on momentum and heat transport processes is qualitatively different in the presence of asymmetry of the stressed state of such a medium.[5,6]

Acoustic (vortex) flows and heat transport due to them near obstacles of different types are ordinarily not established immediately, but rather they develop gradually until the retardation due to the viscosity of the medium compensates the increase in their velocity under the action of the sound. The scale of the flow is determined by the thickness of the acoustic boundary layer $\delta=(\nu/\omega)^{1/2}$ (ν is the kinematic viscosity coefficient and ω is the angular frequency of the sound).

In the present letter a mechanism of stratification of turbulent heat transport into

discrete levels is found which corresponds to interactions between the sound fields of the turbulent vortices and the radiation from the discrete currents of the external flow which are such that the acoustic flows are established so quickly that several (3–7) vortex modes of acoustic origin, giving way to one another in a random manner, are realized near the heat-transfer surface.

The experiments were conducted on a gasdynamic RD apparatus (Institute of Theoretical and Applied Mechanics, Siberian Branch of the Russian Academy of Sciences) with air flow rates of up to 10 kg/s. The distributions of the heat-transfer intensity coefficients, pressure, and pressure pulsations at the walls of a supersonic channel were measured as a function of the position of the channel axis with respect to the subsonic gas flow rate at the entrance. Characteristic acoustic vibrations were excited in the semiclosed volume of the gas flow and then interacted with the sound fields of the turbulent vortices in the boundary layer of the supersonic channel.

The basic arrangement of the experiment and the measurement procedure are presented in Refs. 5 and 6. In the present work, we obtained new data which made it possible to determine the mechanism which results in the stratification of heat transport.

The gas (air), passing through the entrance channel *1* (Fig. 1a), flows into the semiclosed cavity *2* and then into the second channel *3*, which is shaped like a conical Laval nozzle. The diameter of the throat (critical section) equals 38.4 mm. The position of the nozzle *3* was varied by changing the angle β, and the velocity of the flow at the entrance to the nozzle was varied by changing the Mach number M_1 of the jet flowing out of the channel *1*. The measurements were performed along the generatrices of the nozzle *3* on the upstream and downstream sides; this was achieved by rotating the axis relative to the nozzle by 180°.

Three heat-transport regimes are observed on the generatrix of the nozzle *3* (temperature sensors *4*), depending on the values of M_1 and β. The first regime (Fig. 1a) corresponds to an ordinary turbulent heat transport regime in a supersonic channel (here and below in the figures the curve was calculated according to Ref. 7). The second type (Fig. 1b and c) reflects the effect of nonstationary processes due to the instability of large-scale secondary vortex flows, which in turn interact with the sound field of the entrance part of the nozzle *3*. This type of heat transport exhibits the typical nonstationary, irregular character expressed in the random variance, which increases with M_1, in the values of the heat-transfer coefficients. The third regime, first observed in Ref. 5, is characterized by a clearly observed ordering of the heat-transfer coefficients α_n, which are distributed with different probability in several levels n (Fig. 1d), and by the ratio α_n^2/α_1^2 ($n=1, 2, 3, \ldots$) which takes on integer values.

A simple analysis shows that the squared coefficients α_n^2 are related to the acoustic nature of the frequency characteristics ω_n. Indeed, estimating the heat fluxes as $q=\lambda_t \Delta T/\Delta l=\alpha \Delta T$ (here λ_t is the thermal conductivity of a turbulent medium near a wall and ΔT is the temperature difference) and setting $\Delta l \approx \delta$, we obtain

$$\alpha^2 \approx \lambda_t^2/\delta^2=\frac{\lambda_t^2}{\nu}\omega \quad \text{or } \alpha^2 \sim \omega.$$

Measurements of the pressure pulsations at the wall of the channel *3* (Fig. 1a) in

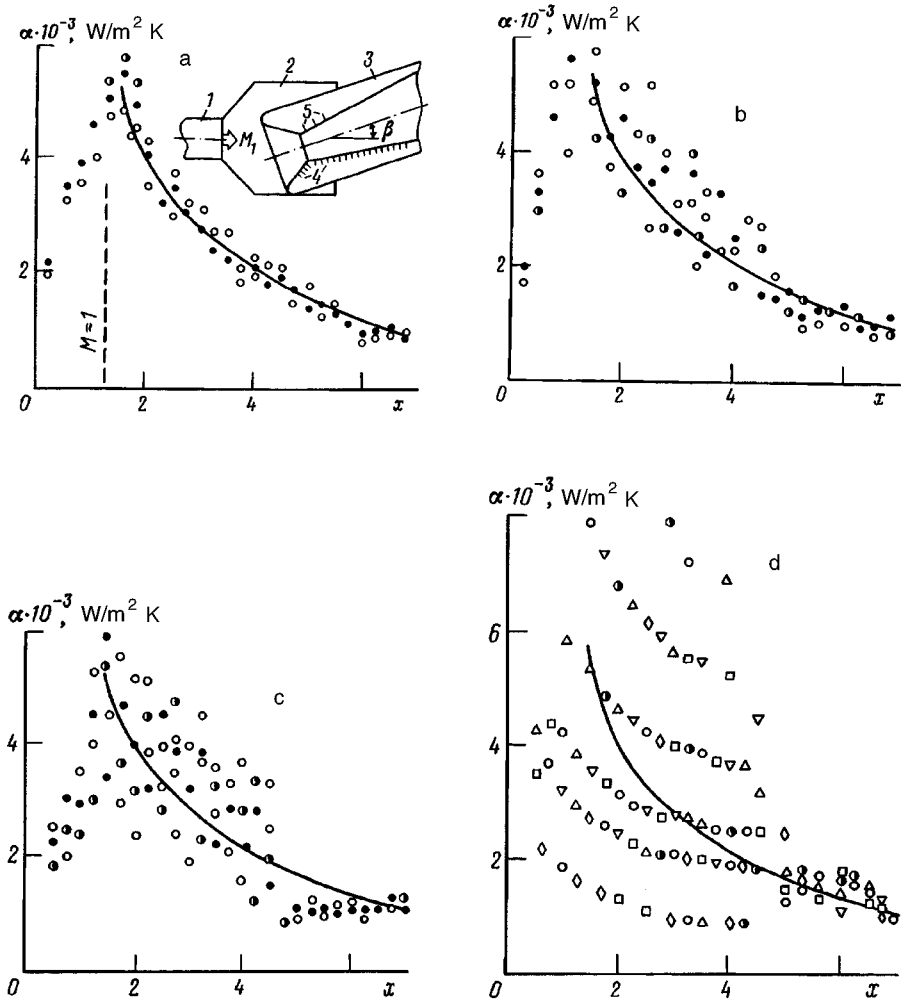

FIG. 1. Distribution of the heat-transport intensity coefficients along the generatrix of the nozzle $x=X/R^*$ (R^* is the radius of the nozzle throat): a — $M_1\approx 0$, $\beta=0°$; b — $M_1=0.18$, $\beta=0°$; c — $M_1=0.35$, $\beta=0°$; d — $M_1=0.35$, $\beta=20°$.

cross sections 5 revealed the following: For the first regime — no large-amplitude vibrations, for the second regime — a nearly random distribution of the amplitudes of the pressure pulsations (Fig. 2a), and for the third regime — a line spectrum, qualitatively correlated with the probability distribution of α_n, of the amplitude of the pressure pulsations (Fig. 2b).[5] The frequency spectrum of the pressure pulsations is characterized by several maxima near the frequencies 0.05, 0.1, 0.2, 0.4, 0.8, 1.6, and 3.2 kHz. Normalizing them to the lowest frequency, we obtain the ratios

$$c^0:c^1:c^2:c^3:c^4:c^5, \quad \text{where } c=2,$$

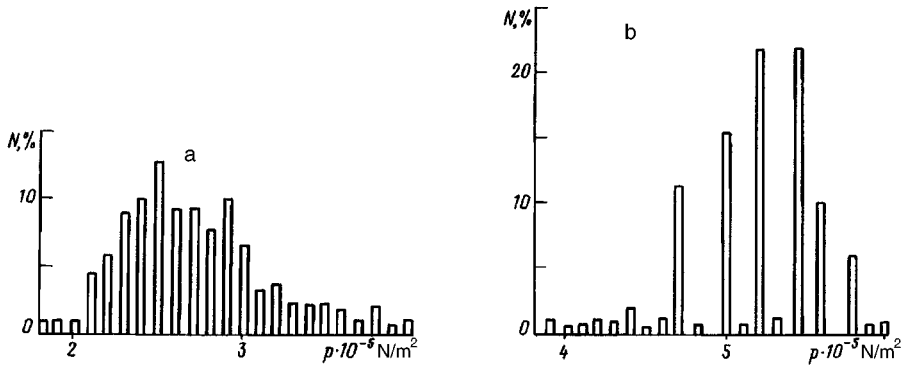

FIG. 2. Spectra of the pressure pulsation amplitudes p (N is the percent content of a given pressure amplitude in the sample): a — $M_1=0.35$, $\beta=0°$; b — $M_1=0.35$, $\beta=20°$.

characteristic for the relative order of the quantities which appears in the sum of the terms of the stress tensor in the expression relating the stress tensor with the pressure field of a multipole,[8] when $c=\omega r/a_0$ (where r is the distance from the multipole).

At the same time, as analysis of the data showed, the ratios a_n^2/a_1^2 are described to within 0.5–10.0% by the formula

$$\alpha_n^2/\alpha_1^2=2^{n-1}, \quad n=1,2,3,\ldots,$$

indicating directly the relation between the structural levels of heat transport α_n and the pressure field of multipole sources.

It is well known that in calculating the acoustic radiation from jets the turbulent vortices are treated as a distribution of quadrupoles.[9] There has been no known interaction between the acoustic radiation of vortices and the external fields of discrete currents that would result in a back effect on heat-transport processes, since the energy of the vortex radiation (far field) is too low.

To analyze a mechanism of this type qualitatively, we write down the main equation of the theory of aerodynamic noise[9]

$$\partial^2\rho/\partial t^2-a_0^2\Delta\rho=\partial^2 T_{ij}/\partial x_i\partial x_j, \tag{1}$$

which describes the generation of a sound field (the left-hand side of Eq. (1), where a_0 is the speed of sound) under the action of continuously distributed acoustic quadrupoles of strength T_{ij} (equal to the components of the stress tensor of an element of the medium). Here the stress tensor has the form

$$T_{ij}=\rho v_i v_j+p_{ij}-a_0^2 p\,\delta_{ij}. \tag{2}$$

The last term on the right-hand side reflects the momentum transport in the ''acoustic'' approximation.

On account of the strong rotational anisotropy of the flow due to the rotation of the channel relative to the direction of the flow at the entrance, we shall describe the turbu-

lent motion as a nonequilibrium motion with respect to the internal angular momenta of the energy-bearing vortices.[3,4] Then the expression (2) can be put into the form

$$T_{ij}=\tau_{ij}+\pi_{ij}^{+}+\pi_{ij}^{-},$$

where τ_{ij} is the symmetric part of the tensor, which includes the momentum transport produced by the terms on the right-hand side of Eq. (2) minus the fluctuation-induced transport; π_{ij}^{+} and π_{ij}^{-} are, respectively, the symmetric and antisymmetric parts of the Reynolds stress tensor. The antisymmetric part of the tensor appears because the characteristic angular momentum vectors of the energy-bearing vortices have a predominant orientation in the rotational anisotropy field. Equation (1) assumes the form

$$\frac{\partial^2\rho}{\partial t^2}-a_0^2\Delta\rho=\frac{\partial^2\tau_{ij}}{\partial x_i\partial x_j}+\frac{\partial^2\pi_{ij}^{+}}{\partial x_i\partial x_j}+\frac{\partial^2\pi_{ij}^{-}}{\partial x_i\partial x_j}. \tag{3}$$

Here the antisymmetric part of the tensor can be represented in the form $\pi_{ij}^{-}=\frac{1}{2}\epsilon_{ijl}M_l$ (ϵ_{ijl} is the Levi-Civita tensor and M_l is an axial vector). The three terms on the right-hand side of Eq. (3) are sources, the latter of which is capable of participating in interactions with an external sound field, similarly to acoustic paramagnetic resonance (APR), if the characteristic angular momenta of the turbulent vortices (and therefore, also the corresponding fields of the quadrupoles) are oriented in the field of the rotation of the flow with $\beta\neq 0$. In Ref. 6 the scales of the turbulent vortices are estimated for the flow being considered here, and the corresponding frequency of an external sound field required to produce an interaction analogous to APR is found.

We note that another property of turbulence discovered in magnetohydrodynamics — the ability to generate and maintain large-scale magnetic fields (the α effect[10]) — was later found in the hydrodynamics of convective media in a Coriolis force field.[11,12] In the latter case, turbulence generates large-scale vortex structures and is called spiral turbulence. As it turned out,[4] the appearance of spirality and the associated losses of symmetry of the stress tensor are also caused by a breakdown of equilibrium between the characteristic angular momenta of the energy-bearing turbulent vortices and the observed angular momenta of the medium in the rotational anisotropy field of the flow.

This work was supported by the Russian Fund for Fundamental Research (Project No. 96-02-19500).

[1] A. Muriel and M. Dresden, Physica D **81**, 221 (1995).
[2] O. A. Nerushev and S. A. Novophashin, JETP Lett. **64**, 47 (1996).
[3] Y. A. Berezin and V. M. Trofimov, Continuum Mech. Thermodyn. **7**, 415 (1995).
[4] Yu. A. Berezin and V. M. Trofimov, Izv. Ross. Akad. Nauk, Mekh. Zhid. i Gaza **1,** 47 (1996).
[5] V. N. Zaĭkovskiĭ and V. M. Trofimov, JETP Lett. **61**, 645 (1995).
[6] V. N. Zaĭkovskiĭ and V. M. Trofimov, Teplofiz. Vys. Temp. **34**, 413 (1996).
[7] Ṣ. S. Kutateladze and A. I. Leont'ev, *Heat and Mass Transfer in a Turbulent Boundary Layer* [in Russian], Energiya, Moscow, 1972.
[8] E. J. Skudrzyk, *The Foundations of Ocean Acoustics*: *Basic Mathematics and Basic Acoustics*, Springer-Verlag, N. Y., 1971 [Russian translation, Mir, Moscow, 1976].
[9] M. J. Lighthill, AIAA J. **1**, 1507 (1963).
[10] F. Krause and K.-H. Radler, *Mean-Field Magnetohydrodynamics and Dynamo Theory*, Pergamon Press, New York, 1981 [Russian translation, Mir, Moscow, 1984].

[11] S. S. Moiseev, P. B. Rutkevich, A. V. Tur, and V. V. YankovskiĭZh. Éksp. Teor Fiz. **95,** 144 (1988) [Sov. Phys. JETP **67**, 294 (1988)].
[12] P. L. Sulem, Z. S. She, H. Scholl *et al.*, Mech. **205,** 341 (1989).

Translated by M. E. Alferieff

Dynamics of a drop of magnetic liquid in a rotating magnetic field

A. V. Lebedev and K. I. Morozov[a)]
Institute of Mechanics of Continuous Media, Urals Branch of the Russian Academy of Sciences, 614013 Perm, Russia

(Submitted 19 December 1996)
Pis'ma Zh. Éksp. Teor. Fiz. **65**, No. 2, 150–154 (25 January 1997)

We report the first observation of the breakup of a rotating drop suspended in a viscous liquid. To produce the motion, a magnetic liquid is used as the material of the drop and the entire system is placed in a uniform, rotating, low-frequency magnetic field. The frequency dependence of the breakup of the drop into two smaller drops is investigated. A theoretical description is given for small Reynolds numbers. The drop is assumed to be ellipsoidal. The flow in the exterior and interior regions and the drag coefficient of the liquid ellipsoid with respect to rotational motion are calculated. A criterion for breakup of the drop is estimated and a comparison is made with experimental data. © *1997 American Institute of Physics.* [S0021-3640(97)00702-0]

PACS numbers: 75.50.Mm, 66.20.+d

The equilibrium shapes of rotating volumes of a liquid have been under investigation for more than a hundred years.[1] The main problem addressed in these investigations is to describe the shapes of the planets modeled by a gravitating volume of liquid. Much later, the possible shapes of assumed by rotating drops as a result of the competition between the centrifugal and surface tension forces characteristic of the liquid were studied.[2] Experimental investigations were held back for a long time by the difficulty of producing rotating volumes of a liquid. Despite the fact that the synthesis of magnetic liquids (MLs) — colloidal dispersions of magnets in ordinary liquids[3] — has made the arrangement of experiments with rotating drops quite obvious, the first experimental work appeared only recently.[4] This work studied the behavior of microdrops in a rotating high-frequency (up to 500 Hz) magnetic field. It was determined that a drop can assume prolate and oblate ellipsoidal shapes, while in strong magnetic fields a drop transforms into a ''starfish'' with a large (up to several tens) number of arms.[4] This latter phenomenon was interpreted in complete analogy with the well-known problem of the instability of a flat surface of a ML in a normal magnetic field.[3] The samples employed in Ref. 4 appear to be quite exotic because of the very small drop sizes (~ 10 μm) and extremely low surface tension at the interface ($\sim 10^{-5}$ dyn/cm). Furthermore, the viscosity of a drop was two orders of magnitude greater than that of the solvent, so that from the standpoint of the problem considered here — the rotational motion of a *liquid* volume, the drops investigated in Ref. 4 were actually solid particles with negligibly small internal motion.

In the present paper we report an experimental investigation of the motion of quite

large (~ 1 mm) drops of a magnetic liquid which were suspended in an electrolytic solution and were characterized by parameters typical of a liquid: The surface tension was ~ 10 dyn/cm at the ML–solution boundary, and the viscosities of the two liquids were of the same order of magnitude. When the sample was placed in a rotating magnetic field, we observed an interesting new phenomenon — at some critical frequency a drop would separate into two equal parts, which, in turn, could break up into drops of even smaller size as the frequency of the field was increased further.

A concentrated ML consisting of magnetite in kerosene with the following parameters, determined from independent experiments, was used as the drop material: viscosity $\eta_1 = 19$ cP, density $\rho = 1.5$ g/cm^3, and surface tension $\sigma_1 = 27$ dyn/cm at a boundary with air. The drops were suspended in a concentrated aqueous solution of zinc dichloride with viscosity $\eta_2 = 3.5$ cP, and the surface tension of the solution at a boundary with air was equal to $\sigma_2 = 54$ dyn/cm. In the absence of a field the drops were, naturally, spheres with radius R. In a constant magnetic field the drops became elongated, and as the field rotated with a low frequency the drops executed a simple forced motion — the long axes of the drops rotated with angular velocity $\Omega = 2\pi f$, where f is the frequency of the field. In our experiments $f \sim 1$ Hz, the magnitude of the field $G = 60$ Oe, and the magnetic permeability of a drop $\mu = 7.1$. The motion of a prolate drop can be easily observed visually. As the frequency of the field changes, the motion occurs without any visible change in shape. Outwardly, the motion of a drop looks like rigid-body rotation, but there is a substantial difference between the rotation of solid and liquid particles. This difference is especially clearly seen if a drop is studied in a coordinate system rotating with velocity Ω. In the case of a liquid drop, there arises inside the drop a flow with a vorticity directed opposite to the direction of rotation of the drop, so that the normal component of the velocity equals zero at any point on the surface of the drop.

The shape of a drop remains unchanged in the entire interval of magnetic field frequencies below a critical frequency f_c. At f_c the drop abruptly becomes several times longer, transforming into a ''dumbbell.'' As the frequency increases further up to a value f_* (which, however, differs so little from f_c that it is impossible to distinguish these frequencies with our apparatus), a dynamic equilibrium is established in the system: A dumbbell-shaped drop separates into two different parts with the same shape as the initial drop. These separate drops execute one to several half-revolutions and once again merge into a single dumbbell-shaped drop, which in turn, after several revolutions, once again divides in two, and so on.

In our experiment we investigated the dependence of the frequency f_* of the field at which drop breakup is observed on the drop diameter d. First, an initial large drop was prepared and then its size was decreased by pumping out some of the ML. The experimental values obtained for f_* in two series of experiments with different initial sizes — $d_1 = 6.1$ mm (triangles in Fig. 1) and $d_2 = 5.8$ mm (circles) — are displayed in Fig. 1. As one can see from the figure, f_* decreases monotonically with increasing drop size, but the onset of breakup itself is apparently of a threshold character: For $d < 3$ mm a drop remains whole for any frequencies f of the external field.

We now proceed to a theoretical analysis of the low-frequency rotational motion of a ML drop suspended in a viscous liquid. We shall solve the problem in the Stokes approximation, regarding the drop to be an ellipsoid with semiaxes $a \geqslant b \geqslant c$. The ratio of

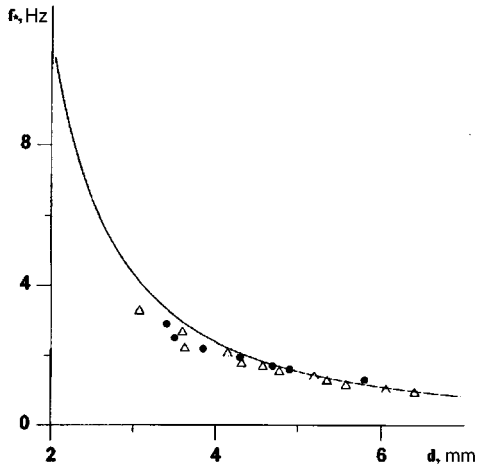

FIG. 1. Critical frequency f_* for drop breakup as a function of drop diameter. The solid curve is the result of a calculation according to formulas (6) and (8); the symbols are experimental data.

any two of the semiaxes is a function of the dimensionless parameters of the problem — the magnetic Bond number $\mathrm{Bo}=G^2R/\sigma$ and the frequency $\Omega\tau$, where σ is the surface tension at the ML–solution boundary and $\tau=\eta_1 R/\sigma$. We shall perform the analysis for $\mathrm{Bo}\geqslant 1$ and $\Omega\tau\ll 1$; this corresponds to the experimental situation. The second inequality expresses the smallness of the characteristic shape relaxation time τ of a drop compared with the period of the field, i.e., the changes in the field can be assumed to occur quasistatically. Therefore, the drop shape is stationary and is determined solely by the parameter Bo as a result of the competition between the magnetic and surface tensions — just as in a static magnetic field.[5] Therefore, in the low-frequency approximation under consideration, a drop is an ellipsoid of revolution ($a>b=c$). This is in complete agreement with our observations in the frequency range from 0 to f_c. Here we also note the high accuracy of the approximation of the shape of a ML drop in a constant magnetic field by an ellipsoid of revolution.[5]

In a rotating coordinate system, the equations of motion for the liquid inside the drop (region 1) and outside the drop (region 2) have the form

$$\eta_{1,2}\Delta\mathbf{v}^{(1,2)}=\nabla p_{1,2}. \tag{1}$$

Here $\mathbf{v}^{(1,2)}$ and $p_{1,2}$ are the velocity and pressure fields, respectively. The absence of volume magnetic forces on the right-hand side of Eq. (1) is due to the uniformity of the magnetic field inside the drop. A system of equations similar to Eqs. (1) was studied in Ref. 6 in application to the solution of the problem of the behavior of an erythrocyte in a shear flow. By analogy to Ref. 6, our problem of a liquid drop can be reduced to the classical Jeffrey problem[7] of the rotational motion of a solid ellipsoid. Indeed, let us choose the axes of the rotating coordinate system as follows: the x axis along the long axis of the ellipsoid and the z axis along the angular velocity vector Ω. Then the solution in the interior and exterior regions has the form

$$v_x^{(1)} = -\nu y a/b, \quad v_y^{(1)} = \nu x b/a, \quad v_z^{(1)} = 0, \quad p_1 = \text{const}, \tag{2}$$

$$v_x^{(2)} = u_J - \nu y a/b, \quad v_y^{(2)} = v_J + \nu x b/a, \quad v_z^{(2)} = \omega_J, \quad p_2 = p_J, \tag{3}$$

where $\mathbf{v}_J = (u_J, v_J, w_J)$ and p_J are the velocity and pressure fields from Jeffrey's problem[7] for a stationary solid ellipsoid in an external flow with a velocity-gradient tensor $\partial v_i / \partial x_k$ which is prescribed at infinity and whose nontrivial symmetric γ_{ik} and antisymmetric ω_{ik} parts are given by

$$\gamma_{12} = \gamma_{21} = \frac{1}{2}\left(\frac{a}{b} - \frac{b}{a}\right), \quad \omega_{12} = -\omega_{21} = \Omega + \frac{1}{2}\left(\frac{a}{b} + \frac{b}{a}\right). \tag{4}$$

The quantity ν, appearing in Eqs. (2)–(4) is a parameter which is to be determined and characterizes the intensity of the motion inside the drop. We call attention to the fact that only the tangential components of the velocity field at the surface of the ellipsoid (see Eqs. (2) and (3)) are different from zero. Using the exact solution,[7] we obtain from Eqs. (2) and (3) an equation of balance of the viscous and magnetic stresses acting on the drop:

$$\eta_2 (A_{12} - A_{21}) = (\mu - 1)^2 (n_2 - n_1) H_x H_y / 4\pi. \tag{5}$$

Here $A_{12} = 2(n_1 \gamma_{12} + b^2 n_3' \omega_{12})/(a^2 n_1 + b^2 n_2) n_3'$, where n_1 and n_2 are the demagnetizing factors along the x and y axes, respectively, and $n_3' = (n_2 - n_1)/(a^2 - b^2)$. The values of A_{21} are obtained from A_{12} by the simple substitutions $1 \leftrightarrow 2$ and $a \leftrightarrow b$. Equation (5) determines the angle α by which the long axis of the ellipsoid (x axis) lags behind the direction of the external field **G**. The components H_x and H_y of the uniform magnetic field inside the ellipsoid equal[8]

$$H_x = G \cos \alpha/(1 + (\mu - 1) n_1), \quad H_y = G \sin \alpha/(1 + (\mu - 1) n_2). \tag{6}$$

We shall calculate ν on the basis of the law of conservation of energy. For this, we equate the work performed on the ML drops per unit time by the magnetic forces generated by the field source ($P_m = MV = \eta_2 (A_{12} - A_{21}) \Omega V$, where M is the moment of the magnetic or viscous forces acting on a drop and V is the volume of the drop) and the power dissipated inside and outside the drop. Omitting the simple but cumbersome calculations, we obtain the following equation for determining ν:

$$\frac{a}{b} A_{12} - \frac{b}{a} A_{21} = \nu \left(\frac{a}{b} - \frac{b}{a}\right)^2 \left(1 - \frac{\eta_1}{\eta_2}\right). \tag{7}$$

As one can see from relations (4), (5), and (6), the moment M of the magnetic forces acting on the drop is connected with the rotational velocity Ω of the long axis by a linear relation. Introducing the ratio $B = \Omega/M$, we shall now determine the rotational mobility of an ellipsoidal liquid particle. The computed mobilities B of a drop in ratio to the mobility $B_{HS} = (6 \eta_2 V)^{-1}$ of a hard spherical particle of the same volume are displayed in Fig. 2 as a function of the eccentricity $e = \sqrt{1 - (b/a)^2}$ of the ellipsoid. The mobilities were calculated for five values of the ratio η_1 / η_2: 0.1, 1, 10, 100, and 1000, indicated next to the corresponding curves. A solid ellipsoid corresponds to the limit $\eta_1 / \eta_2 \to \infty$ and $\nu = 0$ (no internal motion). The particle mobility for this case is determined by Jeffrey's formula[7] (see also Ref. 9). It follows from an analysis of Fig. 2 that the rotation

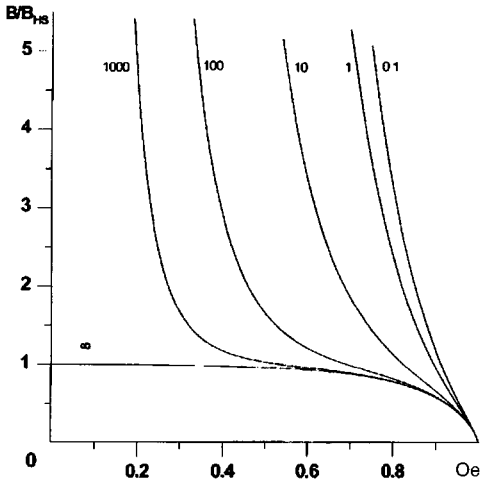

FIG. 2. Mobility B of a liquid drop relative to the mobility B_{HS} of a hard spherical particle as a function of the eccentricity for six values of η_1/η_2 (indicated on the corresponding curves).

of a liquid ellipsoid differs substantially from that of a solid ellipsoid, especially for small drop elongation. This is because the ratio of the viscosities inside and outside the drop appears in relation (6) together with the fourth power of the eccentricity. As a result, in the limit $e \to 0$ (slightly elongated particle) the rotational mobility of the drops increases without bound for any finite value of η_1/η_2, in contrast to the case of a solid ellipsoid, where B approaches the limit B_{HS}. This means that even an infinitesimal field is sufficient to cause a visible rotation of the drop with finite velocity Ω. We recall that by rotation of a drop we mean the rotation of its long axis in the laboratory coordinate system. Of course, the velocities of material particles near the surface of the drop decrease without limit as $e \to 0$.

Thus far we have considered the motion of a drop at field frequencies below f_*. To study dynamics at $f \sim f_*$, when large deformations and breakup of a drop occur, it is necessary to formulate and solve an extremely complicated stability problem. However, the value of f_* itself can be estimated comparatively simply from energy considerations. Indeed, let $\Delta E = E_2 - E_1$ be the difference of the total (surface and magnetic) energy of two equal small drops and one large drop. The increase of the energy by ΔE accompanying the breakup of a drop occurs as a result of the work A performed by the sources of the magnetic field, for which we write approximately $A \approx 2\pi M$, where the latter quantity is the energy dissipated over one period of rotation of the field in a system with one drop. For $f = f_*$, $\Delta E \approx A$, so that to determine the critical frequency we have

$$f_* = \frac{G^2 \Delta E}{4\pi\eta_2} \frac{a^2 n_1 + b^2 n_2}{a^2 + b^2 + 2ab\nu/\Omega}. \tag{8}$$

The theoretical curve $f_* = f_*(d)$ is shown in Fig. 1 by the solid line and was calculated according to Eqs. (8) and (6), allowing for the well-known dependence $e = e(\mathrm{Bo})$ (Ref. 5), and the above-indicated values of the parameters η_1, η_2, μ, and

G. The surface tension σ at the solution — ML boundary was calculated according to Antonov's rule:[10] $\sigma=\sigma_2-\sigma_1=27$ dyn/cm. Without overestimating the significance of relation (8), we nonetheless note the surprising agreement between the computed values of f_* and the data of our experiment. The theoretical curve in Fig. 1, however, does not describe the threshold character of drop breakup as the drop volume decreases; this could be due to both the simplified character of the estimate (8) and the inadequacy of the Stokes approximation at high frequencies of the magnetic field.

We are deeply grateful to A. F. Pshenichnikov for helpful remarks and a discussion of the results of this work. This work was supported by the Russian Fund for Fundamental Research (Grant 95-01-00408).

[a)]e-mail: morozov@psu.ac.ru

---

[1] H. Lamb, *Hydrodynamics*, Dover, New York, 1945 [Russian translation, Gostekhizdat, Moscow, 1947].
[2] S. Chandrasekhar, Proc. R. Soc. **286**, 1 (1965).
[3] M. I. Shliomis, Usp. Fiz. Nauk **112**, 427 (1974) [Sov. Phys. Usp. **17**, 153 (1974)].
[4] J.-C. Bacri, A. Cebers, and R. Perzynski, Phys. Rev. Lett. **72**, 2705 (1994).
[5] J.-C. Bacri and D. Salin, J. Phys. Lett. **43**, 649 (1982).
[6] S. R. Keller and R. Skalak, J. Fluid Mech. **120**, 27 (1982).
[7] G. B. Jeffrey, Proc. R. Soc. A **102**, 161 (1922).
[8] L. D. Landau and E. M. Lifshitz, *Electrodynamics of Continuous Media*, Pergamon Press, New York [Russian original, Nauka, Moscow, 1992].
[9] V. N. Pokrovskiĭ, *Statistical Mechanics of Dilute Suspensions* [in Russian], Nauka, Moscow, 1978.
[10] Yu. G. Frolov, *Surface Phenomena and Disperse Systems* [in Russian], Khimiya, Moscow, 1989.

Translated by M. E. Alferieff

Absence of a ''ferromagnet–spin glass'' reentrant phase transition in quasi-two-dimensional ferromagnetic systems with competing exchange interactions

G. A. Takzeĭ, Yu. P. Grebenyuk, and I. I. Sych
Institute of Magnetism, Ukrainian National Academy of Sciences, 252680 Kiev, Ukraine

L. M. Kulikov
Institute of Problems of Materials Science, Ukrainian National Academy of Sciences, 252680 Kiev, Ukraine

(Submitted 3 December 1996)
Pis'ma Zh. Éksp. Teor. Fiz. **65**, No. 2, 155–158 (25 January 1997)

It is shown on the basis of the results of magnetic investigations for the example of the intercalated layered compounds $Cr_{1/3-x}Ni_xTaS_2$ that in quasi-two-dimensional ferromagnets with competing exchange interactions there is no reentrant ''ferromagnet–spin glass'' phase transition all the way down to liquid-helium temperatures. © *1997 American Institute of Physics.* [S0021-3640(97)00802-5]

PACS numbers: 75.50.−y, 75.30.Kz, 75.10.Nr

The problem of the lowest critical dimension d_L of spin glasses (SGs) occupies a special place in spin-glass physics. If $d_L \geqslant D$, where D is the dimension of the magnetic system, then at finite temperatures a ''paramagnet–spin glass'' (PM–SG) phase transition is impossible. It has been shown[1] theoretically and experimentally in recent years that $2 < d_L < 3$ for classical metallic spin-glass systems of the CuMn type.

We note that, together with a PM–SG phase transition at finite critical temperatures, reentrant temperature transitions, for example, ''ferromagnet–spin glass'' (FM–SG), are very typical in cooled 3D systems with competing exchange interactions.[2] It must be underscored, however, that, as far as we know, the question of the lowest critical dimension for FM–SG phase transitions has not yet been raised either theoretically or experimentally. Such investigations could be performed, by analogy to Ref. 1, on objects in the form of thin and ultrathin films in the crossover regime 3D → 2D. However, such experiments are methodologically and technologically very complicated. At the same time, there exists an entire class of natural quasi-2D systems — intercalated dichalcogenides of transition metals[3] — in bulk samples of which the laws of formation of frozen spin states can be studied by standard methods.

The objective of the present work is to clarify whether a reentrant SG state can appear in magnetic systems with low dimensionality. Synthesized conducting polycrystalline compounds $Cr_{1/3-x}Ni_xTaS_2$ were investigated. This choice of objects of investigation is motivated by the following circumstances. According to Ref. 3, the intercalate $Cr_{1/3}TaS_2$ is a FM with Curie temperature $T_c = 115$ K and the compound $Ni_{1/3}TaS_2$ is an antiferromagnet (AFM) with Néel temperature $T_N = 120$ K. In the compounds indicated above, the intercalating chromium and nickel atoms, which are ordered in octahedral

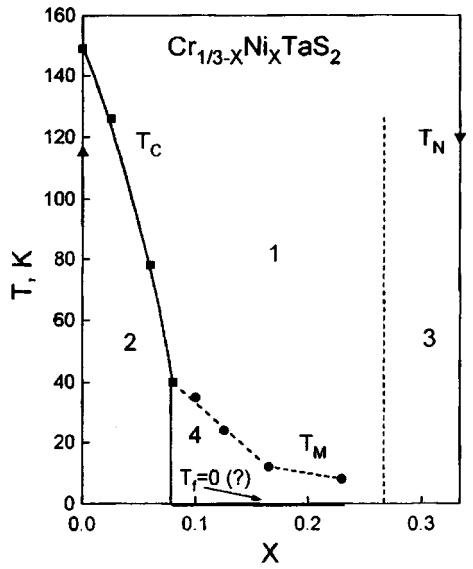

FIG. 1. Magnetic phase diagram of the intercalated dichalcogenide $Cr_{1/3-x}Ni_xTaS_2$: *1* — Paramagnet, *2* — ferromagnet, *3* — possible region of existence of antiferromagnetism, *4* — state with chaotically frozen magnetic moments (spin-glass type). T_c — Curie temperature, T_N — Néel temperature, T_M — temperature of the maximum of the magnetic susceptibility, $T_f=0$ — possible temperature of the ''paramagnet–spin glass'' phase transition; ● — our preliminary investigations, □ — results of the present work, △,▽ — according to the data of Ref. 3.

positions between layers of nonmagnetic tantalum and sulfur atoms, form the above-indicated magnetically ordered states. Therefore, under an isomorphic substitution of nickel for chromium, a FM–AFM concentration phase transition can in principle be realized in the TaS_2 matrix. In this case it can be expected that SG-type states will arise in the concentration range where the type of magnetic order changes, i.e., in the region where the FM and AFM contributions of the exchange interactions to the total exchange energy are approximately the same, as happens, for example, in the fcc alloys FiNiCr (Ref. 4) and FeNiMn (Refs. 5 and 6) in different quasibinary surfaces of section.

In the present work we studied only the FM compounds $Cr_{1/3-x}Ni_xTaS_2$ near the critical concentration $x_0=0.08$ at which long-range FM order appears (Fig. 1). Investigations of the formation of frozen states directly from the PM phase (compounds with $x\geqslant 0.08$) are of interest in themselves and are a subject of a separate analysis. We note only that our investigations show that in the concentration range $0.08<x<0.23$ a frozen magnetic state of the SG-type forms from the PM state on cooling. It is important that this state does not appear as a result of a PM–SG phase transition at a finite critical temperature, as happens in most 3D spin-glass systems, but rather it is formed in a wide temperature range as the indicated compounds are cooled.

Let us now discuss the experimental results. As an example, the temperature dependences of the real and imaginary components, χ' and χ'', respectively, of the dynamic magnetic susceptibility of the compound $Cr_{1/3-x}Ni_xTaS_2$ with $x=0.06$ are displayed in

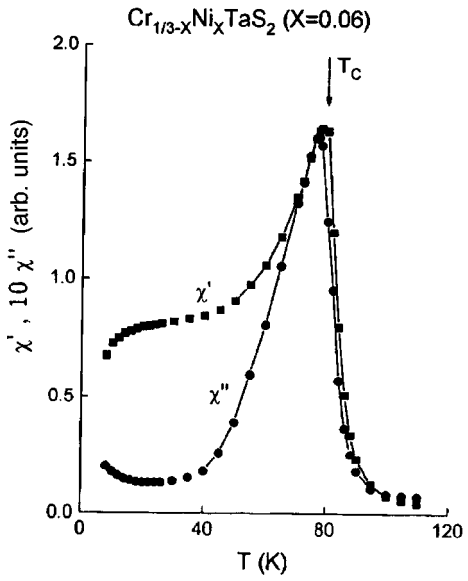

FIG. 2. Temperature dependence of the real part χ' and imaginary part χ'' of the dynamic magnetic susceptibility of the compound $Cr_{1/3-x}Ni_xTaS_2$ ($x=0.06$). The frequency and amplitude of the magnetization reversing field equal 72 Hz and 3.5 Oe.

Fig. 2. The most striking manifestations of SG effects should be expected to occur in the compound with this composition, since this compound lies closest to the critical concentration $x_0=0.08$ in the magnetic phase diagram (Fig. 1), and therefore the contribution of AFM exchange to the total exchange energy is greater in this compound than in any other FM compound in a given quasibinary section. This latter circumstance is a necessary condition for the existence of reentrant temperature transitions.[2]

It follows from the data presented that FM ordering arises in the indicated compound below the Curie temperature $T_c=80$ K. In contrast to 3D systems with reentrant temperature FM–SG transitions,[6] however, appreciable anomalies in the temperature dependences $\chi'(T)$ and $\chi''(T)$ are not observed at lower temperatures. This fact suggests that, at least in the temperature interval 4.2 K $\leqslant T<T_c=80$ K, there is no reentrant FM–SG transition in the compounds which we are studying. Additional confirmations of this can be obtained from investigations of irreversible magnetic phenomena.

Indeed, the temperature dependences obtained for the static magnetization $M(T)$, normalized to the strength H of the measuring magnetic field, after the sample is cooled in a magnetic field (FC) and in a zero magnetic field (ZFC) are absolutely atypical for systems with a reentrant FM–SG temperature transition, since the difference between V^{ZFC} and M^{FC} already appears close to T_c and not at the temperature $T_f \ll T_c$ of the reentrant phase transition (Fig. 3).

It follows from Fig. 4, where the temperature dependence of the thermoremanent magnetization M_r^{TRM} is displayed, that M_r^{TRM} decreases monotonically all the way down to temperatures $T\approx T_c$ and at lower temperatures it is not subject to appreciable anoma-

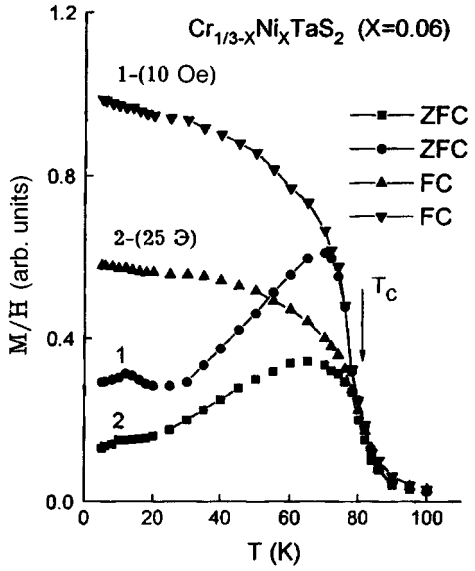

FIG. 3. Static susceptibility M/H of the compound $Cr_{1/3-x}Ni_xTaS_2$ ($x=0.06$) measured after the sample is cooled from a temperature of 100 K in magnetic fields of different intensity (FC) and in zero magnetic field (ZFC).

lies associated with the appearance of a reentrant SG, as happens in frustrated 3D ferromagnets.[6]

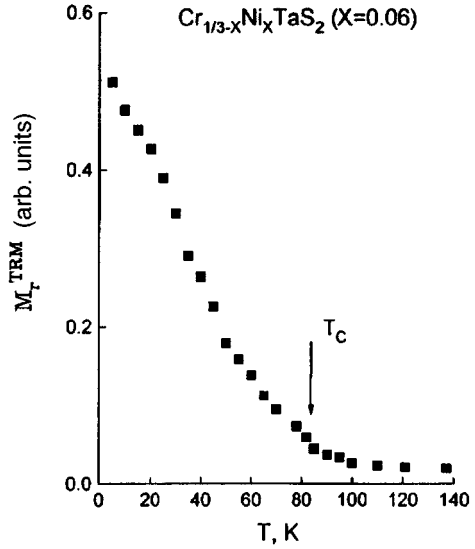

FIG. 4. Thermoremanent magnetization M_r^{TRM} of the compound $Cr_{1/3-x}Ni_xTaS_2$ ($x=0.06$) measured after the compound is cooled from a temperature of 140 K in a 100 Oe magnetic field.

It should be underscored that the existence of appreciable values of M_r^{TRM} and of a difference $M^{\mathrm{FC}}-M^{\mathrm{ZFC}}$ near T_c is not due to the appearance of frozen SG-type spin states in the investigated compound, but rather it is due to the strong nonuniformity of the FM state as a result of the presence of AFM exchange. This is indicated by our discovery in the present work of the existence of an exchange anisotropy in the FM compounds studied that is characteristic of heterogeneous magnetic systems.[7]

In summary, analysis of the experimental results obtained shows that in contrast to 3D systems there are no reentrant FM–SG temperature transitions in the quasi-two-dimensional FM compounds $Cr_{1/3-x}Ni_xTaS_2$ with competing exchange. For this reason, the region *4* in the magnetic phase diagram (Fig. 1) is separated from region *2* by a vertical line, and in the FM region *2* itself there is no line of FM–SG phase transitions. The latter circumstance apparently means that the dimension of the compound studied does not exceed the lowest critical dimension of a reentrant SG.

This work was supported by the German Ministry of Science and Technology as part of the program of collaboration between Leipzig University and the Institute of Magnetism of the Ukrainian National Academy of Sciences.

[1] J. Bass and J. A. Cowen, in *Recent Progress in Random Magnets*, edited by D. H. Ryan, World Scientific Publ. Co., Singapore, 1992, p. 177.
[2] K. Binder and A. P. Young, Rev. Mod. Phys. **58**, 801 (1986).
[3] R. H. Friend and A. D. Yoffe, Adv. Phys. **36**, 1 (1987).
[4] A. Z. Men'shikov, G. A. Takzeĭ, and A. E. Teplykh, Fiz. Met. Metalloved. **54**, 465 (1982).
[5] A. Z. Men'shikov, P. Burlet, A. Chamberod *et al.*, Solid State Commun. **39**, 1093 (1981).
[6] G. A. Takzeĭ, Yu. P. Grebenyuk, and I. I. Sych, Zh. Éksp. Teor. Fiz. **97**, 1022 (1990) [Sov. Phys. JETP **70**, 572 (1990)].
[7] S. V. Vonsovskiĭ, *Magnetism*, Wiley, New York, 1974, Vols. 1 and 2 [Russian original, Nauka, Moscow, 1971, p. 1032].

Translated by M. E. Alferieff

Inelastic resonance tunneling in S–Sm–S tunnel structures

I. A. Devyatov[a)] and M. Yu. Kupriyanov
Scientific-Research Institute of Nuclear Physics at the M. V. Lomonosov Moscow State University, 119899 Moscow, Russia

(Submitted 6 December 1996)
Pis'ma Zh. Éksp. Teor. Fiz. **65**, No. 2, 159–163 (25 January 1997)

Inelastic resonance tunneling through junctions with an amorphous interlayer and superconducting electrodes is studied. The form of the current–voltage characteristic $I(V)$ at low temperature and the temperature dependence of the conductance $G(0)$ at low bias are calculated and are found to be much different from the analogous dependences of structures with normal electrodes. © *1997 American Institute of Physics.* [S0021-3640(97)00902-X]

PACS numbers: 74.50.+r, 73.40.Gk

It has been shown convincingly in a series of experimental works,[1–4] whose purpose was to investigate the transport properties of high-T_c Josephson junctions with semiconductor oxide interlayers, that quasiparticle transport in such structures occurs by means of resonance tunneling through localized states (LSs) in the interlayer. Specifically, it has been shown by comparing the experimental form of the current–voltage characteristic (IVC) in the voltage range $V>2\Delta/e$ (Δ is the modulus of the order parameter of the electrodes) with the results of theoretical calculations[5] that the temperature and voltage dependences of the conductance are close to those predicted for processes with a small number of LSs on the resonant trajectory ($N=2.3$).

However, the results obtained in Ref. 5 are valid only for N–Sm–N structures and neglect the presence of superconducting ordering in the electrodes. Our objective in the present work is to extend the results obtained in Ref. 5 to the case of S–Sm–S structures (superconductor–amorphous interlayer–superconductor).

MODEL OF THE CONTACT

To calculate the contribution of a single two-impurity configuration in the region of the interlayer to the quasiparticle current, we shall proceed from the form proposed in Ref. 5 (Eq. (2.1)) for the tunneling Hamiltonian with additional terms taking into account the superconducting pairing in the electrodes:

$$H_{\text{left}}=\sum_k \xi_k a_k^+ a_k+\sum_k (\Delta a_{k,\uparrow}^+ a_{-k,\downarrow}^+ +\Delta^* a_{k,\uparrow} a_{-k,\downarrow}), \tag{1}$$

$$H_{\text{right}}=\sum_p \xi_p a_p^+ a_p+\sum_p (\Delta a_{p,\uparrow}^+ a_{-p,\downarrow}^+ +\Delta^* a_{p,\uparrow} a_{-p,\downarrow}). \tag{2}$$

Here $\xi_{k,p}$ and $a^{+}_{k,p}$ are, respectively, the energies and the creation operators of electrons in the left(right)-hand superconductor, respectively. Here and below we employ the notation of Ref. 5.

CALCULATION OF THE RESONANT CURRENT THROUGH AND ARRAY OF TWO LSs

Using the unitary transformation

$$i\dot{U}=H_{e-ph}U \tag{3}$$

(H_{e-ph} is determined by Eq. (2.2) of Ref. 5), confining attention to the case of a weak electron–phonon interaction, and making further calculations similar to those performed in Ref. 5 within the limits of applicability of the kinetic equation for the populations of the LSs, deploying the well-known expressions for the correlation functions (see, for example, Ref. 6) for averaging in the kinetic equation over the electron states in the superconducting electrodes,

$$\langle a^{+}_{k}(t)a_{k'}(t')\rangle=\{u^{2}_{k}f_{k}\ \exp\{i\epsilon'_{k}\tau\}+|\nu_{k}|^{2}(1-f_{k})\exp\{-i\epsilon'_{k}\tau\}\}\delta_{k,k'}, \tag{4}$$

$$\langle a_{k'}(t')a^{+}_{k}(t)\rangle=\{u^{2}_{k}(1-f_{k})\exp\{i\epsilon'_{k}\tau\}+|\nu_{k}|^{2}f_{k}\ \exp\{-i\epsilon'_{k}\tau\}\}\delta_{k,k'},$$

$$u^{2}_{k}=\frac{1}{2}(1+\xi_{k}/\epsilon_{k}),\quad |\nu_{k}|^{2}=\frac{1}{2}(1-\xi_{k}/\epsilon_{k}),\quad \epsilon_{k}=\sqrt{\xi^{2}_{k}+|\Delta|^{2}},\quad \tau=t-t',$$

$$f_{k}=f(\epsilon_{k})=(1+\exp\{\epsilon_{k}/k_{B}T\})^{-1},$$

we obtain the following expression for the quasiparticle current in the stationary case:

$$J=J_{+}+J_{-},\quad J_{+}=\frac{4e\chi_{+}}{R_{+}\sqrt{R^{2}_{+}-4\chi_{+}/\Gamma_{1}\Gamma_{2}}},\quad J_{-}=-\frac{4e\chi_{-}}{R_{-}+\sqrt{R^{2}_{-}-4\chi_{-}/\Gamma_{1}\Gamma_{2}}},$$

$$R_{+}=\frac{f_{l}+N}{\Gamma_{2}}+\frac{1-f_{r}+N}{\Gamma_{1}}+\frac{1}{\gamma},\quad \chi_{+}=(f_{l}-f_{r})N+f_{l}(1-f_{r}), \tag{5}$$

$$R_{-}=\frac{f_{r}+N}{\Gamma_{1}}+\frac{1-f_{l}+N}{\Gamma_{2}}+\frac{1}{\gamma},\quad \chi_{-}=-(f_{l}-f_{r})N+f_{r}(1-f_{l}).$$

The terms J_{+} and J_{-} in Eq. (5) correspond to the configurations $\epsilon_{1}>\epsilon_{2}$ and $\epsilon_{1}<\epsilon_{2}$, respectively. In Eq. (5) $f_{l}=f(\epsilon_{1}-eV)$ and $f_{r}=f(\epsilon_{2})$ are the distribution functions for quasiparticle excitations in the left- and right-hand electrodes, ϵ_{1} and ϵ_{2} are the energies of the LSs, $N=N(|\epsilon_{2}-\epsilon_{1}|)=(\exp\{|\epsilon_{2}-\epsilon_{1}|/k_{B}T\}-1)^{-1}$ is the Bose distribution function of the phonons, $\gamma=\pi\Sigma_{q}|T_{12}|^{2}|\lambda_{q}|^{2}\delta(\epsilon_{q}-|\epsilon_{1}-\epsilon_{2}|)$ is the reciprocal of the tunneling time between LSs, T_{12} are the coupling matrix elements between the LSs, the constant λ_{q} is determined in terms of the deformation potential constants at the impurity, and the phonon spectrum is determined by formulas (2.3)–(2.4) of Ref. 5. The quantities $\Gamma_{1,2}$ determine the reciprocal of the tunneling time from the LSs into the superconducting electrodes:

$$\Gamma_{1}=\Gamma_{1}(\epsilon_{1}-eV),\quad \Gamma_{2}=\Gamma_{2}(\epsilon_{2}),$$

$$\Gamma_{1,2}(\epsilon)=\pi\langle T^2_{p1,k2}\rangle N_n(0)\frac{|\epsilon|}{\sqrt{\epsilon^2-\Delta^2}}\{\Theta(\epsilon-\Delta)+\Theta(-\epsilon-\Delta)\}. \tag{6}$$

Here $\langle T^2_{p1,k2}\rangle$ is the angle-averaged, at the Fermi surface, squared tunneling matrix element from the LSs into the left (right)-hand electrode, respectively, and $N_n(0)$ is the density of states of the normal metal at the Fermi surface ($N_n(0)$ is assumed to be the same for both electrodes). As expected, the expression (6) for the current differs from the expression presented in Ref. 5 only by the structure of the coefficients $\Gamma_{1,2}$ (6), which explicitly take into account the singularity in the density of states of the electrodes at $|\epsilon|=\Delta$.

CALCULATION OF THE AVERAGE CURRENT

To calculate the total current through the junction, expression (5) must be averaged over the coordinates and energies of the LSs:

$$\langle J\rangle=g^2S\int d\epsilon_1 d\epsilon_2 dz_1 dz_2 d^2\rho_\perp J(\epsilon_1,\epsilon_2,z_1,z_2,\rho_\perp), \tag{7}$$

where z_1 and z_2 are, respectively, the distances from the LSs to the left- and right-hand electrodes, $\rho_\perp$ is the projection of the vector $\mathbf{r}_1-\mathbf{r}_2$ on the xy plane, which is perpendicular to the direction of the current, S is the contact area, and g is the volume density of LSs.

The calculations simplify substantially and reduce to analytical expressions in the limit $eV,\ \Delta\gg k_BT$. In this limit $J_-=0$, $\chi_+=1$, $R_+=R=\Gamma_1^{-1}+\Gamma_2^{-1}+\gamma^{-1}$, and the expression for the current (5)–(7) reduces to the form

$$\langle J\rangle=g^2S\Theta(eV-2\Delta)\int dz_1 dz_2 d^2\rho_\perp\int_\Delta^{eV-\Delta}d\epsilon_1\int_\Delta^{\epsilon_1}d\epsilon_2\frac{4e}{R+\sqrt{R^2-4/\Gamma_1\Gamma_2}}. \tag{8}$$

Taking into account the exponential character of the decay of the matrix elements T_{k2}, T_{p1}, and T_{12} as a function of the coordinates of the LSs, we find that the reciprocals Γ_i and γ of the tunneling times can be written in explicit form as

$$\begin{aligned}
&\Gamma_1=\Gamma_{10}\exp(-z_1/a)|\epsilon_1-eV|/\sqrt{|\epsilon_1-eV|^2-\Delta^2},\\
&\Gamma_2=\Gamma_{20}\exp((d-z_2)/a)|\epsilon_2|/\sqrt{|\epsilon_2|^2-\Delta^2},\\
&\gamma=\gamma_0|\epsilon_1-\epsilon_2|\exp((z_2-z_1+\rho_\perp^2/(2(z_2-z_1)))/a).
\end{aligned} \tag{9}$$

Here a is the radius of a LS, d is the thickness of the junction, and Γ_{10}, Γ_{20}, and γ_0 are pre-exponential factors, which are weak functions of the coordinates and energies of the LSs. The energy dependence of γ is determined by the Debye phonon model.

One can see from Eqs. (8)–(9) that the denominator in the integrand in Eq. (8) is an exponential function of the coordinates of the LSs and is a much weaker function of their energies. For this reason, just as in the N–Sm–N case,[5] the expression for the average current (8) can be put into a form in which the averaging over the coordinates actually decouples from the averaging over the energies. For this, it is necessary to switch in Eq. (8) from integration over all coordinates $|z_{1,2}|<d$ to integration over neighborhoods of

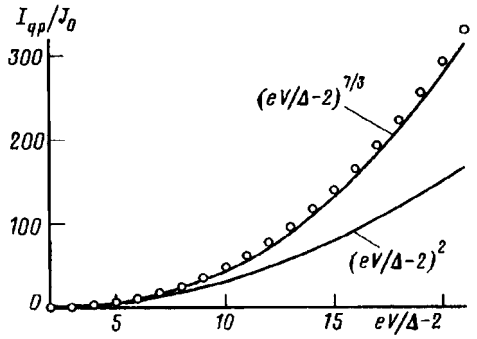

FIG. 1. I–V characteristic of an S–Sm–S junction. The curve was calculated numerically on the basis of formula (10) for a structure with two localized states on the trajectory. Circles — results of numerical calculations, solid lines — fractional power-law and quadratic approximations, J_0 — characteristic magnitude of the current.

the optimal coordinates z_{10} and z_{20} determined by the minimum of the integrand in Eq. (8). Introducing the new variables $\xi_1=z_1-z_{10}$ and $\xi_2=z_2-z_{20}$ and taking into account that the optimal value of $\rho_\perp$ equals zero, we find that, with allowance for relations (9), the expression for the average current (8) reduces to the form

$$\langle J\rangle = Cg^2S\ \exp(-2d/3a)\Theta(eV-2\Delta)$$
$$\times\int_\Delta^{V-\Delta} d\epsilon_1\int_\Delta^{\epsilon_1} d\epsilon_2\left[\frac{|\epsilon_1-eV|}{\sqrt{(\epsilon_1-eV)^2-\Delta^2}}\,\frac{\epsilon_2}{\sqrt{e_2^2-\Delta^2}}(\epsilon_1-\epsilon_2)\right]^{1/3},$$

$$C=2^{5/3}e(\Gamma_{10}\Gamma_{20}\gamma_0)^{1/3}\int d\xi_1 d\xi_2 d^2\rho_\perp\{F+\sqrt{[F^2-4\exp(2(\xi_1-\xi_2))]}\}^{-1}, \qquad (10)$$

$$F=F(\xi_1,\xi_2,\rho_\perp^2)=\exp(2\xi_1/a)+\exp(-2\xi_2/a)$$
$$+\exp\left(2\left(\xi_1-\xi_2+\frac{\rho_\perp^2}{2(z_{20}-z_{10})}\right)\Big/\ a\right).$$

It follows from formula (10) that the exponential dependence on the junction thickness for an array of two LSs in the S–Sm–S case is the same as for a N–Sm–N junction,[5] viz., $(\exp(-2d/3a))$. Therefore estimates of the maximum volume density of LSs at which a transition occurs to current transport predominantly via an inelastic two-LS channel for the N–Sm–N structure[5] are also valid in our case of a S–Sm–S junction. Choosing the corresponding variables in the integral over the energies of the LSs in Eq. (10) makes it possible to determine the form of the IVC: At low voltages, $eV\geqslant 2\Delta$, the IVC is quadratic $\propto(eV-2\Delta)^2$ and at high voltages, $eV\gg 2\Delta$, it assumes the dependence $\propto(eV-2\Delta)^{7/3}\approx(eV)^{7/3}$ as in the case of a N–Sm–N junction. Numerical calculations show (see Fig. 1) that a transition >From a quadratic dependence to a fractional power-law dependence (7/3) occurs at $eV\approx 3\Delta$. It is easy to show that the results of Ref. 5 for $n\geqslant 3$ also obtain for $eV\geqslant 3\Delta$.

Similar calculations yield the following expression for the temperature dependence of the conductance $G(0)$ at low voltages ($eV \ll k_B T$):

$$G(0) \propto T^{4/3} \exp\{-2\Delta(T)/k_B T\} \exp\{-2d/3a\}. \quad (11)$$

The temperature dependence (11) differs from that obtained for N–Sm–N structures[5] by the exponential factor, which arises naturally as a result of the presence of a gap in the quasiparticle excitation spectrum. This factor is proportional to the number of quasiparticles capable of participating at a given temperature in inelastic two-particle resonance tunneling. It is easy to show that this factor also necessarily occurs in the expression for the conductance in the cases when the number of LSs on the trajectory $n \geqslant 3$ ($G_n \propto T^{n-2/(n+1)} \exp\{-2\Delta/k_B T\}$).

Numerous experimental data[1–4] obtained by analyzing the IVCs of high-T_c superconducting junctions show that the expressions (10) do indeed approximate well the form of the IVC at high voltages. However, analysis of the temperature dependence of the conductance at low voltages gives the result $G(0) = G(0,0) + \alpha T^{4/3}$, which is identical to the law for N–Sm–N junctions, i.e., it does not contain the exponential factor $\exp\{-2\Delta/k_B T\}$ which is present in formula (11). This problem will be examined in a separate publication, since it cannot be solved in the framework of the present study.

This work was supported by the program ''Modern problems of condensed-state physics'' and the RFFR–INTAS project RFBR95-1305.

[a)]e-mail: idev@rsfq.npi.msu.su

---

[1] I. I. Vengrus, M. Yu. Kupriyanov, O. V. Snigirev *et al.*, JETP Lett. **60**, 381 (1994).
[2] T. Saton, M. Hidaka, M. Yu. Kupriyanov, and J. S. Tsai, IEEE Trans. Appl. Supercond. **5**, 2612 (1995).
[3] M. Yu. Kupriyanov and J. S. Tsai, IEEE Trans. Appl. Supercond. **5**, 2531 (1995).
[4] M. Siegel, R. Dommel, C. Horstmann, and A. I. Braginskii, in *Extended Abstracts of International Conference on Superconductor Electronics*, Nagoya, Japan, 1995, p. 141.
[5] L. I. Glazman and K. A. Matveev, Zh. Eksp. Teor. Fiz. **94,** 332 (1988) [Sov. Phys. JETP **67**, 1276 (1988)].
[6] A. V. Svidzinskiĭ, *Spatially Nonuniform Problems of the Theory of Superconductivity* [in Russian], Nauka, Moscow, 1982.

Translated by M. E. Alferieff

Inflating antenna: Dynamics of exciton wave packets

E. I. Rashba

L. D. Landau Institute for Theoretical Physics, 117940 Moscow, Russia; Department of Physics, University of Utah, Salt Lake City, UT 84112, USA

(Submitted 15 December 1996)
Pis'ma Zh. Éksp. Teor. Fiz. **65**, No. 2, 164–169 (25 January 1997)

A theory of the free-induction signal from biexcitons and bound excitons is presented. Simultaneous existence of the exciton continuum and a bound state is shown to result in a new type of the time dependence of the free induction. The optically detected signal increases in time and oscillates with increasing amplitude until damped by radiative and dephasing processes. The expanding area of coherent exciton polarization (inflating antenna) produced by the exciting pulse is the underlying physical mechanism. The formalism developed can be applied to various biexciton transients [S0021-3640(97)01002-5]

PACS numbers: 42.50.−p, 71.35.−y

Ultrafast spectroscopy of excitons in the time domain[1] has proven to be a powerful tool to probe the quantum coherence of exciton states, which was originally studied from the polarization of the stationary emission.[2] Most of the experimental data were taken on GaAs quantum wells, but some experiments were performed with bulk excitons. Quantum beats in various response functions are a manifestation of coherence driven by external fields. These beats appear when several states having close energies are excited simultaneously. Quantum beats have been observed for magnetically split exciton levels,[3] bound excitons with different confinement energies,[4] heavy and light hole excitons,[5] free and bound excitons,[6] and with biexcitons and a two-exciton continuum.[7] The last two examples are of principal importance for us in what follows. Experimental data provide convincing evidence of a strong effect of the exciton–exciton and exciton–free-carrier interactions on the nonlinear response functions.[8,9] Different theoretical approaches have been applied, depending on the range of parameter values. When the nonradiative relaxation times τ are short, the mean field approach[10] works rather well. This paper deals with the opposite limit, i.e., the larger-τ region, and is related to papers[11–13] based on microscopic models.

The traditional approach to quantum beats is based on an energy spectrum comprising few (usually two) discrete energy levels. This approach can be applied to beats between heavy and light hole excitons because of momentum conservation and the absence of interaction between these excitons. However, the biexciton and bound exciton problems are more involved because of the existence of the two-exciton and single-exciton continua, respectively. For example, for a two-exciton system it is the exciton–exciton interaction that supports the two-photon coherence, and the lower part of the continuum, with a width of about several biexciton binding energies, ε_b, contributes to the coherent polarization along with the bound biexciton state. In addition

to the theoretical arguments, some experimental data provide weighty, although indirect, evidence of the role of the two-exciton continuum.

Indeed, it has been shown[11] that the four-level biexciton energy scheme can be brought into agreement with the experimental data only if an enhancement factor typical of giant oscillator strengths[14] is invoked. More recent data[15] provide evidence of the significant role of the exciton–exciton interaction in the continuum. Therefore, the frequencies of allowed transitions are distributed continuously, and the frequency spread is about ε_b. Naive consideration suggests that such an energy spectrum should result in beats having a frequency of about ε_b and showing fast nondissipative decay because of accumulating phase differences between different modes. It turns out that the actual physical picture is quite different.

We present an exact solution for a free induction signal excited by a one-sided exponential pulse, $t<0$, in a nondissipative system with a biexcitonic nonlinearity. The special shape of the pulse simplifies calculations but does not influence the basic results. The contribution of the two-exciton continuum is consistently taken into account. With such an approach, free induction, i.e., free oscillations of the two-exciton wave function $\Psi(t)$ for $t>0$, includes two modes. There exists *a beating mode* describing *undamped beats whose frequency is equal to* ε_b. There exists also a *growing mode* whose amplitude increases linearly with time t and whose carrier frequency equals the energy of the bottom of the two-exciton continuum. The growing mode is inherent in interacting systems possessing a continuous spectrum. It describes the inflation in real space of the wave packet created by the pulse. The two modes result in *an optically detected free-induction signal which increases with t and has a monotonic and oscillating parts*. Growth of the signal is restricted by the strong *radiative decay*, resulting in short emission pulses. The same modes exist for excitons bound to impurities. We expect that these modes also contribute to different nonlinear processes, including multiple-pulse processes, and that the technique developed is of general applicability.

To clarify the basic idea and to take into account rigorously the analytical properties of the exciton Green functions, we develop an exactly soluble model. To this end we neglect polariton effects and dephasing. We also neglect the dependence of the scattering amplitude on the polarization of the light, since that is sensitive to the band structure, geometry, etc..[9,16] Excitons are treated as stable particles without internal degrees of freedom. It is convenient to start with the bound exciton problem. If an electromagnetic wave $\mathbf{E}_{\mathbf{q}}(\mathbf{r},t) \propto \exp\{i(\mathbf{q}\cdot\mathbf{r}-\omega t)+\alpha t\}$, $\alpha>0$, is incident upon a crystal at $-\infty<t<0$, the exciton wave function $\Psi_{\mathbf{q}}(\mathbf{q}',t)$ at the instant t $(t>0)$ can be calculated as a linear response to this perturbation:

$$\Psi_{\mathbf{q}}(\mathbf{q}',t)=(iM/\sqrt{v})A_{\mathbf{q}'\mathbf{q}}(t), \quad A_{\mathbf{q}'\mathbf{q}}(t)=\sum_j \frac{\psi_j(\mathbf{q}')\overline{\psi_j}(\mathbf{q})}{\omega-E_j+i\alpha}\, e^{-iE_jt}. \tag{1}$$

Here $\Psi_{\mathbf{q}}(\mathbf{q}',t)$ and $\psi_j(\mathbf{q})$ are, respectively, the time-dependent and stationary exciton wave functions in the momentum representation. The subscript $j\geqslant 1$ labels single-exciton states, both bound and free. The ground-state energy of the crystal is chosen as the origin, $E_0=0$. The coefficient M is the matrix element, per unit cell, of the perturbation produced by the field $\mathbf{E}(\mathbf{r},t)$, and v is the unit cell volume. The momenta $\mathbf{q}$ and $\mathbf{q}'$, which are of importance for optical experiments, are small and will be neglected in the final results.

The amplitude $A_{\mathbf{q}'\mathbf{q}}(t)$ describes the free precession of $\Psi_{\mathbf{q}}(\mathbf{q}',t)$ for positive times. For $t=0$, $A_{\mathbf{q}'\mathbf{q}}(t)$ coincides with the retarded exciton Green function

$$G_{\mathbf{q}'\mathbf{q}}(\omega)=\sum_j \psi_j(\mathbf{q}')\overline{\psi_j}(\mathbf{q})/(\omega-E_j+i0) \tag{2}$$

for $\omega\rightarrow\omega+i\alpha$. For arbitrary t, the functions $A_{\mathbf{q}'\mathbf{q}}(t)$ and $G_{\mathbf{q}'\mathbf{q}}(\omega)$ are related by the equation

$$A_{\mathbf{q}'\mathbf{q}}(t)=\frac{1}{2\pi i}\int_{-\infty}^{\infty} d\omega' \frac{\exp(-i\omega' t)}{\omega'-\omega-i\alpha} G_{\mathbf{q}'\mathbf{q}}(\omega'). \tag{3}$$

Equation (3) can be checked by employing (2), closing the integration path in the lower half of the complex plane, and calculating the residues at the poles of $G_{\mathbf{q}'\mathbf{q}}(\omega')$.

The subsequent transformations of $A_{\mathbf{q}'\mathbf{q}}(t)$ are based on the introduction of the scattering operator $\hat{T}$ (Ref. 17):

$$G_{\mathbf{q}'\mathbf{q}}(\omega)=G^0_{\mathbf{q}}(\omega)\delta_{\mathbf{q}'\mathbf{q}}+G^0_{\mathbf{q}'}(\omega)T_{\mathbf{q}'\mathbf{q}}(\omega)G^0_{\mathbf{q}}(\omega), \tag{4}$$

where $G^0_{\mathbf{q}}(\omega)=(\omega-\varepsilon(\mathbf{q})+i0)^{-1}$ is a free-exciton Green function. Only the second term of Eq. (4) contributes to $A_{\mathbf{q}'\mathbf{q}}(t)$ for $\mathbf{q}'\neq\mathbf{q}$ and will be retained below. It is an important property of this term that it includes a product of two G^0 functions with nearly coincident poles. This property strongly influences the subsequent results. Since $T_{\mathbf{q}\mathbf{q}'}(\omega)$ is analytical in the upper half plane, it obeys the following dispersion relation:

$$\hat{T}(\omega)=-\frac{1}{\pi}\int_{-\infty}^{\infty} d\omega' \hat{T}''(\omega')/(\omega-\omega'+i0), \tag{5}$$

where $\hat{T}''(\omega)=\mathrm{Im}\{\hat{T}(\omega)\}$. Substituting (4) and (5) into (3) and performing the integration over ω', one gets in the $\mathbf{q}',\mathbf{q}\rightarrow 0$ limit:

$$A(t)=-\frac{1}{\pi}\int_{-\infty}^{\infty} d\omega' \frac{d}{d\varepsilon}\left[\frac{T''(\omega')}{\omega'-\varepsilon}\left(\frac{\exp(-i\omega' t)}{\omega-\omega'+i\alpha}-\frac{\exp(-i\varepsilon t)}{\omega-\varepsilon+i\alpha}\right)\right]. \tag{6}$$

Here $\varepsilon=\varepsilon(0)$ is the energy of long-wavelength excitons, and $A(t)$ and $T''(\omega')$ are the limits of $A_{\mathbf{q}'\mathbf{q}}(t)$ and $T_{\mathbf{q}'\mathbf{q}}(\omega)$, respectively, for $\mathbf{q},\mathbf{q}'\rightarrow 0$. Equation (6) is the final equation for the time-dependent amplitude $A(t)$. It is completely determined by the operator $\hat{T}$.

Two basic properties of Eq. (6) follow from general arguments.

First, the derivative $d/d\varepsilon$ results in a contribution to $A(t)$ proportional to $t\exp(-i\varepsilon t)$. The term in $A(t)$ which increases with t will be referred to below as *the growing mode*. It originates from the product of two G^0 functions with coincident poles; Eq. (4). The growing mode is reminiscent of the growing solutions of differential equations with degenerate characteristic numbers. This mode describes the global evolution of the wave packet prepared by the pulse. As t increases, the packet expands in $\mathbf{r}$ space. For translationally invariant systems this expansion is accompanied by changes in the phases of different Fourier components, whereas their moduli remain unchanged. However, the impurity potential violates momentum conservation, and the amplitude of the $\mathbf{q}=0$ mode increases with t. The giant oscillator strengths observed in steady-state experiments are

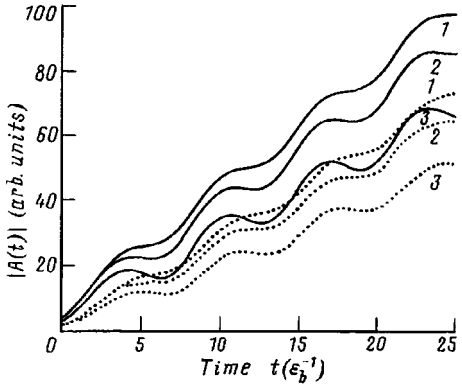

FIG. 1. Time dependence of the amplitude $|A(t)|$ for $\alpha=\varepsilon_b$, $E_B=10\varepsilon_b$. 3D—solid lines, 2D—dotted lines. (*1*) $\omega-\varepsilon=0$, (*2*) $\omega-\varepsilon=-0.5\varepsilon_b$, (*3*) $\omega-\varepsilon=-\varepsilon_b$. For $t2\pi/\varepsilon_b$ the amplitude shows a linear growth and undamped oscillations with a period $2\pi/\varepsilon_b$.

ascribed to *exciton antennas*.[18] In these terms *the growing mode is an inflating exciton antenna*. This picture explains why the growing mode is specific for systems possessing a continuous spectrum and, hence, extended states.

Second, the bound state is a pole of $\hat{T}(\omega)$. Therefore, $T''(\omega')$ includes a term proportional to $\delta(\omega'-\varepsilon+\varepsilon_b)$. It contributes to Eq. (6) an oscillating exponential $\exp[-i(\varepsilon-\varepsilon_b)t]$. The width of the exciton band is assumed to be large compared to ε_b. Under these conditions the integration along the cut in the complex plane contributes a factor $\exp(-i\varepsilon t)$. The two oscillatory terms in Eq. (6), $\exp[-i(\varepsilon-\varepsilon_b)t]$ and $\exp(-i\varepsilon t)$, result in beats at a frequency of ε_b with a time independent amplitude. This oscillating contribution to $A(\omega)$ will be termed as *the beating mode*.

The integral of Eq. (6) can be easily performed for a Frenkel exciton when the impurity potential is described by a degenerate perturbation $U_{\mathbf{mn}}=-U\delta_{\mathbf{m}0}\delta_{0\mathbf{n}}$ (Ref. 19). Here $\mathbf{m}$ and $\mathbf{n}$ label lattice sites, and the impurity resides at the site $\mathbf{m}=\mathbf{n}=0$. In this case $T_{\mathbf{qq}'}(\omega)$ does not depend on the momenta $\mathbf{q}$ and $\mathbf{q}'$. For a two-dimensional (2D) system, the density-of-states inside the exciton band can be chosen as $\rho(\omega)=1/E_B$, where E_B is the width of the band. The amplitude $A(t)$ is shown in Fig. 1 for three values of ω. Both the linear-in-t growth and the oscillations with a time-independent amplitude are distinctly seen in the asymptotic region, $t2\pi\varepsilon_b^{-1}$. Actually, they are seen even for small values of $t>0$, but the shape of the first oscillation is somewhat distorted. It also depends on the shape of the exciting pulse. The data for a 3D system with $\rho(\omega)=8\sqrt{\omega(E_B-\omega)}/\pi E_B^2$ are also shown in Fig. 1. The dependence of $A(t)$ on dimensionality is rather weak.

Therefore, after a short transient the growing and beating modes dominate the amplitude $A(t)$. The optically detected free-induction signal, $I(t)$, is related to the zero-momentum component of the wave function. Therefore, $I(t)\propto|\Psi_0(0,t)|^2$. In the asymptotic region $A(t)\propto\{t+b/2\exp[i(\varepsilon_b t+\phi)]\}e^{-i\varepsilon t}$, where b and ϕ are real parameters, and $I(t)$ obeys the law:

$$I(t)\propto\{t^2+bt\ \cos(\varepsilon_b t+\phi)\}. \tag{7}$$

Interference of the two modes results in an unusual shape of the signal $I(t)$. It consists of the monotonic and oscillatory contributions, both of them growing (rather than decaying!) with t. If one neglects the oscillating part in Eq. (7), the radiative time $\tau_R(t)$ decreases with t as $\tau_R(t)\propto t^{-2}$. This rapid increase in the emission probability establishes the applicability limit for Eq. (7). One can infer from the data of Fig. 1 that $\tau_R^{-1}(t)\approx(\tau_R^0)^{-1}(1+\beta\varepsilon_b t)^2$, where $\beta\sim 1$, and τ_R^0 can be estimated as the bound-exciton radiative lifetime. The radiative lifetime $\tau_{\rm em}$ can be evaluated from the phenomenological equation

$$\int_0^1 dn=\int_0^{\tau_{\rm em}} dt/\tau_R=1, \tag{8}$$

which yields $\tau_{\rm em}\approx(\tau_R^0/\varepsilon_b^2)^{1/3}$. This estimate is crude because $A(t=0)$ from Eq. (1) depends on ω and α. For $\tau_R^0\approx 1$ ns and $\varepsilon_b\approx 10$ meV, we get $\tau_{\rm em}\varepsilon_b\approx 25$, which corresponds to about three oscillations in $|A(t)|$; Fig. 1. Therefore, the radiative response has the shape of a short train of oscillations with a total duration of only about $\tau_{\rm em}$ and an efficiency of up to 100%. Polariton effects, neglected above, are expected to contribute at this fast stage of the radiative decay, and this contribution should be dimensionality dependent.[20]

In what follows we generalize these results for biexcitons. There exist two processes which result in optical production of biexcitons.[7,14] The first process is two-step absorption with an exciton level as a real intermediate state. In this process an exciton produced in the first step acts as an ''impurity''. All the above results are applicable to this process without any serious modifications. The second process is two-phonon absorption from the ground state. The theory of this process is more cumbersome than for impurity absorption. Nevertheless, the final results are nearly identical.

Biexciton eigenfunctions can be written in operator form as

$$|\mathbf{K}j\rangle=\frac{1}{\sqrt{2}}\int\frac{d\mathbf{k}}{(2\pi)^3}\,\psi_j(\mathbf{k})\,\psi^\dagger_{\mathbf{K}/2+\mathbf{k}}\psi^\dagger_{\mathbf{K}/2-\mathbf{k}}, \tag{9}$$

where $\psi^\dagger_{\mathbf{K}/2\pm\mathbf{k}}$ are exciton creation operators, and $\mathbf{K}$ is the center-of-mass momentum of a biexciton. The functions $\psi_j(\mathbf{k})$ are eigenfunctions in the momentum representation. The biexciton wave function at positive times can be found in the second order of perturbation theory in the field $\mathbf{E}_\mathbf{q}(\mathbf{r},t)$. In the momentum representation

$$\Psi_\mathbf{q}(\mathbf{k},t)=\frac{2M^2\sqrt{V}/v}{\omega-\varepsilon(\mathbf{q})+i\alpha}\,A_{k0}(t),\quad A_{k0}(t)=\sum_j\frac{\psi_j(\mathbf{k})\overline{\psi_j}(0)}{2\omega-E_j+2i\alpha}\,\mathrm{e}^{-iE_jt}. \tag{10}$$

Here E_j are the energy levels of a two-exciton system, and V is the normalization volume; the momentum $\mathbf{K}=2\mathbf{q}$. If biexcitons are excited by two light beams with momenta $\mathbf{q}_1$ and $\mathbf{q}_2$, the function $\psi_j(0)$ in (10) should be replaced by $\psi_j((\mathbf{q}_1-\mathbf{q}_2)/2)$.

Equation (10) differs from Eq. (1) only in the coefficient and in the change in variables $\omega\to\Omega=2\omega$ and $\alpha\to 2\alpha$. Therefore, the transformations which led us from Eq. (1) to Eq. (6) can be repeated step-by-step for biexcitons. The equation for the scattering

operator $T_{\mathbf{k},\mathbf{k}}(\Omega)$ depends on the interaction between excitons. The zero-radius potential provides a satisfactory approximation for giant oscillator strengths.[14] With this potential, the operator $\hat{T}(\Omega)$ is known for three-dimensional systems,[17] and it does not depend on the momenta. Finally, $A(t)$ actually shows the same behavior as for bound excitons.

One can infer from Eq. (9) that the quantum state $\Psi_{\mathbf{q}}$ decays into two photons with momenta $\mathbf{K}/2\pm\mathbf{k}$. The intensity of the free-induction signal is proportional to $|\Psi_{\mathbf{q}}(\mathbf{k},t)|^2\approx|\Psi_0(0,t)|^2$. In the asymptotic region $A(t)\propto\{t+b/2\exp[i(\varepsilon_b t+\phi)]\}\times\exp(-2i\varepsilon t)$, and Eq. (7) describes the optically detected signal.

In conclusion, the coexistence of a continuous spectrum and a bound state results in the existence of growing and beating modes in the free induction $\Psi(t)$, following the exciting pulse, for biexcitons and bound excitons. The duration of the induction signal is controlled by the radiative decay rate and dephasing. If the first mechanism dominates, the signal is emitted in a short pulse with a radiative yield close to unity.

I am grateful to M. D. Sturge and J. M. Worlock for helpful discussions and suggestions and for critical reading of the manuscript. The support of the Office of Naval Research under Contract No. N000149410853 is acknowledged.

[1] Y. Masumoto, S. Shionoya, and T. Takagahara, Phys. Rev. Lett. **51**, 923 (1983); L. Schultheis, M. D. Sturge, and J. Hegarty, Appl. Phys. Lett. **47**, 995 (1985); L. Schultheis, J. Kuhl, A. Honord, and C. T. Tu, Phys. Rev. Lett. **57**, 1797 (1986); B. Fluegel, N. Peyghambarian, G. Olbright *et al.*, Phys. Rev. Lett. **59**, 2588 (1987).
[2] G. E. Pikus and E. L. Ivchenko, in *Excitons*, edited by E. I. Rashba and M. D. Sturge (North Holland, Amsterdam, 1982).
[3] V. Langer, H. Stolz, and W. von der Osten Phys. Rev. Lett. **64**, 854 (1990).
[4] E. O. Göbel, K. Leo, and T. C. Damen *et al.*, Phys. Rev. Lett. **64**, 1801 (1990).
[5] B. F. Feuerbacher, J. Kuhl, R. Eccleston, and K. Ploog, Solid State Commun. **74**, 1279 (1990).
[6] K. Leo, T. C. Damen, J. Shah, and K. Köhler, Phys. Rev. B **42**, 11 359 (1990).
[7] S. Bar-Ad and I. Bar-Joseph, Phys. Rev. Lett. **68**, 349 (1992); D. J. Lovering, R. T. Phillips, G. J. Denton, and G. W. Smith, Phys. Rev. Lett. **68**, 1880 (1992); B. Oberhauser, K. H. Pantke, W. Langbein *et al.*, Phys. Status Solidi B **173**, 53 (1992).
[8] S. Weiss, M.-A. Mysek, J.-Y. Bigot *et al.*, Phys. Rev. Lett. **69**, 2685 (1992); D.-S. Kim, J. Shah, and T. C. Damen *et al.*, Phys. Rev. Lett. **69**, 2765 (1992).
[9] H. Wang, J. Shah, T. C. Damen, L. N. Pfeiffer, Solid State Commun. **91**, 869 (1994).
[10] S. Schmitt-Rink and D. S. Chemla, Phys. Rev. Lett. **57**, 2752 (1986).
[11] G. Finkelstein, S. Bar-Ad, O Carmel *et al.*, Phys. Rev. B **47**, 12 964 (1993); T. Saiki, M. Kuwata-Gonokami, T. Matsusue, and H. Sakaki, Phys. Rev. B **49**, 4817 (1994).
[12] K. Bott, O. Heller, D. Bennhardt *et al.*, Phys. Rev. B **48**, 17 418 (1993).
[13] H. Wang, J. Shah, and T. C. Damen *et al.*, Solid State Commun. **98**, 807 (1996).
[14] E. I. Rashba, Opt. Spektrosk. **2**, 568 (1957); A. A. Gogolin and E. I. Rashba, JETP Lett. **17**, 478 (1973); E. Hanamura, Solid State Commun. **12**, 951 (1973).
[15] S. T. Cundiff, M. Koch, W. H. Knox *et al.*, Phys. Rev. Lett. **77**, 1107 (1996).
[16] S. T. Cundiff, H. Wang, and D. G. Steel, Phys. Rev. B **46**, 7248 (1992).
[17] A. I. Baz', Ya. B. Zel'dovich, and A. M. Perelomov, *Scattering, Reactions, and Decays in Nonrelativistic Quantum Mechanics* (Wiley, New York, 1975), Chapter 4, §9.
[18] D. G. Thomas and J. J. Hopfield, Phys. Rev. **175**, 1021 (1968).
[19] V. L. Broude, E. I. Rashba, and E. F. Sheka, *Spectroscopy of Molecular Excitons* (Springer, Berlin, 1985).
[20] L. C. Andreani, F. Tassone, and F. Bassani, Solid State Commun. **77**, 641 (1991); D. S. Citrin, Phys. Rev. B **50**, 17 655 (1994); and references therein.

Published in English in the original Russian journal. Edited by Steve Torstveit.

Phase diagram of a 2D metal system with a variable number of carriers

V. P. Gusynin, V. M. Loktev,[a)] and S. G. Sharapov
N. N. Bogolyubov Institute of Theoretical Physics, Ukrainian National Academy of Sciences, 252143 Kiev, Ukraine

(Submitted 28 October 1996; resubmitted 17 December 1996)
Pis'ma Zh. Éksp. Teor. Fiz. **65**, No. 2, 170–175 (25 January 1997)

It is shown that the phase diagram of a 2D metal undergoing a superconducting transition consists of regions of a normal phase where the modulus of the order parameter is absent, an ''anomalous normal'' phase where the modulus of the order parameter is different from zero but the phase of the order parameter is a random quantity, and a Berezinskiĭ–Kosterlitz–Thouless phase. The characteristic temperatures of transitions between the phases and the behavior of the chemical potential as a function of the fermion density and temperature are found. © *1997 American Institute of Physics.*
[S0021-3640(97)01102-X]

PACS numbers: 74.72.−h, 74.20.Fg, 74.20.Mn, 64.60.Cn

1. Crossover between the limiting cases of Cooper-pair superconductivity and composite-boson superfluidity is drawing attention in connection with the problem of describing high-T_c superconductors (see, for example, Ref. 1). The crossover region is now understood for 3D systems at arbitrary temperatures[2] and crossover has been studied, though incompletely, in quasi-two-dimensional systems,[3] while for 2D systems only the case $T=0$ has been studied.[2,4] The latter circumstance is well known to be due to the fact that the fluctuations of the phase of the charged (complex) order parameter (OP) in 2D systems are so large that they make it impossible for long-range order to be established in such systems at any finite T (Mermin–Wagner–Hohenberg theorem). The description of the appearance of a nonuniform condensate with power-law decay of the correlations (so-called Berezinskii–Kosterlitz–Thouless (BKT) phase), however, entails a number of difficulties. Nonetheless, several steps been made even in this direction. For example, the BKT transition in the relativistic $(2+1)$-theory was studied in Ref. 5, and crossover from superconductivity to superfluidity was studied in Ref. 6 according to the value of the carrier density n_f. However, the method employed in Ref. 6 to obtain the temperature T_{BKT} of the BKT transition has a number of drawbacks. Specifically, the equation for T_{BKT} was obtained neglecting the existence of a neutral (real) order parameter ρ, whose appearance at finite T, being due to the breaking of only a discrete symmetry, is consistent with the theorem mentioned above. As we shall see below, ρ gives the modulus of a multivalued complex order parameter of a 2D system as a whole, and only the modulus determines the possibility of the formation of nonuniform (including vortex) configurations in the system. However, as a result of allowing for a neutral order parameter, a region where ρ decays gradually to zero appears in the phase diagram of the

system; this region separates the standard normal phase (NP) with $\rho=0$ from the BKT phase. Despite the exponential decay of the correlations in it, this new region of states very likely possesses unusual properties, since ρ appears in all expressions in the same manner as does the energy gap Δ in the theory of ordinary superconductors, though to calculate the observed single-particle spectrum, of course, the carrier losses due to scattering of carriers by fluctuations of the phase of the order parameter and, in the case of real systems, by dopants must be taken into account.[7] The possible existence of such a phase, which is also in some sense normal, might shed light on the frequently anomalous (see, for example, Ref. 1) behavior of the normal state of high-T_c superconductors, specifically, the temperature dependences of the spin susceptibility, resistivity, specific heat, photoemission spectra, and so on (see Refs. 8 and 9), for the explanation of which the idea of a pseudogap (and also spin gap) in the region $T>T_c$ is now widely employed.

Our objective in the present work is to establish the n_f–T phase diagram of a 2D metal whose carriers attract one another and to calculate n_f as a function of the temperatures $T_{\rm BKT}$ and T_c^{MF} (T_c^{MF} is the temperature at which $\rho\to 0$), between which lies the region of the ''anomalous normal'' phase (ANP).

2. We write down the simplest model Hamiltonian describing 2D fermions in a volume v:

$$H=\psi_\sigma^\dagger(x)\left[-\frac{\nabla^2}{2m}-\mu\right]\psi_\sigma(x)-V\psi_\uparrow^\dagger(x)\psi_\downarrow^\dagger(x)\psi_\downarrow(x)\psi_\uparrow(x). \tag{1}$$

Here $x\equiv\mathbf{r},\ \tau$; $\psi_\sigma(x)$ is the Fermi field; m is the fermion effective mass; σ is the fermion spin; μ is the chemical potential; V is the attraction constant; and, $\hbar=k_B=1$.

The desired phase diagram was calculated using the Hubbard–Stratonovich method (see, for example, Ref. 4), which has become standard in such problems. In this method the partition function $Z(v,\ \mu,\ T)$ is a functional integral of the Fermi fields (Nambu spinors) and an auxiliary field $\Phi=V\psi_\uparrow^\dagger\psi_\downarrow^\dagger$. In the 2D case, however, instead of using the accepted method for calculating Z in the variables Φ and Φ^*, it is better to perform the calculation in modulus–phase variables, introducing according to Ref. 10 the parameterization $\Phi(x)=\rho(x)\exp[-i2\theta(x)]$, which corresponds to the obvious transformation $\psi_\sigma(x)=\chi_\sigma(x)\exp[i\theta(x)]$, where the field operator $\chi_\sigma(x)$ describes neutral fermions and $\exp[i\theta(x)]$ corresponds to the charge degree of freedom. Making the corresponding substitution in Eq. (1) and integrating over the fields χ, we arrive at the expression $Z=\int\rho\mathcal{D}\rho\mathcal{D}\theta\ \exp[-\beta\Omega(\rho,\partial\theta)]$, where

$$\Omega(\rho,\partial\theta)=\frac{T}{V}\int_0^\beta d\tau\int d\mathbf{r}\rho^2-T\ \mathrm{Tr}\ \ln\ \mathcal{G}^{-1} \tag{2}$$

is the effective thermodynamic potential of the system and $\mathcal{G}$ is its single-particle Green's function, so that

$$\mathcal{G}^{-1}=-\hat{I}\partial_\tau+\tau_3\left(\frac{\nabla^2}{2m}+\mu\right)+\tau_1\rho-\tau_3\left(i\partial_\tau\theta+\frac{(\nabla\theta)^2}{2m}\right)+\hat{I}\left(\frac{i\nabla^2\theta}{2m}+\frac{i\nabla\theta\nabla}{m}\right)$$
$$\equiv G^{-1}(\rho)-\Sigma(\partial\theta); \tag{3}$$

in Eq. (2) Tr is taken with respect to the space $\mathbf{r}$, the imaginary time τ ($\leqslant\beta\equiv 1/T$), and the Nambu indices, which appear in the Pauli matrix τ_j. It is important to note that neither the smallness nor slowness of the variation of the phase of the order parameter was assumed in obtaining expression (3).

Since the low-energy dynamics in the phases in which $\rho\neq 0$ is determined mainly by the long-wavelength fluctuations of $\theta(x)$, only the lowest order derivatives need be retained in the expansion of $\Omega(\rho,\partial\theta)$:

$$\Omega(\rho,\partial\theta)=\Omega_{\rm kin}(\rho,\partial\theta)+\Omega_{\rm pot}(\rho);\quad \Omega_{\rm kin}(\rho,\partial\theta)=T\ {\rm Tr}\sum_{n=1}^{\infty}\frac{1}{n}(G\Sigma)^n\Bigg|_{\rho={\rm const}};$$

$$\Omega_{\rm pot}(\rho)=\frac{1}{V}\int d\mathbf{r}\rho^2-T\ {\rm Tr\ ln}\ G^{-1}\Big|_{\rho={\rm const}}. \tag{4}$$

3. In the expansion of $\Omega_{\rm kin}$ in Eq. (4) it is sufficient to retain terms with $n=1$, 2, right up to $\sim(\nabla\theta)^2$. The computational scheme is similar to that employed in Ref. 11, where only the case of high densities n_f at $T=0$ is studied, and gives[b)]

$$\Omega_{\rm kin}=\frac{T}{2}\int_0^{\beta}d\tau\int d\mathbf{r}J(\mu,T,\rho(\mu,T))(\nabla\theta)^2, \tag{5}$$

where

$$J(\mu,T,\rho)=\frac{1}{m}n_F(\mu,T,\rho)-\frac{T}{\pi}\int_{-\mu/2T}^{\infty}dx\,\frac{x+\mu/2T}{\cosh^2\sqrt{x^2+\dfrac{\rho^2}{4T^2}}}, \tag{6}$$

and the function

$$n_F(\mu,T,\rho)=\frac{m}{2\pi}\left\{\sqrt{\mu^2+\rho^2}+\mu+2T\ \ln\left[1+\exp\left(-\frac{\sqrt{\mu^2+\rho^2}}{T}\right)\right]\right\} \tag{7}$$

corresponds to the density of Fermi quasiparticles (for $\rho=0$ the expression (7) is simply the free-fermion density). A direct comparison of expression (5) with the Hamiltonian of the XY model[12] and the closeness of the physical situations (two-component order parameter in a 2D system) make it possible to write an equation for $T_{\rm BKT}$:

$$\frac{\pi}{2}J(\mu,T_{\rm BKT},\rho(\mu,T_{\rm BKT}))=T_{\rm BKT}. \tag{8}$$

Although mathematically the problem reduces to a well-known problem, the analogy is incomplete. Indeed, in the standard XY model (as well as the nonlinear σ model) the vector (spin) subject to ordering is assumed to be a unit vector with no dependence[c)] on T. In our case this is fundamentally not the case, and a self-consistent calculation of $T_{\rm BKT}$ as a function of n_f requires additional equations for ρ and μ, which together with Eq. (8) form a complete system. (In the BCS theory, which we recall is valid for ordinary metals, it is assumed that $\mu=\epsilon_F$, where ϵ_F is the Fermi energy, and the chemical potential is therefore not an unknown quantity.)

4. The effective potential $\Omega_{\rm pot}$ (see Eq. (4)), after some calculations, acquires the form

$$\Omega_{\rm pot}(\rho)=v\left[\frac{\rho^2}{V}-\int\frac{d\mathbf{k}}{(2\pi)^2}\left\{2T\ \ln\cosh\frac{\sqrt{\xi^2(\mathbf{k})+\rho^2}}{2T}-\xi(\mathbf{k})\right\}\right], \tag{9}$$

where $\xi(\mathbf{k})=\mathbf{k}^2/2m-\mu$. Then the desired missing equations are the condition $\partial\Omega_{\rm pot}(\rho)/\partial\rho=0$ that the potential (9) be minimum and the equality $v^{-1}\partial\Omega_{\rm pot}/\partial\mu=-n_f$, which fixes n_f. For them we have, respectively,

$$\frac{1}{V}=\int\frac{d\mathbf{k}}{(2\pi)^2}\frac{1}{2\sqrt{\xi^2(\mathbf{k})+\rho^2}}\tanh\frac{\sqrt{\xi^2(\mathbf{k})+\rho^2}}{2T}, \tag{10}$$

$$n_F(\mu,T,\rho)=n_f. \tag{11}$$

The equations (10) and (11) obtained above comprise a self-consistent system for determining the modulus ρ of the order parameter[d)] and the chemical potential μ in the mean-field approximation for fixed T and n_f. As we have already mentioned, ρ and μ serve as the initial values for calculating $T_{\rm BKT}$. The fact that the potential (9) depends explicitly on ρ^2 is a consequence only of a definite symmetry of the spectrum of eigenvalues of the operator (3).

Setting $\rho=0$ in Eqs. (10) and (11), we arrive (in the same approximation) at equations for the critical temperature T_c^{MF} and the corresponding value of μ:

$$\ln\frac{|\varepsilon_b|}{T_c^{MF}}\frac{\gamma}{\pi}=-\int_0^{\mu/2T_c^{MF}}du\frac{\tanh u}{u}\ (\gamma=1.781), \tag{12}$$

$$T_c^{MF}\ \ln\left[1+\exp\left(\frac{\mu}{T_c^{MF}}\right)\right]=\epsilon_F. \tag{13}$$

Here $\varepsilon_b=-2W\exp(-4\pi/mV)$ is the energy of two-particle bound states, where W is the width of the conduction band, $\epsilon_F=\pi n_f/m$, and the change to ε_b means renormalization or, in other words, passage to the limits $W\to\infty$ and $V\to 0$. The parameter ε_b is physically equivalent to the four-fermion constant V but is much more convenient to use. For example, after renormalization Eq. (10) becomes

$$\ln\frac{|\varepsilon_b|}{\sqrt{\mu^2+\rho^2}-\mu}=2\int_{-\mu/T}^{\infty}du\frac{1}{\sqrt{u^2+\left(\frac{\rho}{T}\right)^2}\left[\exp\sqrt{u^2+\left(\frac{\rho}{T}\right)^2}+1\right]}. \tag{14}$$

It is easy to show that at $T=0$ the system (14), (11) possesses an exact solution[2,4] $\rho=\sqrt{2|\varepsilon_b|\epsilon_F}$ and $\mu=-|\varepsilon_b|/2+\epsilon_F$. This shows that both the magnitude and sign of μ are determined by the ratio between ϵ_F and $|\varepsilon_b|$. Otherwise, there arises a natural separation of metallic systems into systems with low ($\epsilon_F\ll|\varepsilon_b|$), high ($\epsilon_F\gg|\varepsilon_b|$), and intermediate ($\epsilon_F\sim|\varepsilon_b|$) carrier densities. The first case corresponds to the formation of local pairs and condensation scenarios according to the type of superfluidity; the second case corresponds to Cooper pairs and BCS-type superconductivity; and, finally, the third case corresponds to composite bosons of intermediate radius (of the order of the average

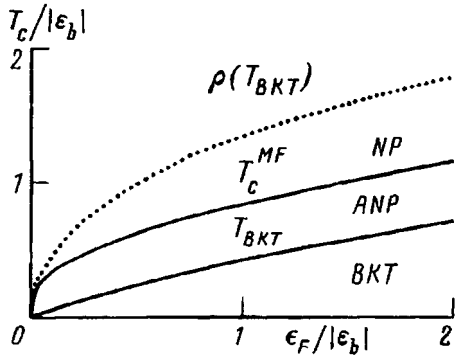

FIG. 1. $T_{\rm BKT}$ and T_c^{MF} versus the seed-fermion density. The dots represent the function $\rho(\epsilon_F)$ at $T=T_{\rm BKT}$. The regions of the NP, ANP, and BKT phases are indicated.

distance between fermions) and a crossover-type condensate. We also note that the quantity (6) vanishes on (and above) the mean-field critical line, which bounds the NP and the ANP.

Finally, we underscore that in the equation for the variable ρ we restricted ourselves to the mean-field approximation, since allowance for fluctuations of ρ is not fundamental for the final results. The non-single-valuedness of the phase of the order parameter is taken into account systematically — only $\nabla\theta(x)$ were assumed to be small.

5. The numerical investigation of the systems (8), (11), (14) and (12), (13) gives the following very interesting results, which are displayed graphically. a) The ANP region (see Fig. 1) in the present model is commensurate with the BKT region. But it has not been ruled out that in the case of an indirect interaction or the quasi-two-dimensional model this region will narrow as n_f increases. b) For low ϵ_F ($\ll|\varepsilon_b|$) the function $T_{\rm BKT}(\epsilon_F)$ is linear, as is also confirmed by the analytical solution of the system (8), (11), and (14), which gives $T_{\rm BKT}=\epsilon_F/2$. We note that the temperature of formation of a uniform order parameter $T_c=\epsilon_F/(2\alpha)$ (where $\alpha\gg 1$) even for the quasi-two-dimensional model[3] in the limit of low density n_f. This shows that the weak three-dimensionalization can preserve (in any case, for low n_f) the regions of the ANP and BKT phases, which, for example, happens in the relativistic quasi-two-dimensional model.[13] At the same time, as the three-dimensionalization parameter increases, the BKT phase can vanish, provided, however, that the ANP region and both temperatures T_c^{MF} and T_c are preserved. c) Figure 2 shows the values of n_f for which μ differs substantially from ϵ_F and, in other words, the Landau Fermi-liquid theory becomes inapplicable for metals with low or intermediate carrier density. As expected, the kink in μ at $T=T_c^{MF}$, experiments on the observation of which were discussed in Ref. 14 and have been interpreted for the 1–2–3 cuprate,[15] becomes increasingly less pronounced as ϵ_F increases. But in the present case it is interesting that in the approximation employed it happens at the NP–ANP boundary or before superconductivity actually appears. Therefore it would be of great interest to perform experiments which would reveal the temperature dependence $\mu(T)$, especially for strongly anisotropic (quasi-two-dimensional) and relatively weakly doped cuprates. d)

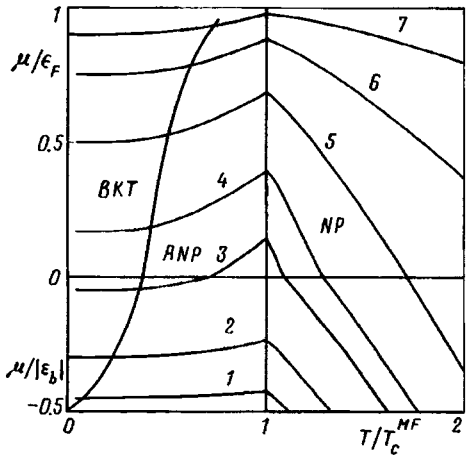

FIG. 2. $\mu(T)$ for different values of $\epsilon_F/|\varepsilon_b|$: *1* — 0.05; *2* — 0.2; *3* — 0.45; *4* — 0.6; *5* — 1; *6* — 2; *7* — 5. (For $\mu>0$ and $\mu<0$ the chemical potential was scaled to ϵ_F and $|\varepsilon_b|$, respectively.) The thick lines bound regions of the BKT, ANP, and NP phases.

It follows from curve *3* in Fig. 2 that the transition (change in sign of μ) from local to Cooper pairs is possible not only as ϵ_F increases, which is more or less obvious, but also (for some n_f) as T increases. e) Finally, the calculations showed that the ratio $2\Delta/T_{\mathrm{BKT}}$ is always greater than 4.4; the value of $2\Delta/T_c^{MF}$ is, however, somewhat lower and reaches the BCS theory limit of 3.52 only for $\epsilon_F \gg |\varepsilon_b|$. It is interesting that this behavior is consistent with numerous measurements of this ratio in high-T_c superconductors.[16,17]

6. Even though the phase diagram found was obtained under simplifying assumptions (for example, fluctuations of only the phase of the order parameter were taken into account systematically), it does show how sensitive the parameters of its critical lines are to the value of n_f. At the same time, it should be kept in mind that in contrast to the 3D transition, which occurs at $\rho=0$, the BKT transition occurs in a state where $\rho\neq 0$ and therefore, as was noted above, the fluctuations of the modulus of the order parameter should be weaker here and they should not suppress T_c^{MF} completely. Allowing for them is unlikely to affect the qualitative picture, but undoubtedly it would be interesting to estimate separately the role of the corresponding contributions of fluctuations of ρ and θ. The correlated and uncorrelated pairs, whose existence in a high-T_c superconductor is being widely discussed (see the reviews in Refs. 1, 8, and 9), can be qualitatively compared with regions where the phase diagram has been computed: Thus the pairs are correlated for $T<T_{\mathrm{BKT}}$ and uncorrelated for $T>T_{\mathrm{BKT}}$. In the NP region it is not so much the fluctuations of θ but rather of ρ that are important, and one should talk not about a correlation of different pairs but rather about fluctuations in the number of pairs.

In this letter only the existence of the ANP was established and the boundaries of this phase were calculated. However, the physical properties of this phase, primarily the spectrum, require a special study, though it is obvious that in the ANP, which does not

exhibit superconducting properties, a gap (pseudogap) is present in the Fermi excitation spectrum.

One of us (V. M. L.) thanks V. A. Gasparov for a discussion of the possibilities of observing the BKT phase in high-T_c superconductors and also V. F. Gantmakher for his interest in this work and for encouragement.

[a)]e-mail: vloktev@gluk.apc.org

[b)]The total derivative with respect to τ and terms which are not important for the further calculations are dropped.

[c)]There is no doubt that in certain situations (for example, very high T) it also can become a thermodynamic variable, i.e., dependent on T, as happens in problems of phase transitions between ordered (magnetic) and disordered (paramagnetic) phases when the spin itself vanishes. Specifically, for quasi-two-dimensional spin systems it is virtually obvious that as one proceeds from high-T regions, at first a spin modulus forms in 2D clusters of finite size and only then does global (3D) ordering occur.

[d)]It should be kept in mind that in the local-pair regime ($\mu<0$) the gap Δ in the quasiparticle excitation spectrum equals not ρ (as in the case $\mu>0$) but rather $\sqrt{\mu^2+\rho^2}$ (see the review in Ref. 2 and the literature cited there).

[1] V. M. Loktev, Fiz. Nizk. Temp. **22**, 490 (1996) [Low Temp. Phys. **22**, 376 (1996)].
[2] M. Randeria, in *Bose Einstein Condensation*, edited by A. Griffin, D. W. Snoke, and S. Stringari, Cambridge University Press, New York, 1995, p. 355.
[3] E. V. Gorbar, V. M. Loktev, and S. G. Sharapov, Physica C **257**, 355 (1996).
[4] É. V. Gorbar, V. P. Gusynin, and V. M. Loktev, Sverkhprovodimost' KIAE **6**, 483 (1992) [Fiz. Nizk. Temp. **19**, 1171 (1993) [Low Temp. Phys. **19**, 832 (1993)]; Preprint ITP-92-54E (1992).
[5] R. MacKenzie, P. K. Panigrahi, and S. Sakhi, Int. J. Mod. Phys. A **9**, 3603 (1994).
[6] M. Drechsler and W. Zwerger, Ann. Phys. (Germany) **1**, 15 (1992).
[7] V. M. Loktev and Yu. G. Pogorelov, Fiz. Nizk. Temp. **22**, 1018 (1996) [Low Temp. Phys. **22**, 776 (1996)].
[8] B. G. Levi, Physics Today **49**, 17 (1996).
[9] H. Ding, T. Yokoya, I. C. Campuzano *et al.*, Nature **382**, 51 (1996).
[10] I. J. R. Aitchison, P. Ao, D. J. Thouless, and X.-M. Zhu, Preprint CERN-TH.7385/94 (1994).
[11] A. M. J. Schakel, Mod. Phys. Lett. B **4**, 927 (1990).
[12] Yu. A. Izyumov and Yu. N. Skryabin, *Statistical Mechanics of Magnetically Ordered Systems* [in Russian], Nauka, Moscow, 1987, Chapter 15.
[13] H. Yamamoto and I. Ichinose, Nucl. Phys. B **370**, 695 (1992).
[14] D. van der Marel, Physica C **165**, 35 (1990).
[15] A. V. Dotsenko and O. P. Sushkov, Preprint cond-mat/9601031.
[16] T. P. Devereaux, Phys. Rev. Lett. **74**, 4313 (1995).
[17] C. Kendziora *et al.*, Phys. Rev. Lett. **77**, 727 (1996).

Translated by M. E. Alferieff

Contact phenomena in a semiconductor film with activational conduction

V. B. Shikin

Institute of Solid-State Physics, Russian Academy of Sciences, 142432 Chernogolovka, Moscow District, Russia

(Submitted 28 November 1996; resubmitted 18 December 1996)
Pis'ma Zh. Éksp. Teor. Fiz. **65**, No. 2, 176–181 (25 January 1997)

It is noted that the contact of an unscreened, two-dimensional electronic system with ''external'' metallic electrodes destroys the spatial uniformity of its electron density, which decreases slowly (inversely as the distance from the interface) away from the contact zone. These effects are especially pronounced in systems with a small number of carriers, for example, semiconductor films with an exponentially low electron (hole) density, when the nonuniform part of the contact density competes without difficulty with its initial, uniform component. The effect of contact phenomena on the conductivity of a semiconductor film, which is the central part of a Corbino disk, for different temperatures, doping levels and doping composition, sample dimensions in the direction of the current, and so on is described in detail. A comparison with existing experiments is presented. © *1997 American Institute of Physics.* [S0021-3640(97)01202-4]

PACS numbers: 73.50.Jt, 73.50.Gr

Contact phenomena are well known in the physics of three-dimensional (3D) conducting media (see, for example, Refs. 1 and 2). These phenomena are accompanied by a breakdown of the local neutrality of conductors in the contact zone as a result of the need for some free carriers to be transferred from one medium into another. Neutrality in the volume of the contact pair is destroyed exponentially at interatomic distances for good metals and at the corresponding Debye screening length in typical semiconductors. In the case of the free faces of conductors the contact electric fields ''extend'' into the vacuum and are screened by the conductors much more weakly (power-law manner) than in the interior.[1]

Surface effects are clearly not important in various three-dimensional problems of the type where Schottky barriers or the properties of p–n junctions must be described.[1,2] However, the situation changes in contact problems involving two-dimensional (2D) conductors. The initial factors leading to the appearance of a contact potential difference (mainly, different work functions of the media in contact) also remain for such contacts. But in a 2D system, screening of the contact fields through the vacuum is the only possible way. As a result, the slowly decreasing contact surface charge density, which is of no importance in three-dimensional problems, is at center stage in the study of low-dimensional contact phenomena.

Among the as yet few, examples of an explicit manifestation of ''long-range action'' in the effect of contacts on the properties of low-dimensional electronic systems, we mention the fact that the real dimensions of the region with an integer filling factor in the 2D part of a Corbino disk under conditions of the quantum Hall effect (the experiment in Ref. 3 and interpretation in Ref. 4) are different from the nominal dimensions of this region; specific oscillations of the Corbino conductivity as a function of the magnetic field,[5] when the resistance of the apparatus is determined mainly by its central part, where the filling factor is small, and the period of the oscillations assumes a value that is characteristic for the metallic Corbino ''electrodes'' with a quasiclassically large filling factor; and, so on.

Our objective in the present work is to discuss in the spirit of Ref. 4 the properties of a quasi-one-dimensional Corbino disk whose central part is a 2D semiconductor film with activational conductivity. For simplicity, the metallic contacts are also assumed to be two-dimensional. The requirement that the film be two-dimensional means that the thickness d of the film is less than the corresponding Debye radius for the given semiconductor. The quasi-one-dimensionality of the Corbino geometry presupposes that

$$R_2 - R_1 \ll (R_2 + R_1)/2, \tag{1}$$

where R_2 and R_1 are the outer and inner radii of the semiconductor part of the Corbino disk.

Specifically, we shall consider below an extreme version of the problem, in which the semiconductor film occupies the strip $z=0$, $-w<x<+w$ and is in contact with semi-infinite metallic ''electrodes'', which also lie in the $z=0$ plane. The composite character of the system is determined mainly by a jump in the work function $\Phi(x)$:

$$\Phi(x)=\Phi_m, \quad |x|>w; \quad \Phi(x)=\Phi_s, \quad |x|<w. \tag{2}$$

Here $2w$ is the width of the semiconductor-filled strip along the x axis. Besides the work function, the characteristics of the semiconductor include also the donor density n_d and acceptor density n_a, as well as the position of the donor level E_d and the acceptor level E_a with respect to the bottom of the conduction band.

The electrons occupy the same plane $z=0$ as the donors, and the electron density $n(x)$ varies along the x axis, corresponding to the radial direction of the Corbino disk. The properties of the film in the vertical direction are not specified. It is assumed that the film is quite thin and that its characteristics are all uniform over its thickness d.

The model (2) is convenient from the formal standpoint because of its simplicity. It contains the well-known (from Ref. 1) singularities of the electron density in the contact zones (see the definition of $\delta n_0(x)$ in Eq. (4)) and permits regularization of the singularities by the methods presented in Ref. 4.

1. Proceeding to the study of the properties of the system (2), we consider first the equilibrium results, comparing in so doing the ''pictures'' of 3D and 2D metal–semiconductor contacts for the case when a *n*-type semiconductor is enriched with extra electrons.

In the 3D case the transfer of electrons into the semiconductor results in the appearance of a band with high electron density[2] near a contact placed at the point $x=0$:

$$\delta n(x)=n_k\left(\frac{a}{a+x}\right)^2, \quad a^2=\kappa T/2\pi n_k e^2, \quad x>0. \tag{3}$$

Here n_k is a 3D electron density at the metal–semiconductor boundary and is proportional to the difference of the work functions, and κ is the dielectric constant.

For the two-dimensional problem with the same accuracy as in Eq. (3), the distribution $\delta n_o(x)$ of the perturbed electron density of contact origin is given by (the origin of the coordinates lies at the point $x=0$, according to the model in Eq. (2))

$$\delta n_o(x)=\frac{\kappa w\varphi_{ms}}{\pi^2 e(w^2-x^2)}, \quad e\varphi_{ms}=\Phi_m-\Phi_s>0, \tag{4}$$

where Φ_m and Φ_s are the work functions for the metallic ''electrodes'' and the semiconductor. The symbol >0 in the definition of φ_{ms} in Eq. (4) corresponds to the case of enrichment for the semiconductor film. The power-law singularities at the ends of the interval $2w$ are not very important for the effective conductivity of the system (see below for a more detailed discussion) and can be eliminated if so desired (see Ref. 4). In the central part, where the distribution $\delta n_o(x)$ (4) possesses a minimum, the definition (4) can be used, just as in the case (3), so long as

$$\delta n_o(x)>n_e, \quad n_e=\sqrt{n_c n_d}\,\exp(-E_d/2T), \quad n_c=\frac{4\pi m_* T}{h^2}; \tag{5}$$

Here n_c and m_* are the 2D density of states and the electron effective mass in the conduction band of a n-type semiconductor and E_d is the activation energy (position of the donor level relative to the bottom of the conduction band).

In the situation $\delta n_o(x)<n_e$ the problem of the electron distribution in the film must be solved more accurately than was done in the derivation of Eq. (4). Qualitatively, just as in the 3D theory, the interpolation

$$n_e(x)=n_e+\delta n_o(x), \quad -w\ll x\ll +w, \tag{6}$$

where n_e is taken from Eq. (5) and $\delta n_o(x)$ is taken from Eq. (4), is a good approximation for this region.

Comparing Eqs. (3) and (4), it is easy to see their similarity (the weak dependence on T) and difference (the distribution (4) is much more even and does not contain even a power-law radius of convergence, as in Eq. (3)). The accuracy of the asymptotic expressions (3) and (4) at large distances from the contacts is also the same. This justifies the interpolation (6) for $n_e(x)$ constructed by analogy to the 3D case.

2. The next part of the calculation concerns the introduction of a correction $\delta n(x)$ to Ohm's law for a Corbino disk. Here we shall restrict ourselves to the simplest possibility — the Drude approximation:

$$j=\frac{n_e(x)e^2\tau}{m_*}\frac{d\mu}{dx}, \quad n_e(x)=n_e+\delta n_o(x), \tag{7}$$

where μ is the electrochemical potential, τ is the momentum relaxation time, n_e is taken from Eq. (5), and $\delta n_o(x)$ is taken from Eq. (4). Assuming now that the current density

j is conserved in the radial direction of the Corbino disk, the effective relation between j and the potential difference V at the edges of the high-resistance part of the disk can be determined:

$$V=\int_{-w}^{+w} ds d\mu/ds=\frac{m_* j}{e^2\tau}\int_{-w}^{+w}\frac{ds}{n_e+\delta n_o(s)}. \tag{8}$$

The definition (8) attests to the fact that the singular points of the function $\delta n_o(x)$ from Eq. (4) make no contribution to the integral.

Expression (8) can ultimately be reduced to the following effective Ohm's law:

$$j=\sigma\frac{V}{2w}, \quad \sigma=\sigma_0 f(\delta), \quad \sigma_0=e^2\tau n_0/m_* \tag{9}$$

$$f(\delta)=\frac{\delta}{\delta-0.5(1-\delta^2)\ln\dfrac{1+\delta}{1-\delta}}, \quad \delta=(1+l/w)^{-1/2}, \quad l=\frac{\kappa e\varphi_{ms}}{\pi^2 e^2 n_e}.$$

Here φ_{ms} is given by Eq. (4) and n_e by Eq. (5).

If $\delta=1-\epsilon$, $\epsilon\ll 1$,

$$f(\delta)\simeq\frac{1}{1-\epsilon\ln(2/\epsilon)}, \quad \epsilon=0.5l/w. \tag{10}$$

In the opposite limiting case $\delta\to 0$ $(l\gg w)$

$$f(\delta)\simeq 3/2\delta^2. \tag{11}$$

Formulas (9)–(11) contain the canonical part of the IVC, viz., $j=\sigma_o V/2w$, and a correction factor $f(\delta)$ that takes into account the effect of the contacts. As w decreases, at fixed temperature, this factor effectively increases the conductivity as a result of the variation of the parameter l/w. If w is fixed and the temperature varies, however, then in accordance with the definition of the length l (9) this factor modifies the activational temperature dependence of σ_0 contained in the definition of n_e.

3. As a supplement to the problem of a film of a *n*-type semiconductor we shall also study the case of mixed doping: donors + acceptors. The degree of compensation

$$k=n_a/n_d, \quad k\leqslant 1, \tag{12}$$

is assumed to be quite high, and the temperature interval corresponds to simple hopping conduction.

It is obvious that in this case the contact electrons, which are not confined in the conduction band, reach the acceptors, charge them, and thereby locally change the degree of compensation of the semiconductor, which in turn results in a renormalization of the basic parameters of hopping conduction. On this basis, we write with the aid of Ref. 6 the effective resistance of the film in the limiting case of a deep compensation, which we are interested in here:

$$V=\int_{-w}^{+w}\rho(x)j\,dx;\quad \rho(x)=\rho_o\exp\left[\left(\frac{2.86}{a\sqrt{n_d}}\right)+\left(\frac{\varepsilon(x)}{T}\right)\right], \tag{13}$$

$$\varepsilon(x)=\epsilon\,\ln\left[\frac{1}{1-k(x)}\right],\quad k(x)=\frac{n_a(x)}{n_d},\quad [1-k(x)]\ll 1,$$

$$n_a(x)=n_a-\delta n_0(x),\quad \epsilon=e^2\kappa^{-1}\sqrt{n_d}\,. \tag{14}$$

Here n_a and n_d are the corresponding two-dimensional acceptor and donor densities and a is the characteristic Bohr radius of an electron on a separate donor. As noted above, the contact electrons with density $\delta n_o(x)$ (4) influence the local acceptor density $n_a(x)$ (14) (the extra electrons escape to the acceptors, decreasing their active number, and the number of donor locations via which the hops occur remains unchanged).

It is obvious that the integral (13) possesses a saddle point at $x=0$. On this basis, we rewrite the definition (13) in the form

$$V=\rho j,\quad \rho=\rho_0 w^*\exp\left[\left(\frac{2.86}{a\sqrt{n_d}}\right)+\left(\frac{\varepsilon(0)}{T}\right)\right], \tag{15}$$

$$\varepsilon(0)=\epsilon\,\ln\left[\frac{1}{1-k(0)}\right],\quad k(0)=\frac{n_a(0)}{n_d},\quad [1-k(0)]\ll 1,$$

$$w^*=\sqrt{\frac{\pi T}{|\varepsilon''(0)|}},\quad \varepsilon''(0)=-\frac{2\epsilon\delta n_o}{n_d w^2(1-\Delta)},\quad \Delta=\frac{n_a-\delta n_o}{n_d}.$$

Here $n_a(0)$ is given by Eq. (14).

Formula (15) for ρ shows that contact phenomena have an exponential effect on the activation energy for hopping conduction. In the strong compensation regime, the activation energy is determined mainly by the ''distance'' between the position of the Fermi level and the maximum of the donor density of states. As excess electrons appear and change the degree of compensation at the center of the semiconductor, this ''distance'' decreases, as a result of which the activation energy for hopping conduction decreases.

Size effects in hopping conduction in semiconductor films have been observed in Ref. 7. For a quantitative analysis of the data in Ref. 7 it is convenient to rewrite the definition of $\varepsilon(0)$ in Eq. (15) with the geometric factor l/w singled out:

$$\varepsilon_w\equiv\varepsilon(0)=e^2\kappa^{-1}\sqrt{n_d}\,\ln\left[\frac{1}{1-k(1-l/w)}\right],\quad k=n_a/n_d, \tag{16}$$

$$l=\frac{\kappa\phi_{ab}}{\pi^2e^2n_d}. \tag{17}$$

The definition (16) of the activation energy contains three parameters: n_a, n_d, and l. To estimate their numerical values, we employ the data of Ref. 7. Figure 29 of that dissertation makes it possible to distinguish the following pairs of numbers for a channel of length w in microns and the corresponding activation energy ε_w in degrees Kelvin:

$$(w,\varepsilon_w)=(145;15);\quad (12;10.8);\quad (3.5;9.0);\quad (1;7.6);\quad (0.45;4.4). \tag{18}$$

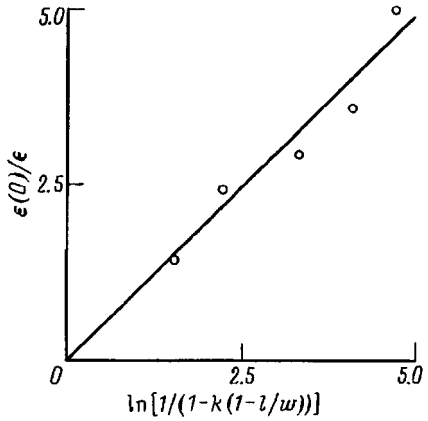

FIG. 1. Relative activation energy $\varepsilon(0)/\epsilon$ versus the channel width w for fixed values of k and l. The plot is constructed in rectilinearizing coordinates for $k=0.99$ and $l=0.1$ μm. The open circles represent the experimental points from Ref. 7, whose values are presented in Eq. (18).

Formula (16) fits the data (18) best if

$$k=0.99, \quad l=0.1\ \mu\text{m}. \tag{19}$$

The degree to which the points (18) correspond to the defnitions (16) and (19) is illustrated in Fig. 1.

Knowing k and l, we shall estimate n_d and $e\varphi_{ms}$ with the aid of expressions (15) and (17) for $\varepsilon(0)$ and l, respectively. For $\kappa=10$

$$n_d=10^9\ \text{cm}^{-2}, \quad e\varphi_{ms}=\pi^2 e^2 n_d \kappa^{-1} l \simeq 10\ \text{K}. \tag{20}$$

Hence it follows that the average distance between the nominal donors and acceptors is greater than or of the order of 10^{-5} cm. This distance is greater than the thickness of the films employed in the experiments of Ref. 7, and as noted above this makes it possible to employ the 2D approximation in writing formula (13) for $\rho(x)$.

Comparing the quantity $e\varphi_{ms}\simeq 10$ K in Eq. (20) with the known values of the contact potential difference shows that it is relatively small. But it is necessary to take into account the fact that the activiation energies (18) are also small for typical semiconductor objects. In this case, it is important that even small values of the contact potential difference are sufficient to account for the observed dependence of the activation energy on the dimensions of the channel.

In closing, we note that contact phenomena in low-dimensional systems and, specifically, in semiconductor films appreciably influence the equilibrium and transport properties of the films. This occurs in cases when the spatially nonuniform contact correction to the electron density is comparable to the initial electron density of the semiconductor. Taking account of the strong dependence of the nonuniform part of the density on the geometric parameters of the problem and the temperature, it is possible to predict the various size and temperature effects of contact origin in the conductivity of semiconductor films. Some of these effects have already been observed experimentally.

I thank V. F. Gantmakher for bringing Ref. 7 to my attention and for helpful discussions. This work is supported by the Russian Fund for Fundamental Research (Grants 95-02-06108a and 96-02-19568).

[1] L. D. Landau and E. M. Lifshitz, *Electrodynamics of Continuous Media*, Pergamon Press, New York [Russian original, Gostekhizdat, Moscow, 1957, p. 133].
[2] V. L. Bonch-Bruevich and S. G. Kalashnikov, *Semiconductor Physics* [in Russian], Nauka, Moscow, 1977.
[3] W. Dietsche, K. von Klitzing, and K. Ploog, Workbook Program of the Conference ''Electronic Properties of Two Dimensional Systems,'' Nottingham, U.K., 1995, p. 311.
[4] V. B. Shikin and N. I. Shikina, JETP Lett. **62**, 879 (1995).
[5] V. T. Dolgopolov, A. A. Shaṣhkin, G. V. Kravchenko *et al.*, JETP Lett. **63**, 55 (1996).
[6] B. I. Shklovskiĭ and A. L. Ėfros, *Electronic Properties of Doped Semiconductors*, Springer-Verlag, New York, 1984 [Russian original, Nauka, Moscow, 1979].
[7] D. Kowal, *Characterization of the Percolative Resistor Network in the Hopping Regime*, PhD Thesis, Hebrew University, 1995.

Translated by M. E. Alferieff

Thermoelectric effect in high-T_c superconductors: The role of density-of-states fluctuations

A. A. Varlamov
Department of Physics ''A. Volta,'' University of Pavia, Strada Nuova 65, 27100 Pavia, Italy

D. V. Livanov
Moscow Institute for Steel and Alloys, 117936 Moscow, Russia

F. Federici
Department of Physics, University of Florence, 50125 Florence, Italy

(Submitted 19 December 1996)
Pis'ma Zh. Éksp. Teor. Fiz. **65**, No. 2, 182–187 (25 January 1997)

We study the effect of the density-of-states (DOS) fluctuations on the thermoelectric coefficient of a highly anisotropic superconductor above the critical temperature. It is shown that it is the DOS contribution which gives rise to the leading correction to the thermoelectric coefficient, in spite of previous results where only the Aslamazov–Larkin term was taken into account. This conclusion is valid for an arbitrary impurity concentration. © *1997 American Institute of Physics.* [S0021-3640(97)01302-9]

PACS numbers: 72.15.Jf, 74.40.+k

1. The problem of the thermoelectric effect in the fluctuation regime has been attracting the attention of theoreticians for more than twenty years, ever since the paper of Maki.[1] The main question which should be answered is whether or not the correction to the thermoelectric coefficient β has the same temperature singularity in the vicinity of the critical temperature T_c as does the correction to the electrical conducticity σ. In the paper of Maki[1] only a logarithmically divergent contribution was predicted in the two-dimensional (2D) case, and its sign was found to be opposite to the sign of the normal-state thermoelectric coefficient β_0. Later on, in a number of papers[2–4] it was claimed that the temperature singularity of the fluctuation correction to β is the same as it is for σ ($\propto(T-T_c)^{-1}$ in 2D). Finally, Reizer and Sergeev[5] have recently revised the problem using both the quantum kinetic equation and linear response methods and have shown that, in the case of an isotropic electron spectrum, the strongly divergent contributions[2–4] are canceled out for any dimensionality, and the final result has the same logarithmic singularity as was found by Maki, but with the opposite sign. We should emphasize that in all papers cited above only the Aslamazov–Larkin (AL) contribution was taken into account, while the anomalous Maki–Thompson (MT) term was shown to be absent.[2,5] It has been mentioned[5] that an incorrect evaluation of the interaction corrections to the heat-current operator in Refs. 2–4 produced erroneously large terms, which really are canceled out within the adequate procedure. Due to this strong cancelation the AL term

turns out to be less singular as compared to the corresponding correction to the conductivity.[5]

On the other hand, it is now well established that in every case, where the leading AL and MT fluctuation corrections are suppressed for some reason, the contribution connected with fluctuation renormalization of the one-electron density of states (DOS) can become important. As examples we can mention c-axis fluctuative transport,[6,7] the NMR relaxation rate,[8] and infrared optical conductivity.[9] In this communication we show that an analogous situation also takes place in the case of the thermoelectric coefficient. In what follows we study the DOS contribution to the thermoelectric coefficient of superconductors with an arbitrary impurity concentration above T_c. We will be mostly interested in the 2D case, but the generalization to the case of a layered superconductor will be done at the end. We show that, although the DOS term has the same temperature dependence as the AL contribution,[5] it turns out to be the leading fluctuation contribution in both the clean and dirty cases, due to its specific dependence on the electron mean free path.

2. We use units in which $\hbar = c = k_B = 1$. We introduce the thermoelectric coefficient β in the framework of linear response theory as:

$$\beta = \lim_{\omega \to 0} \frac{\mathrm{Im}[Q^{(eh)R}(\omega)]}{T\omega}, \tag{1}$$

where $Q^{(eh)R}(\omega)$ is the retarded Fourier component of the correlation function of the electric and heat current operators. This correlation function in the diagrammatic technique is represented by the two exact electron Green's functions loop with two external field vertices, the first, $-e\mathbf{v}$, associated with the electric current operator and the second, $i/2(\epsilon_n + \epsilon_{n+\nu})\mathbf{v}$, associated with the heat current operator [$\epsilon_n = \pi T(2n+1)$ is the fermionic Matsubara frequency and $\mathbf{v} = \partial\xi(\mathbf{p})/\partial\mathbf{p}$, where ξ is the quasiparticle energy]. Taking into account the first order of perturbation theory in the Cooper interaction and averaging over impurity configurations, one can find the ten diagrams presented in Fig. 1. The solid lines represent $G(\mathbf{p},\epsilon_n) = 1/(i\tilde{\epsilon}_n - \xi(\mathbf{p}))$, the single-quasiparticle normal-state Green's function averaged over impurities, which contains the scattering lifetime $\tau(\tilde{\epsilon}_n = \epsilon_n + 1/2\tau \,\mathrm{sign}\, \epsilon_n)$. The shaded objects are the vertex impurity renormalization $\lambda(\mathbf{q}=0,\epsilon_n,\epsilon_{n'})$ (see Ref. 7). The wavy line represents the fluctuation propagator $L(\mathbf{q},\Omega_k)$:

$$L^{-1}(\mathbf{q},\Omega_k) = -\rho\left[\ln\frac{T}{T_c} + \psi\left(\frac{1}{2} + \frac{|\Omega_k|}{4\pi T} + \frac{2\eta q^2}{\pi^2}\right) - \psi\left(\frac{1}{2}\right)\right], \tag{2}$$

where

$$\eta = -\frac{v_F^2\tau^2}{2}\left[\psi\left(\frac{1}{2} + \frac{1}{4\pi T\tau}\right) - \psi\left(\frac{1}{2}\right) - \frac{1}{4\pi T\tau}\,\psi'\left(\frac{1}{2}\right)\right]$$

is a positive constant which appears in the expression for the current in Ginzburg–Landau theory in the 2D case (ρ is the one-electron density of states and $\psi(x)$ and $\psi'(x)$ are the digamma function and its derivative, respectively). The first diagram describes the AL contribution to the thermoelectric coefficient and was calculated in Ref. 5 with the electron–hole asymmetry factor taken into account in the fluctuation propagator. Dia-

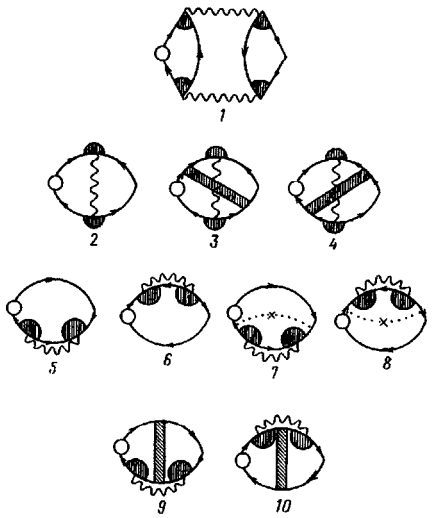

FIG. 1. The Feynman diagrams for the fluctuation correction to thermoelectric coefficient are shown. The shaded partial circles are impurity vertex corrections, the dashed curves with central crosses are additional impurity renormalizations, and the shaded heavy lines are additional impurity vertex corrections.

grams 2–4 represent the Maki–Thompson contribution. As was mentioned in Refs. 2 and 5, neither the anomalous nor the regular parts of this diagram contribute to β in any order of electron–hole asymmetry. In what follows we will discuss the contribution from diagrams 5–10, which describes the correction to β due to DOS renormalization.

For diagrams 5 and 6 we have

$$Q^{(5+6)}(\omega_\nu)=-2eT\sum_{\Omega_k}\int(d\mathbf{q})L(\mathbf{q},\Omega_k)T\sum_{\epsilon_n}\frac{i(\epsilon_{n+\nu}+\epsilon_n)}{2}\int(d\mathbf{p})v^2$$
$$\times[\lambda^2(\epsilon_n,-\epsilon_n)G^2(\mathbf{p},\epsilon_n)G(\mathbf{q}-\mathbf{p},-\epsilon_n)G(\mathbf{p},\epsilon_{n+\nu})$$
$$+\lambda^2(\epsilon_{n+\nu},-\epsilon_{n+\nu})G^2(\mathbf{p},\epsilon_{n+\nu})G(\mathbf{q}-\mathbf{p},-\epsilon_{n+\nu})G(\mathbf{p},\epsilon_n)]. \tag{3}$$

(We use the shorthand notation $(d\mathbf{q})=d^dq/(2\pi)^d$, where d is the dimensionality). Evaluating Eq. (3), one naturally obtains a zero result without taking into account the electron–hole asymmetry. The first possible source of such a factor is contained in the fluctuation propagator and was used in Ref. 5 for the AL diagram. Our calculations show that for the DOS contribution this correction to the fluctuation propagator results in a non-singular correction to β in the 2D case and can be neglected. Another source of electron–hole asymmetry is connected with the expansion of the energy-dependent functions in power of ξ/E_F near the Fermi level in performing the **p**-integration in Eq. (3) (E_F is the Fermi energy):

$$\rho v^2(\xi)=\rho v^2(0)+\xi\left[\frac{\partial(\rho v^2(\xi))}{\partial\xi}\right]_{\xi=0}. \tag{4}$$

Only the second term in Eq. (4) contributes to the thermoelectric coefficient. The contribution of diagrams 7 and 8 can be calculated in analogous way. Diagrams 9–10 do not give any singular contribution to the thermoelectric coefficient on account of the vector character of the external vertices, and, as a result, an additional q^2 factor appears after **p**-integration. The same conclusion concerns the MT-like diagram.[3,4]

Performing the integration over ξ, we find the contribution of the important diagrams 5–8 in the form

$$Q^{(5-8)}(\omega_\nu)=\frac{eT^2}{4}\left[\frac{\partial(\rho v^2(\xi))}{\partial\xi}\right]_{\xi=0}\int (d\mathbf{q})L(\mathbf{q},0)(\Sigma_1+\Sigma_2+\Sigma_3), \tag{5}$$

where we have separated the sums over semi-infinite ($(-\infty,-\nu-1]$, $[0,\infty)$) and finite ($[-\nu,-1]$) intervals:

$$\Sigma_1=2\sum_{n=0}^{\infty}\frac{2\epsilon_n+\omega_\nu}{2\tilde{\epsilon}_n+\omega_\nu}\left(\frac{\tilde{\epsilon}_n+\omega_\nu}{(\epsilon_n+\omega_\nu)^2}+\frac{\tilde{\epsilon}}{\epsilon_n^2}\right),$$

$$\Sigma_2=\frac{1}{(1/\tau+\omega_\nu)^2}\sum_{n=-\nu}^{-1}(2\epsilon_n+\omega_\nu)^2\left(\frac{\tilde{\epsilon}_{n+\nu}}{\epsilon_{n+\nu}^2}-\frac{\tilde{\epsilon}_n}{\epsilon_n^2}\right),$$

$$\Sigma_3=(1+\omega_\nu\tau)\sum_{n=-\nu}^{-1}(2\epsilon_n+\omega_\nu)\left(\frac{1}{\epsilon_{n+\nu}^2}-\frac{1}{\epsilon_n^2}\right). \tag{6}$$

Σ_1 and Σ_2 are associated with diagram 5–6, while Σ_3 is associated with diagram 7–8. In calculating the sums (6) we are interested in terms which are linear in the external frequency ω_ν. Sum Σ_1 turns out to be an analytic function of ω_ν and it is sufficient to expand it in a Taylor series after analytical continuation $\omega_\nu\to-i\omega$. The last two sums over finite intervals require more attention because of their nontrivial ω_ν dependence, and before analytical continuation they have to be calculated rigorously. The result is

$$\Sigma_1^R=\frac{i\omega}{4T^2};\quad \Sigma_2^R=-\frac{2i\omega\tau}{\pi T};\quad \Sigma_3^R=-\frac{i\omega}{2T^2}. \tag{7}$$

Finally, we perform the integration over **q**, and the total contribution associated with DOS renormalization in 2D case takes the form:

$$\beta^{\mathrm{DOS}}=\frac{1}{8\pi^2}\frac{eT_c}{v_{\mathrm{F}}^2\rho}\left[\frac{\partial(v^2\rho)}{\partial\xi}\right]_{\xi=0}\ln\left(\frac{T_c}{T-T_c}\right)\kappa(T_c\tau), \tag{8}$$

$$\kappa(T\tau)=-\frac{1+\dfrac{\pi}{8T\tau}}{T\tau\left[\psi\left(\dfrac{1}{2}+\dfrac{1}{4\pi T\tau}\right)-\psi\left(\dfrac{1}{2}\right)-\dfrac{1}{4\pi T\tau}\,\psi'\left(\dfrac{1}{2}\right)\right]}$$

$$= \begin{cases} \dfrac{8\pi^2}{7\zeta(3)}\, T\tau \approx 9.4 T\tau & \text{for } T\tau \ll 1, \\ \dfrac{1}{T\tau} & \text{for } T\tau \ll 1. \end{cases} \tag{9}$$

To generalize this result to the important case of a layered superconductor one has to make the substitution to $\ln(1/\epsilon) \to \ln[2/(\sqrt{\epsilon}+\sqrt{\epsilon+r})]$ ($\epsilon = (T-T_c)/T_c$ and r is an anisotropy parameter[7]) and to multiply Eq. (8) by $1/p_F s$, where s is the interlayer distance. In the limiting case of a 3D superconductor ($r \gg \epsilon$) both the AL[5] and DOS contributions are nonsingular.

3. Comparing Eq. (8) with the results of Ref. 5 for the AL contribution, we conclude that in both the limiting cases of clean and dirty systems the decrease of β due to fluctuation DOS renormalization dominates the thermoelectric transport due to the AL process. In fact, the total relative correction to thermoelectric coefficient in the case of a 2D superconducting film of thickness s can be written in the form:

$$\frac{\beta^{\mathrm{DOS}}+\beta^{\mathrm{AL}}}{\beta_0} = -0.09\, \frac{1}{E_F \tau}\, \frac{1}{p_F s}\, \ln\left(\frac{T_c}{T-T_c}\right)\left[\kappa(T_c\tau) + 10.6\, \ln\frac{\Theta_D}{T_c}\right], \tag{10}$$

where the first term in square brackets corresponds to the DOS contribution (8) and the second term describes the AL contribution from Ref. 5 (Θ_D is the Debye temperature). Assuming $\ln(\Theta_D/T_c) \approx 2$ one finds that the DOS contribution dominates the AL contribution for any value of the impurity concentration: κ as a function of $T\tau$ has a minimum at $T\tau \approx 0.3$, and even at this point the DOS term is larger. In the two limiting cases $T\tau \ll 1$ and $T\tau \gg 1$ this difference increases strongly.

The temperature and impurity-concentration dependences of the fluctuation corrections to β can be evaluated through a simple qualitative consideration. The thermoelectric coefficient may be estimated in terms of the electrical conductivity σ as $\eta \sim (\epsilon^*/eT) f_{\mathrm{as}} \sigma$, where ϵ^* is the characteristic energy involved in thermoelectric transport and f_{as} is the electron–hole asymmetry factor, which is defined as the ratio of the difference between the numbers of electrons and holes to the total number of particles. The conductivity can be estimated as $\sigma \sim e^2 \mathcal{N} \tau^*/m$, where $\mathcal{N}$, τ^*, and m are the density, lifetime, and mass of the charge (and heat) carriers, respectively. In the case of the AL contribution the heat carriers are nonequilibrium Cooper pairs with energy $\epsilon^* \sim T - T_c$ and density

$$\mathcal{N} \sim p_F^d\, \frac{T}{E_F}\, \ln\frac{T_c}{T-T_c}$$

and with a characteristic time given by the Ginzburg–Landau time $\tau^* \sim \tau_{\mathrm{GL}} = \pi/8(T-T_c)$. Thus in the 2D case

$$\Delta\eta^{\mathrm{AL}} \sim (T-T_c)/(eT_c) f_{\mathrm{as}} \Delta\sigma^{\mathrm{AL}} \sim e f_{\mathrm{as}}\, \ln\frac{T_c}{T-T_c}.$$

One can easily see that the fluctuation correction due to AL process is less singular (logarithmic in 2D case) than the corresponding correction to the conductivity and does not depend on impurity scattering.[5]

An analogous consideration of the single-particle DOS contribution ($\epsilon^* \sim T$, $\tau^* \sim \tau$) evidently results in the estimate

$$\beta \sim e f_{\rm as} T_c \tau \ln \frac{T_c}{T - T_c},$$

which coincides with Eq. (8) in the clean case. The dirty case is more ''sophisticated'' because the fluctuation density-of-states renormalization depends strongly on the character of the electron motion, especially in the case of diffusive motion.[10] The same density-of-states redistribution in the vicinity of the Fermi level enters directly into the rigorous expression for β, and it is not enough to write the fluctuation Cooper pair density $\mathcal{N}$ but it is necessary to take into account some convolution with $\delta\rho_{\rm fl}(\epsilon)$. This is what was actually done in the previous calculations.

Experimentally, although the Seebeck coefficient $S = -\eta/\sigma$ is probably the easiest to measure of thermal transport coefficients, the comparison between experiment and theory is complicated by the fact that S cannot be calculated directly; it is rather a composite quantity made up of the electrical conductivity and thermoelectric coefficient. As both η and σ have corrections due to superconducting fluctuations, the total correction to Seebeck coefficient is given by

$$\Delta S = S_0 \left(\frac{\Delta\beta}{\beta_0} - \frac{\Delta\sigma}{\sigma_0} \right). \tag{11}$$

Both these contributions provide a positive correction $\Delta\beta$, thus resulting in a decrease of the absolute value of S at the edge of superconducting transition ($\Delta\beta/\beta_0 < 0$). As to the fluctuation correction to the conductivity, $\Delta\sigma/\sigma_0 > 0$, we see from Eq. (11) that thermodynamic fluctuations above T_c always reduce the overall Seebeck coefficient as the temperature approaches T_c. So the very sharp maximum in the Seebeck coefficient of high-T_c materials experimentally observed in several papers[11] seems to be unrelated to fluctuation effects within our simple model, even leaving aside the question of the experimental reliability of these observations.

The authors are grateful for Collaborative NATO Grant 941187 and for RFFR Grant 18878 for support. One of the authors (A.V.) thanks the CARIPLO Foundation and Landau network for kind hospitality in Pavia.

[1] K. Maki, Sov. J. Low Temp. Phys. **14**, 419 (1974).
[2] A. A. Varlamov and D. V. Livanov, Zh. Éksp. Teor. Fiz. **98**, 584 (1990) [Sov. Phys. JETP **71**, 325 (1990)].
[3] A. V. Rapoport, Fiz. Tverd. Tela (Leningrad) **33**, 542 (1991) [Sov. Phys. Solid State **33**, 309 (1991)].
[4] D. Kumar, J. Phys. Condens. Matter **5**, 8227 (1993).
[5] M. Yu. Reizer and A. V. Sergeev, Phys. Rev. B **50**, 9344 (1994).
[6] L. B. Ioffe, A. I. Larkin, A. A. Varlamov, and L. Yu, Phys. Rev. B **47**, 8936 (1993).
[7] A. I. Buzdin, V. V. Dorin, R. A. Klemm *et al.*, Phys. Rev. B **48**, 12951 (1993).
[8] M. Randeria and A. A. Varlamov, Phys. Rev. B **50**, 10401 (1994).
[9] F. Federici and A. A. Varlamov, JETP Lett. **64**, 433 (1996).
[10] C. Di Castro, C. Castellani, R. Raimondi, and A. A. Varlamov, Phys. Rev. B **42**, 10211 (1990).
[11] M. A. Howson, M. B. Salamon, T. A. Friedmann *et al.*, Phys. Rev. B **41**, 300 (1990); N. V. Zavaritsky, A. A. Samoilov, and A. A. Yurgens, JETP Lett. **55**, 127 (1992).

Published in English in the original Russian journal. Edited by Steve Torstveit.

Momentum dependence of the dimensionality of the electronic states in heterostructures

V. V. Kapaev and Yu. V. Kopaev[a)]
P. N. Lebedev Physics Institute, Russian Academy of Sciences, 117924 Moscow, Russia

(Submitted 20 December 1996)
Pis'ma Zh. Éksp. Teor. Fiz. **65**, No. 2, 188–193 (25 January 1997)

Bound states of electrons (holes) in quantum wells and wires with asymmetric barriers can exist in bounded regions of two- and one-dimensional momentum space, respectively. As the corresponding momentum increases, both the disappearance (increase of dimensionality) and appearance (decrease of dimensionality) of bound states as well as the existence of a sequence of several such transformations of dimensionality are possible. In the case of anisotropic effective masses in the quantum wells and barriers, the forms of the lines of disappearance and appearance of bound states are different from the forms of the isoenergy lines. Therefore there is a finite energy interval (i.e., electron density interval) where bound states exist on only a part of an isoenergy line. The dimensionality of the states can be controlled with an electric field; this should be observable in a number of the experiments discussed.
[S0021-3640(97)01402-3]

PACS numbers: 68.65.+g

For quantum wells the in-layer wave-vector components (k_x, k_y) are conserved. Since the effective-mass components are different in the materials in contact, the effective potentials will depend on k_x and k_y. This can even change the sign of the effective potential, i.e., a potential well can be converted into a barrier and vice versa. This fact was discussed in Refs. 1–3. However, the critical values k_c of the wave vectors for which bound states appear or disappear are too high from the standpoint of both the possibility of observation and the correctness of the description. This letter shows that these problems can be solved in principle for quantum wells and wires with asymmetric barriers.

1. The wave function of the quantum wells can be represented in the form $\psi(x,y,z)=Z(z)\exp(ik\rho)$, where z is the coordinate in the direction of the growth axis, ρ lies in the plane of the layers, and $k=(k_x^2+k_y^2)^{1/2}$. The Schrödinger equation for $Z(z)$ in the case of isotropic masses in each layer of the heterostructure has the form

$$Z''(z)+\frac{2m_n}{\hbar^2}\left(E-\frac{\hbar^2k^2}{2m_n}-U_n\right)Z(z)=0, \tag{1}$$

where m_n and U_n are the effective mass and potential in the nth layer. The functions Z and Z'/m_n are continuous at the boundaries of the layers. For a quantum well of thickness d this results in a dispersion relation for the energy E of the bound states

$$\left(\frac{\kappa_1}{m_1}+\frac{\kappa_2}{m_2}\right)\cos\,\kappa d+\left(\frac{\kappa_1\kappa_2}{m_1m_2}\,\frac{m}{\kappa}-\frac{\kappa}{m}\right)\sin\,\kappa d=0, \tag{2}$$

where

$$\kappa=\left[\frac{2m}{\hbar^2}(E-V_0(k))\right]^{1/2}, \quad \kappa_{1,2}=\left[\frac{2m_{1,2}}{\hbar^2}(V_{1,2}(k)-E)\right]^{1/2},$$

m_1, m_2, and m are the effective masses in the left- and right-hand barriers and in the well; $V_{1,2}(k)=U_{1,2}+\hbar^2k^2/2m_{1,2}$ and $V_0(k)=\hbar^2k^2/2m$ are equal to the potentials of the barriers and the well for finite k and to U_i for $k=0$.

For $U_1\neq U_2$ a bound state appears for well width above a critical value.[4] The asymmetry of the barriers can be characterized by the parameter

$$\beta(k)=[V_2(k)-V_0(k)]/[V_1(k)-V_0(k)].$$

For $m<m_1$ the sign of the derivative $\partial\beta(k)/\partial k$ is the same as that of the parameter α:

$$\alpha=\frac{U_2}{U_1}-\frac{m_2-m}{m_1-m}\,\frac{m_1}{m_2}, \tag{3}$$

i.e., as k increases, the system becomes increasingly asymmetric for $\alpha>0$ (for definiteness, we assume that $U_2>U_1$) and increasingly symmetric for $\alpha<0$. If $m>m_1$, then $\partial\beta(k)/\partial k$ and α have opposite signs.

For type-I heterostructures the relations $m<m_1<m_2$ are typical. In this case, for $k_i=[2U_imm_i/\hbar^2(m_i-m)]^{1/2}$ the barrier vanishes on the left ($i=1$) or right ($i=2$) side and for $k_s=[2(U_2-U_1)m_1m_2/\hbar^2(m_2-m_1)]^{1/2}$ the barrier heights are equal. The relative arrangement of k_1, k_2, and k_s is determined by the sign of α: $k_1<k_s<k_2$ for $\alpha>0$ and $k_s<k_2<k_1$ for $\alpha<0$.

Barrier asymmetry results in vanishing of a bound state for values of k_c much less than k_1 and k_2. To determine k_c, Eq. (2) must be solved for k under the additional condition $E=V_i(k_{ci})$. For $\alpha>0$ there is one critical value k_{c1}, and the equation for k_{c1} is

$$\frac{d}{\lambda}=\frac{1}{2\pi\tilde{\kappa}}\tan^{-1}\left[\frac{m}{m_2}(\beta(k_{c1})-1)\right]^{1/2}+\frac{n}{2\tilde{\kappa}}, \tag{4}$$

where

$$\tilde{\kappa}=\left[1-(k_{c1}/k_0)^2\left(1-\frac{m}{m_1}\right)\right]^{1/2}, \quad k_0=2\pi/\lambda, \quad \lambda=(2\pi^2\hbar^2/2mU_1)^{1/2},$$

$n=0$, 1, ... is the number of the subband. For $\alpha<0$ there is a second value k_{c2} which is obtained from Eq. (4) with $\tilde{\kappa}=[U_2/U_1-(k_{c2}/k_0)^2(1-m/m_2)]^{1/2}$ and the substitutions $m_1\Leftrightarrow m_2$ and β replaced by $1/\beta$.

A state diagram in the variables $d(k)$, which describes the limit between the bound (2D) and unbound (3D) states, is displayed in Fig. 1. Curve *1* corresponds to $\alpha>0$. A bound state exists above and to the left of this curve. For $d<d_{c1}$ there is no bound state for any k. For $d>d_{c1}$ a bound state exists in the interval $0<k<k_{c1}$, and the value of

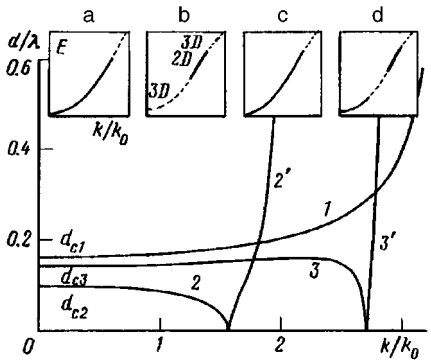

FIG. 1. Diagram of the states of a quantum well. The lines *1*, *2*, and *3* correspond to the condition $E=V_1$; lines *2′* and *3′* to $E=V_2$, $m_1=1.1m$, and $m_2=2.0m$ for $U_2/U_1=6$ (curve *1*); 4 (*2*, *2′*), and 2 (*3*, *3′*). Inset: Dispersion curves $E(k)$: a) for curve *1*; b, c) — *2*, *2′*; d) — *3*, *3′*.

k_{c1} increases from 0 to k_1 as d increases. The function $E(k)$ for $d>d_1$ is displayed in inset a in Fig. 1 (solid lines — 2D states, dashed lines — 3D states).

Curves *2* and *2′* correspond to $E=V_1$ and $E=V_2$ for $\alpha<0$; inset b corresponds to the case $d<d_{c2}$ and inset c corresponds to $d>d_{c2}$. For $\alpha<0$ the function $d(k_c)$ can possess a maximum (curve *3* in Fig. 1). In this case three critical values k_c exist in a narrow range of layer thicknesses $d_{c2}<d<d_{\max}$ (see inset d). The disappearance of the state as $k\rightarrow k_{c1}$ is due to the fact that despite the symmetrization of the system, the well depth decreases more rapidly than the barrier heights equalize.

The condition $m<m_1<m_2$ and $\alpha>0$ holds for the widely investigated heterostructures based on three-component substances of the type $A_xB_{1-x}C$, where barrier asymmetry is achieved as a result of different values of x on the left and right sides. For $GaAs/Al_xGa_{1-x}As$ structures with $x_1=0.1$, $x_2=0.4$, and $d=25$ Å we have $k_c=0.3k_0$, which is approximately an order of magnitude less than the value of k_1. The Fermi wave vector k_F in this case equals k_c with electron density $N=10^{18}$ cm^{-3} in the well. For small well widths the matching of the lattices is not of fundamental importance. This increases the number of possible compounds with $\alpha<0$ for observing the effect described. An example is the heterostructure $Al_xGa_{1-x}As/In_yGa_{1-y}As/GaAs$. For $x=0.4$ and $y=0.03$ the parameter $\alpha=-20$, asymmetry decreases with increasing k, and the critical width d_c at $k=0$ equals 36.6 Å.

Applying an electric field F_z changes the ratio of the potential barriers, leaving the masses in the layers unchanged. This ''decoupling'' of the masses and potentials makes it possible to control the parameter α. A transition from $\alpha>0$ to $\alpha<0$ (and vice versa) is possible in the case when the voltage ΔU is positive (negative) at the higher barrier, i.e., all the situations examined above can be realized in structures with the same composition. Specifically, a function $E(k)$ of the type shown in the inset d in Fig. 1 is obtained in the structure $Al_{0.1}Ga_{0.9}As/GaAs/Al_{0.4}Ga_{0.6}As$ with a well width of 18 Å by applying a voltage of the order of 0.1 V.

We note several possibilities for observing the lines of disappearance (appearance) of bound states in momentum space (k_x, k_y).

1. The character of the electron motion in a magnetic field will change both with the field oriented in the plane of the layers and along the z axis. Depending on the relative arrangement of the disappearance lines and the Fermi line, the oscillations of the kinetic and thermodynamic quantities in a magnetic field will correspond to the two-dimensional (2D) or three-dimensional (3D) cases. The quantum Hall effect should vanish at a 2D–3D transformation. The transformation phenomenon itself can be observed in the same sample by controlling the carrier density and the position of the disappearance lines by means of an electric field.

2. In the case of a 2D–3D transformation induced by an electric field, the character of the phase transformations can change. For example, if ferromagnetic ordering is determined by magnetic ions in quantum wells by means of an indirect exchange interaction via the carriers, then ferromagnetism can vanish at a 2D–3D transformation.

3. In the case when the position of the disappearance (appearance) line changes, a sharp change in the binding energy of excitons or impurity states can be observed, since the binding energy for the 2D case is four times higher than for the 3D case. This sharp change will occur when the momentum of the disappearance (appearance) line equals the corresponding reciprocal of the Bohr radius.

4. It is possible to observe the inverse Franz–Keldysh effect in superlattices constructed from asymmetric quantum wells, i.e., under the action of a field F_z the width of the forbidden miniband increases on account of a 3D–2D transformation. As a result of the formation of bound 2D states, the overlap integral of the wave functions between neighboring quantum wells decreases, and this results in a decrease of the widths of the allowed minibands.

5. The 2D–3D transformation under the action of a lateral electric field can also be observed directly. The 2D–3D defocusing (or 3D–2D focusing) of electronic states which occurs in this case can be observed in transient processes. In time-resolved experiments, the shift in the position of the excitonic line will be determined by the change in the binding energy.

6. A system of two quantum wells, one of which possesses asymmetric barriers, may be attractive for decreasing the threshold current in a quantum cascade laser.[5] If the lower subband corresponds to an asymmetric well, then the line of disappearance of the subband can lie much lower than the minimum of the top band. This will result in the suppression of one-phonon intersubband relaxation and a decrease of the threshold current.

2. The foregoing analysis can be easily extended to the case of anisotropic masses. This case occurs if the extrema of the volume spectra do not lie at the Γ points of the Brillouin zone. For hole states in Ge, Si, and III–V semiconductors, the masses are anisotropic even at the Γ points. Then the equation for determining the energies of the bound states has the form (2), where m, m_1, and m_2 must be interpreted as the z components of the masses and the potentials V_i in the quantities κ and κ_i must be replaced by $V_i = U_i + \hbar^2/2(k_x^2/m_{ix} + k_y^2/m_{iy})$, where m_{ix} and m_{iy} are the effective mass components in the ith layer. To make a classification of the situations which are possible

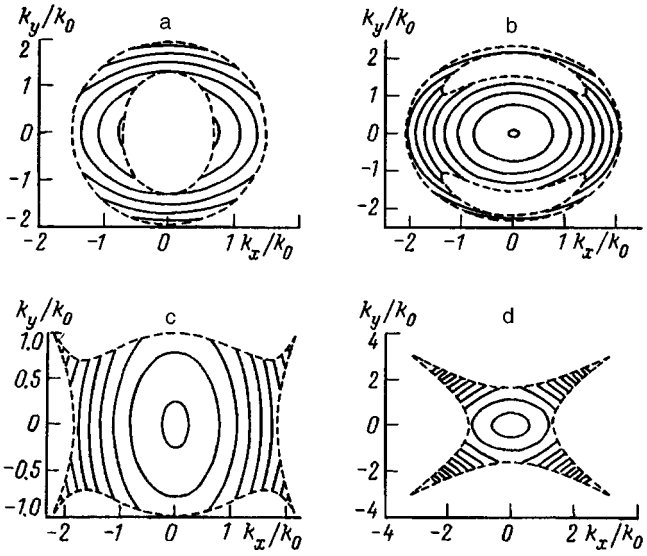

FIG. 2. Isoenergy lines (solid lines) and lines of disappearance (dashed lines) of quantum wells with anisotropic masses for $U_2/U_1=2$, $m_{iz}=m_{ix}$, and a) $m_{1x}=1.2m$, $m_{2x}=3.0m$, $m_{1y}=1.15m$, $m_{2y}=1.7m$, $d=0.08\lambda$; b) $m_{1x}=1.2m$, $m_{2x}=1.7m$, $m_{1y}=1.17m$, $m_{2y}=1.5m$, $d=0.08\lambda$; c) $m_{1x}=1.2m$, $m_{2x}=2.0m$, $m_{1y}=1.25m$, $m_{2y}=0.7m$, $d=0.14\lambda$; d) $m_{1x}=1.5m$, $m_{2x}=0.7m$, $m_{1y}=0.8m$, $m_{2y}=3.0m$, $d=0.30\lambda$. The isoenergy lines are plotted with a step of 0.5 starting with $E/U_1=1.5$ for part a and 1.0 for parts b–d.

here, let us analyze the form of the lines of disappearance of the barriers $V_0=V_1$ and $V_0=V_2$. The equations of these lines have the form

$$k_x^2/a_i+k_y^2/b_i=1,$$

where

$$a_i=2U_i m_x m_{ix}/\hbar^2(m_{ix}-m_x), \quad b_i=2U_i m_y m_{iy}/\hbar^2(m_{iy}-m_y), \quad i=1,2.$$

These are ellipses if a_i and b_i are positive and hyperbolas if either a_i or b_i are negative. The relative arrangement of the points of disappearance of the barriers along each axis can be characterized by the parameters α_x and α_y. The relation between k_y and k_x for lines of appearance (disappearance) of the bound states is obtained from Eq. (2) with the additional condition $E=V_i(k_x, k_y)$. The most important characteristics of the system are lines of equal energy (isoenergy lines), which are obtained from Eq. (2) with $E=$ const.

Examples of the isoenergy lines (solid lines) and lines of disappearance of the bound states (dashed lines) are presented in Fig. 2. Without loss of generality, we shall assume that the masses in the well are isotropic and that $m_{iz}=m_{ix}$. For Figs. 2a,b the lines of disappearance of the barriers are ellipses, and in both cases $a_2>a_1$ and $b_2>b_1$. Figure 2c corresponds to the situation when the line $V_0=V_1$ is an ellipse and $V_0=V_2$ is a hyperbola intersecting an ellipse ($a_2<a_1$ and $b_2<0$). For Fig. 2d the lines $V_0=V_1$ and $V_0=V_2$ are hyperbolas with mutually perpendicular axes ($a_1>0$, $a_2<0$, $b_1<0$, $b_2>0$).

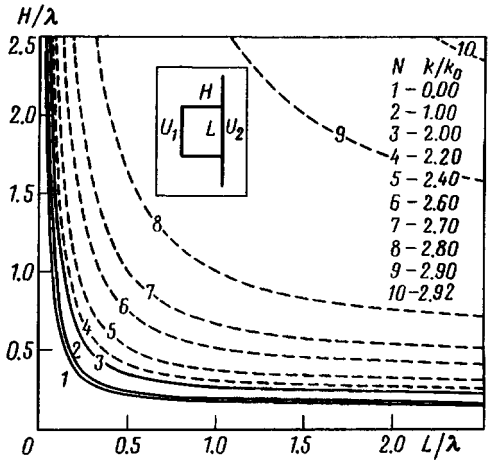

FIG. 3. Boundaries $H(L)$ of the bound states in a quantum wire.

The most characteristic feature is that the forms of the lines of disappearance and appearance are the same as those of the isoenergy lines. Therefore there is an energy interval (and hence an interval of carrier densities) where bound states exist on part of the isoenergy line. In this case the transformation of dimensionality accompanying a change in the controlling parameter (for example, the electric field F_z) extends over some region. The isoenergy lines of 2D states in this region are unclosed, and magnetic breakdown due to tunneling from one section of the isoenergy curve to another can be observed in a magnetic field H_z.

3. To investigate the bound states of asymmetric quantum wires, we shall employ an approximate method consisting of reducing the two-dimensional problem to a sequence of one-dimensional problems.[6] The problem is solved in two stages. First, a one-dimensional Schrödinger equation with potential $V(y,k_z)$ is solved in each section $x=$ const. The resulting energy level $\epsilon(x,\ k_z)$, which depends on the coordinate x and wave vector k_z, serves as an effective potential $V(x,k_z)$ for electron motion along the x axis.

We shall investigate the dispersion law $E(k_z)$ and calculate the existence region of bound states for quantum wires with asymmetric barriers for the example of wires with a rectangular cross section (see inset in Fig. 3) of width L and height H. The effective mass in the wire is m and the potential and mass in the barrier equal U_1 and m_1 for $x<L$ and m_2 and U_2 for $x>L$. For such a structure, the reduction to a one-dimensional problem leads to the effective potential $V(x)\equiv V_1(k_z)=U_1+\hbar^2k_z^2/2m_1$ for $x<0$, $V(x)\equiv V_2(k_z)=U_2+\hbar^2k_z^2/2m_2$ for $x>L$, and the value of $V(x)\equiv V_0(k_z)$ for $0<x<L$ is determined from the solution of the transcendental equation

$$\tan[L(2mV_0/\hbar^2-k_z^2)^{1/2}]=2f/(1-f^2), \tag{5}$$

where

$$f=\frac{m}{m_1}\left[\frac{2m_1(U_1-V_0)+\hbar^2k_z^2}{2mV_0-\hbar^2k_z^2}\right]^{1/2}.$$

The solution of the 1D Schrödinger equation with the potential $V(x)$ gives the desired wave-number dependence of the energy $E(k_z)$ of the localized state.

As in the case of quantum wells, the asymmetry of the structure can be characterized by the parameter α (3). For $\alpha>0$, there is a single condition for the appearance (disappearance) of a bound state $E=V_1(k_z)$, and there are only points of disappearance of the spectrum (in quantum wells these were lines). An example of a calculation of the family of curves $H(L)$ for different k_z for a wire based on GaAs/Al_xGa_{1-x}As with $x=0.4$ for the high barrier and $x=0.1$ for the low barrier is presented in Fig. 3. For fixed k_z, bound states exist above and to the right of the line $H(L)$. For fixed H the critical value k_{zc} increases monotonically with L. For example, for $H=30$ Å one has $k_{zc}=0.2k_0$ for $L=110$ Å, $k_{zc}=0.9k_0$ for $L=140$ Å, and $k_{zc}=1.2k_0$ for $L=200$ Å.

The situation for $\alpha<0$ is more complicated. In this case, together with the lines $H(L)$ corresponding to $E=V_1$, there exist solutions with $E=V_2$. The latter solutions have a form similar to that displayed in Fig. 3. The main feature of the solutions with $E=V_1$ is the existence of points of intersection of the lines $H(L)$ for different values of k_z. For H and L corresponding to a point of intersection there are two values of k_z (k_{z1} and k'_{z1}) for which $E=V_1$. The form of the dispersion law $E(k_z)$ in this case is similar to that shown in the inset d in Fig. 1 (solid lines — 1D, dashed lines — 3D).

In the case of a 1D–2D (or 1D–3D) transformation, for example, induced by a transverse electric field, a transition is possible from a Tomonaga–Luttinger electronic liquid of the type in Ref. 7 (bound state in a wire) to a Fermi liquid.

This work was supported by the Russian Fund for Fundamental Research and the Russian Interdisiplinary Science and Technology Program ''Physics of solid-state nanostructures,'' and INTAS.

[a)]e-mail: kopaev@sci.lpi.ac.ru

[1] B. A. Volkov, B. G. Idliş, and M. Sh. Uşmanov, Usp. Fiz. Nauk **165**, 799 (1995).
[2] Z. S. Gribnikov and O. É. Raĭchev, Zh. Éksp. Teor. Fiz. **96**, 996 (1989) [Sov. Phys. JETP **69**, 564 (1989)].
[3] A. V. Kolesnikov and A. P. Silin, Zh. Éksp. Teor. Fiz. **109**, 2125 (1996) [JETP **82**, 1145 (1996)].
[4] L. D. Landau and E. M. Lifshitz, *Quantum Mechanics*, Pergamon Press, New York [Russian original, Nauka, Moscow, 1974].
[5] J. Faist, F. Capasso, D. L. Sivco *et al.*, Science **264**, 553 (1994).
[6] Yu. A. Aleshchenko, V. V. Kapaev, Yu. V. Kopaev, and N. N. Mel'nik, JETP Lett. **63**, 278 (1996).
[7] S. Tarucha, T. Honda, and T. Saku, Solid State Commun. **94**, 413 (1995).

Translated by M. E. Alferieff

Shallow acceptors in Ge/GeSi strained multilayer heterostructures with quantum wells

V. I. Gavrilenko,[a] I. V. Erofeeva, A. L. Korotkov, Z. F. Krasil'nik, O. A. Kuznetsov, M. D. Moldavskaya, V. V. Nikonorov, and L. V. Paramonov
Institute of Microstructure Physics, Russian Academy of Sciences, 603600 Nizhniĭ Novgorod, Russia

(Submitted 23 December 1996)
Pis'ma Zh. Éksp. Teor. Fiz. **65**, No. 2, 194–198 (25 January 1997)

The impurity photoconductivity spectra of $Ge/Ge_{1-x}Si_x$ strained heterostructures with quantum wells are investigated. It is established that the built-in deformation in quantum-size Ge layers substantially changes the spectrum of shallow acceptors, shifting it into the long-wavelength region of the far-IR range. In strong magnetic fields the photoconductivity lines are observed to split and shift as a function of the field. This makes it possible to carry out a classification of the transitions. © *1997 American Institute of Physics.*
[S0021-3640(97)01502-8]

PACS numbers: 78.66.Db, 79.60.Jv

Size quantization in semiconductor heterostructures (HSs) substantially alters the spectra of shallow impurities in quantum wells as compared with bulk semiconductors. At present, shallow donor impurities in quantum wells in the heterostructures $GaAs/Al_xGa_{1-x}As$ have been studied in greatest detail.[1,2] At the same time, impurities in strained HSs, such as $Ge/Ge_{1-x}Si_x$, have practically escaped study. Here it is of greatest interest to investigate shallow acceptors, since the deformation arising as a result of the mismatch of the lattice parameters of Ge and $Ge_{1-x}Si_x$ results in splitting of the valence band, which is degenerate at the point $\mathbf{k}=0$, and a radical restructing of the hole dispersion law. In the present work we have investigated experimentally the shallow acceptors in $Ge/Ge_{1-x}Si_x$ strained multilayer HSs with quantum wells, in which the spectra of the impurity states are determined simultaneously by both the elastic deformation of the layers and size-quantization effects.

The $Ge/Ge_{1-x}Si_x$ heterostructures ($x\approx 0.1$, d_{Ge}, $d_{GeSi}\approx 200$ Å, 80–160 layers) were grown by the gas hydride method on *n*-type Ge(111) substrates ($\rho_{300K}=40-45$ $\Omega\cdot$ cm). For these values of x and layer thicknesses, quantum wells for both holes and electrons exist in the germanium layers.[3] The first investigations of the spectra of shallow impurities were performed in the undoped HS $Ge/Ge_{0.88}Si_{0.12}$ (No. 306),[4] in which impact ionization of the residual shallow acceptors was observed when a weak static electric field (of the order of 10 V/cm) was applied in the plane of the layers of the HS at $T=4.2$ K.[5,6] In this case, an absorption line of two-dimensional holes appeared in the cyclotron resonance (CR) spectrum; the impurity density was estimated to be $N\approx 3\cdot 10^{14}$ cm^{-3}, based on the intensity of absorption at the CR. Next, we investigated both undoped and specially doped $Ge/Ge_{1-x}Si_x$ HSs. In the latter case, the center of the

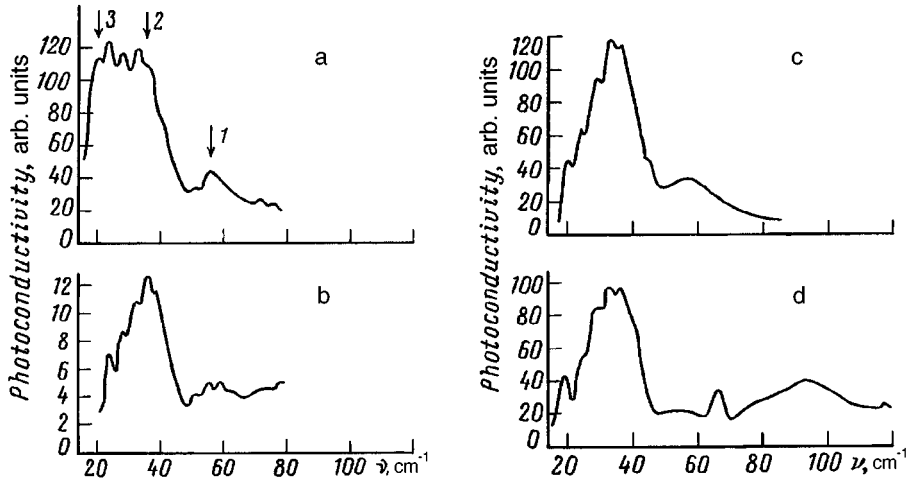

FIG. 1. Photoconductivity spectra of $Ge/Ge_{1-x}Si_x$ heterostructures ($d_{Ge}, d_{GeSi} \approx 200$ Å) at $T=4.2$ K: a) No. 306, undoped, $x=0.12$, 162 layers, $P_{equiv}=4$ kbar; b) No. 379, Ge:B, $x=0.15$, 81 layers, $P_{equiv}=1.7$ kbar; c) No. 406, undoped, $x=0.11$, 162 layers, $P_{equiv}=3.7$ kbar; d) No. 406 under illumination by a GaAs light-emitting diode.

quantum well (approximately 1/7 of its thickness) was doped with boron up to the minimum possible carrier density ($N \approx 10^{16}$ cm^{-3}). The most sensitive method of photothermal ionization spectroscopy was used to investigate the spectra of the shallow impurities. A ''BOMEM DA3.36'' Fourier spectrometer was used to record the photoconductivity spectra of heterostructures in the far-IR range at $T=4.2$ K.

The photoconductivity spectra of two undoped samples, Nos. 306 and 406, and sample No. 379 with doped wells are displayed in Figs. 1a–c. One can see that a photoconductivity line near 55 cm^{-1} (1) and a wide band in the interval 20–40 cm^{-1} (2) are characteristic for all spectra, while in bulk germanium the photoconductivity spectrum of shallow acceptors has a maximum at shorter wavelengths near 100 cm^{-1} (see, for example, Ref. 7). The fact that the spectral features *1* and *2* are common to all three spectra shows that they are related with the shallow acceptors A^0 located at the center of the well. Another feature *3*, which lies next to the feature *2* on the long-wavelength side, can be distinguished in the spectrum of the undoped sample No. 306 (Fig. 1a).

A model of an impurity center for the case of an anisotropic parabolic band, considered previously in investigations of shallow donors in germanium and silicon, was used to interpret the observed photoconductivity spectra. The Ge layers in ''thick'' HSs (in our case the characteristic thicknesses of the structures were equal to 2.5–5 μm) undergo biaxial compression in the plane of the heterostructure. Such a deformation can be considered as being the result of hydrostatic compression plus uniaxial tension along the axis of the HS. It is well known that uniaxial deformation along the [111] axis, lowering the symmetry of the crystal lattice, results in splitting of the edges of the valence bands of the light and heavy holes ($\Delta_\nu \approx 4$ meV/kbar) and it also lifts the intervalley degeneracy in the conduction band.[8] The equivalent uniaxial tension P_{equiv}, de-

termined by the x-ray diffraction method, equal several kilobars for our samples. Therefore the splitting Δ_ν in our experimental samples is of the order of or greater than the binding energy of shallow acceptors in bulk undeformed germanium ($E_b \approx 10$ meV). Under uniaxial tension along the [111] direction the effective hole masses parallel ($\|$) and perpendicular ($\perp$) to the deformation axis near the bottom of each subband become substantially different:[8]

$$m_\|^{(1)} \approx 0.49 m_0, \quad m_\perp^{(1)} \approx 0.053 m_0; \tag{1}$$

$$m_\|^{(2)} \approx 0.048 m_0, \quad m_\perp^{(2)} \approx 0.13 m_0. \tag{2}$$

Thus, the longitudinal hole mass in the bottom subband (*1*) is an order of magnitude larger than in the top subband (*2*). For this reason, the quantization of the hole spectrum in thin Ge layers results in an even greater repulsion of the subbands *1* and *2*. This makes it possible to neglect, to a first approximation, the effect of the top subband *2* and the nonparabolicity of the hole dispersion law in the bottom subband *1* on the spectrum of shallow impurities. The calculations of the dependences of the energies of the ground and excited states of the impurity center in a bulk semiconductor on the effective-mass anisotropy parameter $\gamma^{1/3}$ ($\gamma = m_\perp / m_\|$), performed in Ref. 9, can be used to analyze the impurity photoconductivity spectra of the Ge/$Ge_{1-x}Si_x$ HSs. Size quantization should not produce any strong changes in the spectrum, since on account of the large value of the mass $m_\|^{(1)}$ the characteristic extent of the wave function along the axis of the structure $a_\| = (4/\pi)^{2/3}\gamma^{1/3}(\hbar^2\epsilon/e^2 m_\perp^{(1)})/3 \approx 30$ Å (Ref. 10) is much less than the well width. It is natural to conjecture that, just as for shallow donors in bulk semiconductors, the transition $1s \rightarrow 2p_\pm$ should be the strongest transition in the photoconductivity spectrum of Ge/$Ge_{1-x}Si_x$ heterostructures. For a shallow acceptor A^0 in uniaxially stretched Ge $\gamma = 0.108$ (see Eq. (1)) and the energy of the transition $1s \rightarrow 2p_\pm$, calculated according to Ref. 9, equals 36.4 cm^{-1}, which agrees well with the spectral position of the strongest feature *2* in Fig. 1. The large width and great extent of this spectral band in the long-wavelength region in samples Nos. 379 and 406 (Figs. 1b and c) can be explained by the dependence of the spectrum on the arrangement of the impurity atom in the well: The binding energy is maximum at the center of the well and decreases as the heterojunction is approached.[1,2] The spectral feature *1* is evidently associated with transitions from the ground state into upper-lying excited states and into the continuum. The longest-wavelength spectral feature *3* (Fig. 1a), observed only in sample No. 306, could be associated with photoexcitation of A^+ centers, which form when an additional hole, whose ''parent'' ion is located in a barrier, is trapped by a neutral acceptor in the quantum well.[11] However, to confirm this hypothesis additional experiments must be performed with samples in which both the wells and the barriers are doped.

Figure 1d shows the spectrum of sample No. 406, measured with continuous illumination by radiation from a GaAs light-emitting diode ($\lambda \approx 0.9$ μm). One can see that a new structure, consisting of a narrow line at 67 cm^{-1} and a wide band near 70–110 cm^{-1}, appears in the spectrum under illumination. The new structure is apparently associated with transitions between states of compensating donors which are neutralized by illumination from the fundamental absorption region. For the technology used, the most likely shallow donor is antimony. It is well known that for antimony the chemical shift is small (about 3 cm^{-1}; Ref. 12) and the deviation from the model of Ref. 9, caused by the

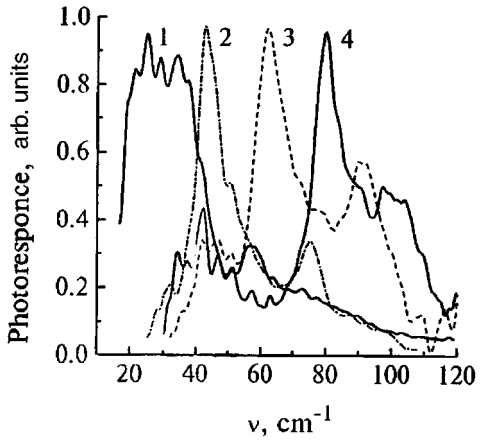

FIG. 2. Photoconductivity spectra of heterostructure No. 306 in magnetic fields $\mathbf{H}\|[111]$ at $T=4.2$ K. H, kOe: *1* — 0, *2* — 20, *3* — 40, *4* — 50.

centrocellular potential, is insignificantly small. This statement is valid for both the bulk material and for strained Ge layers in $Ge/Ge_{1-x}Si_x$ heterostructures ($P_{\text{equiv}}\|[111]$), where only three electronic valleys remain at the bottom of the conduction band (under uniaxial extension along the [111] axis the fourth valley shifts upwards in energy by 12 meV/kbar). Size-quantization effects should be small for the same reason as for acceptors. The observed spectral line $\nu\approx 67$ cm^{-1} (Fig. 1d) can be attributed to the transition $1s\rightarrow 2p_{\pm}$ of shallow donors in Ge ($\nu_{1s\rightarrow 2p_{\pm}}\approx 65$ cm^{-1}; Ref. 9) and the transition $1s\rightarrow 3p_{\pm}$ ($\nu_{1s\rightarrow 2p_{\pm}}\approx 71$ cm^{-1}) — transitions into upper lying states — can be attributed to the band 75–110 cm^{-1}.

To obtain additional information about the nature of the spectral lines, investigations of the photoconductivity of sample No. 306 in strong magnetic fields $\mathbf{H}\|[111]$ were performed. As one can see from Figs. 2 and 3, the spectral feature *2* splits in a magnetic field into two peaks. The most intense peak 2^+ shifts linearly with increasing magnetic field into the short-wavelength region of the spectrum. The position of the second peak 2^- is virtually independent of the field. The other spectral line *1* (1^+) also shifts linearly with the magnetic field (the corresponding peak 1^- was not observed, apparently because of superposition with the stronger line 2^+). As one can see From Fig. 3, the magnetic-field dependences of the positions of the maxima 1^+ and 2^+ are parallel and in strong fields they have the same slope $e/(2\pi m_c c^2)$, where $m_c=0.07m_0$, which equals the two-dimensional hole mass measured in CR experiments.[5,6] This magnetic field dependence is characteristic for the transitions $1S\rightarrow nP^+$, $n=2, 3,\ldots$(and the behavior of the peak 2^- is characteristic for the transitions $1S\rightarrow 2P^-$),[13] which confirms the above classification of the transitions.

In summary, in the present work we have investigated the spectra of shallow impurities in strained quantum-size heterostructures $Ge/Ge_{1-x}Si_x$. The experiments showed that elastic deformation of the quantum-size Ge layers in a HS radically changes the spectrum of shallow acceptors as compared with a bulk single crystal, shifting the spec-

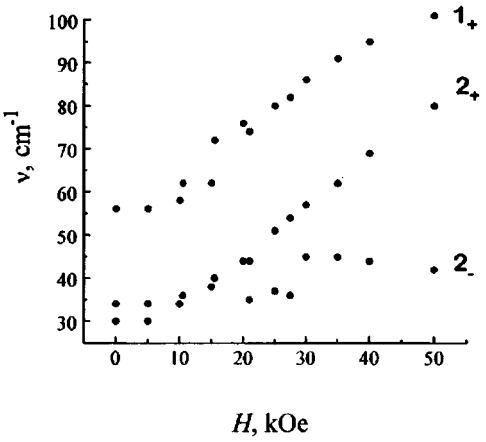

FIG. 3. Positions of the lines *1* and *2* (Fig. 1) in the spectrum of sample No. 306 versus the magnetic field.

trum into the long-wavelength region of the far-IR range. The possibility of controlling the magnitude of the deformation and the thickness of the quantum wells and also the possibility of selective doping of wells and barriers in the HSs in order to produce A^0 and A^+ centers open up new prospects for producing solid-state detectors for the far-IR range. The power–voltage sensitivity of one of the samples (No. 306), measured using a standard source of radiation (an absolutely black body), was found to be quite high: $S \approx 10^4$ V/W ($NEP \approx 10^{-11}$ W/Hz$^{1/2}$). This makes it possible to use this structure as a photoelectric detector for the far-IR range.

This work was supported by the Russian Fund for Fundamental Research (Grant 94-02-05445), the Russian Interdisciplinary Science and Technology Progam ''Physics of solid-state nanostructures'' (Project 2-027/4), the Russian Interdisciplinary Science and Technology Program ''Physics of microwaves'' (Project 4.5), and the State Science and Technology Program ''Physics of quantum and wave processes'' (subprogram ''Fundamental spectroscopy,'' Project 7.8). We thank E. A. Uskova for assisting in the preparation of the contacts to the samples and Yu. N. Drozdov and L. D. Moldavskaya for performing the x-ray diffraction investigation of the heterostructures.

[a)]e-mail: gavr@ipm.sci-nnov.ru

[1] A. A. Reeder, J.-M. Mercy, and B. D. McCombe, IEEE J. Quantum Electron. **24**, N8 (1988).
[2] R. L. Greene and P. Lane, Phys. Rev. B **34**, 8639 (1986).
[3] V. Ya. Aleshkin and N. A. Bekin, Fiz. Tekh. Poluprovodn. **31**, No. 2 (1997), in press.
[4] V. I. Gavrilenko, I. V. Erofeeva, Z. F. Krasil'nik *et al.*, in *Abstracts of Reports at the 2nd Russian Conference on Semiconductor Physics* [in Russian], Zelengorsk, 1996, Vol. 2, p. 43.
[5] V. Ya. Aleshkin, N. A. Bekin, I. V. Erofeeva *et al.*, Lith. J. Phys. **35**, 368 (1995).
[6] V. Ya. Aleshkin, N. A. Bekin, I. V. Erofeeva *et al.*, in *Abstracts of Invited Lectures and Contributed Papers of the International Symposium on ''Nanostructures: Physics and Technology-95,''* 1995, p. 271.
[7] R. L. Jones and P. Fisher, Phys. Rev. B **2**, 2016 (1970).
[8] G. L. Bir and G. E. Pikus, *Symmetry and Deformation Effects in Semiconductors* [in Russian], Nauka, Moscow, 1972.

[9] R. A. Foulkner, Phys. Rev. **184**, 713 (1969).
[10] W. Kohn and J. M. Luttinger, Phys. Rev. **98**, 915 (1955).
[11] S. Holmes, J.-P. Cheng, B. D. McCombe *et al.*, Phys. Rev. Lett. **69**, 2571 (1992).
[12] Reuszer and P. Fisher, Phys. Rev. **135**, A1125 (1964).
[13] W. S. Boyle and R. E. Howard, J. Phys. Chem. Solids **19**, 181 (1961).

Translated by M. E. Alferieff

Squeezed states of long-lived terahertz vibrations in quantum dots

V. A. Kovarskiĭ
ul. Akademii 6/2-37, Kishinev 2028, Moldova

(Submitted 10 December 1996)
Pis'ma Zh. Éksp. Teor. Fiz. **65**, No. 2, 199–200 (25 January 1997)

Quantum dots based on materials with long-lived terahertz vibrations are studied. It is shown that squeezed states of such vibrations can result in microwave-frequency modulation of the optical radiation absorbed at electronic transitions in quantum dots. © *1997 American Institute of Physics.* [S0021-3640(97)01602-2]

PACS numbers: 73.20.Dx

Long-lived high-frequency (terahertz) vibrational modes in some amorphous and crystalline materials have been observed in recent years.[1–4] At the same time, the so-called frequency effect — a change in the vibrational frequencies accompanying a quantum transition of an electron from one localized state into another — is well known for localized electronic states. This frequency effect can result in the formation of a squeezed vibrational state when the electronic–vibrational system is excited by an ultrashort laser pulse (for a more detailed discussion, see Ref. 5 and the references cited therein). For long-lived vibrations with $\tau \sim 10^{-9}$ s a vibrational packet corresponding to the squeezed state can undergo $10^3 - 10^4$ vibrations and can be detected by means of a second (read-out) pulse, as has been done in an experiment in molecular systems (see Ref. 6 for a more detailed discussion).

In a solid, the frequency effect can arise when electrons are localized in so-called quantum dots. An intensification of the electron–phonon interaction as a result of electron localization in quantum dots was noted in Ref. 7.

In what follows, a quantum dot in which long-lived vibrations with frequency ω and lifetime $\tau \sim 10^{-9}$ s exist will be studied. The effect of the quantum dot is manifested mainly in that the luminescence band is shifted in the blue direction, as compared with the bulk material, by an amount ΔE determined by the size-quantization effect (for example, in porous silicon $\Delta E \simeq 0.5$ eV).[8]

When the quantum dot is excited by a laser pulse with $\tau_0 \simeq 1$ fs, local levels (arising from the conduction band) are populated. The vibrational packet has the form

$$|\psi^{sq}(x,t)|^2 = \frac{1}{\sqrt{\pi}\sigma(t)} \exp\left\{ -\frac{x^2}{\sigma^2(t)} \right\}, \tag{1}$$

$$\sigma^2(t) = \sigma_0^2 \left(\eta^2 \cos \omega_2 t + \frac{1}{\eta^2} \sin \omega_2 t \right),$$

$$\eta = \frac{\omega_1}{\omega_2}; \quad \sigma_0^2 = \hbar / M \omega_2; \quad \omega_1 > \omega_2,$$

where M is the mass of the oscillator x, η is the compression factor, and $\omega_{1,2}$ are the vibrational frequencies of the nuclei when an electron is localized in discrete levels of the valence and conduction bands, respectively.

Formula (1) was written for the simple case of a ''squeezed vacuum,'' when the frequency effect plays the main role in the preparation of the squeezed state and the Stokes shift can be neglected. The frequency ω_2 differs from the frequency ω_1 by the amount $\Delta\omega$ determined by the matrix elements of the electronic–vibrational interaction, and it can be calculated theoretically. It is better to determine this quantity experimentally, for example, by measuring the Raman spectra of α-Si for sufficiently intense laser illuminations. In my opinion, the additional lines observed in the Raman spectra in Refs. 1 and 2 could be due to the frequency effect, since the laser source in Refs. 1 and 2 was more powerful than the source in Ref. 9. In the method employing a readout pulse at a transition from a lower discrete state 2 of the conduction band into an excited state 3 of the conduction band, a photon with frequency Ω_{23} is absorbed. If the state 2 is unoccupied, then the photon $\hbar\Omega_{23}$ is not absorbed and passes freely through the material.

Let $\hbar\Omega_{23}$ be less than the energy gap Δ_{23} between the states 2 and 3. Then, when state 2 is populated, the absorption of light involves an additional absorption of phonons. The rate $W_{23}(\Omega)$ of this transition per unit time is described by the formula

$$W_{23}(\Omega)\sim\exp\left\{-\frac{(\hbar\Omega-\Delta_{23})^2}{2a(\hbar\omega_2)^2\overline{n}}\right\}, \tag{2}$$

where a is the dimensionless Stokes constant and $\overline{n}$ is the average occupation number of the squeezed vibration with frequency ω_2.

It is easy to show that $\overline{n}$ is determined by the variance of the vibrational coordinate of the squeezed state, i.e., $\overline{n}\sim\sigma^2(t)$, where the time t is measured from the time at which the squeezed state is prepared and corresponds to the time at which the readout pulse is switched on. In the method in which the radiation Ω_{23} is always present, this absorption will be modulated with frequency ω_2.

I thank E. Yu. Kanarovskiĭ, my colleague at the Institute of Applied Physics at the Moldavian Academy of Sciences, for helpful remarks.

[1] A. T. Scholten, A. V. Akimov, and T. I. Dijkhuis, Phys. Rev. B **47**, 13910 (1993).
[2] A. T. Scholten, A. V. Akimov, P. A. W. E. Verleg *et al.*, J. Non-Cryst. Solids **164**–**166**, 923 (1993).
[3] R. Orbach, J. Non-Cryst. Solids **164**–**166**, 917 (1993).
[4] A. V. Akimov, A. A. Kaplyanskiĭ, and E. S. Moskalenko, Fiz. Tverd. Tela (Leningrad) **29**, 509 (1987) [Sov. Phys. Solid State **29**, 288 (1987)].
[5] V. A. Kovarskiĭ, Zh. Éksp. Teor. Fiz. **110**, 1216 (1996) [JETP **83**, 670 (1996)].
[6] M. Gruebele and A. H. Zewail, Phys. Today, May 1990, p. 24.
[7] V. A. Kovarskiĭ and V. N. Chevotar', Fiz. Tekh. Poluprovodn. **26**, 1828 (1992) [Sov. Phys. Semicond. **26**, 1052 (1992)].
[8] N. V. Gushchina, V. S. Dneprovskiĭ, E. Yu. Davydenko *et al.*, Zh. Éksp. Teor. Fiz. **106**, 1830 (1994) [JETP **79**, 994 (1994)].
[9] D. Bermejo and M. Cardona, J. Non-Cryst. Solids **32**, 405 (1979).

Translated by M. E. Alferieff

Comment on vortex mass and quantum tunneling of vortices

G. E. Volovik

Low Temperature Laboratory, Helsinki University of Technology 02150 Espoo, Finland; L. D. Landau Institute for Theoretical Physics, 117940 Moscow, Russia

(Submitted 30 December 1996)
Pis'ma Zh. Éksp. Teor. Fiz. **65**, No. 2, 201–206 (25 January 1997)

Vortex mass in Fermi superfluids and superconductors and its influence on quantum tunneling of vortices are discussed. The vortex mass is essentially enhanced due to the fermion zero modes in the core of the vortex: the bound states of the Bogoliubov quasiparticles localized in the core. These bound states form the normal component, which is nonzero even in the low-temperature limit. In the collisionless regime $\omega_0\tau \gg 1$ the normal component trapped by the vortex is unbound from the normal component in a bulk superfluid/superconductor and adds to the inertial mass of the moving vortex. In a d-wave superconductor the vortex mass has an additional factor of $(B_{c2}/B)^{1/2}$ due to the gap nodes. © *1997 American Institute of Physics.*
[S0021-3640(97)01702-7]

PACS numbers: 74.60.Ge

The vortex mass is thought to be an important issue for the problem of the quantum tunneling of vortices. The latter problem is popular now, and many experiments are discussed in terms of the macroscopic quantum tunneling of vortices in superfluids or superconductors. Firm experimental proof of the quantum nucleation of vortices is still lacking. On the other hand, the characteristic plateau in the temperature dependence of the critical velocity, which is always ascribed to quantum nucleation, has been also observed in superfluid ^{3}He-B (Ref. 1). However, the time required for quantum nucleation of a vortex in ^{3}He-B is 10^{10^6}, which is extremely large in any units. The vortices in ^{3}He-B are created in the course of development of the classical instability of the superflow at the pair-breaking velocity. The cause of the plateau is that the characteristic physical quantities, such as the gap amplitude Δ, which determine the threshold of instability become temperature independent at low T. The intrinsic instability thus provides an alternative explanation of the plateau observed in many different systems, including superfluid ^{4}He.

In the vortex tunneling problem the inertial mass becomes important only if its effect is comparable to the effect of the Magnus force. That is why the magnitude of the inertial mass is of prime importance. It appears that in Fermi superfluids and superconductors the mass of the vortex is substantially enhanced as compared to the vortex mass in superfluid ^{4}He, where it is determined by the compressibility. In Fermi systems the fermions bound to the vortex core give the dominant contribution, as was first found by Kopnin.[2] We discuss this effect in detail and relate it to the normal component trapped by

the vortex. This effect is even more enhanced in d-wave superconductors, where the vortex traps a substantial part of the bulk excitations due to the gap nodes.

VOLUME LAW AND AREA LAW FOR THE QUANTUM TUNNELING

In the earlier estimations of the vortex tunneling rate the mass of a vortex line was neglected.[3,4] When the mass is neglected the tunneling exponent $\exp -S_{\rm eff}$ is determined by the volume V within the surface swept by the classical trajectory of the vortex in the process of the quantum tunneling:

$$S_{\rm eff}/\hbar = 2\pi \mathcal{N}, \quad \mathcal{N} = nV. \tag{1.1}$$

Here n is the particle density; $\mathcal{N}$ is the number of particles in the volume V. The volume law for the vortex action follows from the general laws of vortex dynamics governed by the Magnus force.[5]

In Ref. 3 the tunneling trajectory between the ground state of the superfluid and the state with a vortex was generated by an irregularity (pinning center) on the container wall in the presence of the superflow with the asymptotic superfluid velocity v_s. For small v_s the tunneling exponent does not depend on the pinning center and corresponds to a volume

$$V = \frac{4\pi}{3} R_0^3. \tag{1.2}$$

Here R_0 is the radius of the nucleated vortex ring:

$$R_0 = (\kappa/2\pi v_s) \ln \frac{R_0}{R_{\rm core}} \tag{1.3}$$

and $R_{\rm core}$ is the core size, which is of the order of the coherence length ξ.

The volume law for the tunneling exponent $S_{\rm eff}$ was confirmed in Ref. 4, where $S_{\rm eff}$ was found as the overlap integral of the many-body wave function. This $S_{\rm eff}$ was then minimized with respect to the velocity field in the vortex. The extremal trajectory corresponds to the formation of an intermediate vortex state with a deformed velocity field around the vortex loop. The resulting volume V is logarithmically reduced compared with Eq. (1.2) for the direct formation of the equilibrium vortex:

$$S_{\rm eff}/\hbar = 2\pi n V, \quad V = \frac{27}{\pi \ln \dfrac{R_0}{R_{\rm core}}} R_0^3. \tag{1.4}$$

In this approach the volume law reflects a general property of macroscopic quantum tunneling: the tunneling exponent is proportional to the number $\mathcal{N}$ of particles which effectively participate in the tunneling. This has also been found in other systems.[6,7]

When the problem of vortex tunneling was revived due to the experiments on vortex creep in superconductors, the effect of the vortex mass was discussed.[8] If the mass term is more important for quantum tunneling than the Magnus force, then the volume law of Eq. (1.1) should give way to an area law. A quadratic dependence of $S_{\rm eff}$ on R_0 (area law) was also obtained using field theory in Refs. 9 and 10, where the vortex nucleation was

considered as a process analogous to the Schwinger production of electron–positron pairs in an electric field. The result for the semi-classical tunneling exponent is

$$S_{\rm eff}=\int_0^{R_0} dR\sqrt{2M(R)E_{\rm vortex}(R)}, \tag{1.5}$$

where $E_{\rm vortex}(R)\sim R\ln R/R_{\rm core}$ is the energy of a vortex ring of radius R and $M(R)$ is the mass of the vortex loop. Since $M(R)$ is also $\propto R$, the tunneling rate is proportional to the area R_0^2 of the nucleated vortex ring.

This area law for the action is typical for the dynamics of string loops in systems without a Magnus force, such as cosmic strings (see Ref. 11), vortex rings in charge-density-wave systems,[12] in antiferromagnets, etc. The breaking of the time inversion symmetry introduces the Magnus force even in these systems (see Ref. 13 on vortices in planar magnets and Ref. 14 on spinning global strings), and the volume law can be restored.

HYDRODYNAMIC MASS OF A VORTEX

In the hydrodynamic theory the mass of a vortex is nonzero due to compressibility of the liquid, which leads to the ''relativistic'' expression[9,15,10,16]

$$M_{\rm hydro}=\frac{E_{\rm vortex}}{s^2}, \tag{2.1}$$

where s is the sound velocity. For Fermi superfluids s is of the order of the Fermi velocity $v_F\sim p_F/m$ (m is the mass of the electron or of the ^{3}He atom), and the estimate for the hydrodynamic mass of a vortex loop of length L is

$$M_{\rm hydro}\sim Lmk_F\ln\frac{L}{\xi}. \tag{2.2}$$

However in this analysis the fermions in the vortex core[17] are neglected. They produce an effective mass proportional to the core area $R_{\rm core}^2\sim\xi^3$ (Refs. 2, 18, 19, 20):

$$M_{\rm bound\ states}\sim Lmk_F(k_F\xi)^2. \tag{2.3}$$

Even though it does not contain a logarithmic divergence, this gives the main contribution, since the core radius $\sim\xi$ in superfluid ^{3}He-B and superconductors is large compared with the interatomic spacing: $k_F\xi\gg 1$. The mass of the vortex is substantially enhanced, and so the arguments that the effect of the vortex mass on the vortex tunneling is negligible[3,25] become shaky. That is why it is worthwhile to consider the effect of core fermions more thoroughly.

BOUND-STATES CONTRIBUTION TO THE VORTEX MASS: NORMAL COMPONENT IN THE VORTEX CORE IN THE COLLISIONLESS REGIME

The core contribution to the vortex mass was obtained by Kopnin[2] in a rigorous microscopic theory for the vortex dynamics developed by Kopnin and Kravtsov.[26] Here we associate it with the normal component trapped by the core texture. At low T the core contribution to the vortex dynamics is completely determined by the low-energy excitations in the vortex core, the energy spectrum of which is $E=-Q\omega_0(k_z)$ in the vortex

frame.[17] Here Q is the angular momentum of the fermions and $\omega_0(k_z)$ is the interlevel spacing, which depends on the linear momentum $k_z = k_F \cos\theta$ along the vortex axis ($\omega_0 \sim \Delta^2/E_F \ll \Delta$). If the temperature is large enough, $\omega_0 \ll T \ll T_c$, this branch is characterized by a density of states $N(0) = 1/\omega_0(k_z)$.

If the vortex moves with velocity $\mathbf{v}_L$ with respect to the superfluid component, the fermionic spectrum in the vortex frame is Doppler shifted: $E = -Q\omega_0(k_z) - \mathbf{k}\cdot\mathbf{v}_L$. In the collisionless regime, $\omega_0\tau \gg 1$, the exchange between the fermions in the vortex core and in the heat bath vanishes, and the linear momentum of the bound-state fermions adds to the momentum of the moving vortex. The summation of fermionic momenta in the moving vortex leads to an extra linear momentum of the vortex $\propto \mathbf{v}_L$ (see also Eq. (5.7) of Ref. 20):

$$\mathbf{P} = \sum \mathbf{k}\theta(-E) = M_{\text{bound states}}\mathbf{v}_L, \tag{3.1}$$

$$M_{\text{bound states}} = L\int_{-k_F}^{k_F} \frac{dk_z}{4\pi}\frac{k_\perp^2}{\omega_0(k_z)}. \tag{3.2}$$

This is an extra vortex mass which is larger by a factor $(k_F\xi)^2$ than the hydrodynamic mass of the vortex.

Equation (3.2) represents the dynamical mass of the vortex in the low-temperature limit and only in the clean (or collisionless) regime, when the exchange between the core fermions and the heat bath is suppressed. Actually it was assumed that $T_c \gg T \gg \omega_0 \gg 1/\tau$. In this regime there is no spectral flow between the bound fermions and the heat bath, and, as a result, during the vortex motion the momentum of the core fermions is not transferred to the heat bath and adds to the momentum of the vortex, producing an extra inertia. In other words, this is the contribution of the normal component associated with the vortex core, which in the collisionless regime is trapped by the vortex and is transferred together with the vortex.

For vortices with a core size $R_{\text{core}} \gg \xi$, this extra vortex mass can be represented as the integral over the local density of the normal component:

$$M_{\text{bound states}} = \int d^3r\ \rho_n(\mathbf{r}, T=0). \tag{3.3}$$

This nonzero normal component at $T=0$ is produced by the inhomogeneous order parameter, the texture. This can be seen for the extremely simple example of a continuous vortex in the ^{3}He-A phase, where the corresponding texture is the field of the unit vector $\hat{\mathbf{l}}$ along the orbital angular momentum of the Cooper pairs. Let us choose the texture in the form

$$\hat{\mathbf{l}}(\mathbf{r}) = \hat{\mathbf{z}}\cos\eta(r) + \hat{\mathbf{r}}\sin\eta(r), \tag{3.4}$$

with $\hat{\mathbf{l}}(0) = -\hat{\mathbf{z}}$ and $\hat{\mathbf{l}}(\infty) = \hat{\mathbf{z}}$. This texture represents a doubly quantized continuous vortex in ^{3}He-A (see Eq. (5.21) in the review[21]); the latest experiments on such vortices are discussed in Ref. 22.

The $\hat{\mathbf{l}}$-texture leads to the normal component tensor even at $T=0$ (Ref. 23; see Eq. (5.24) of Ref. 24):

$$(\rho_n)_{ij}(\mathbf{r}) = \frac{k_F^4}{2\pi^2\Delta_A} \left|(\hat{\mathbf{l}}\cdot\vec{\nabla})\hat{\mathbf{l}}\right| \hat{l}_i\hat{l}_j , \tag{3.5}$$

where Δ_A is the gap amplitude in ^{3}He-A. For the texture in Eq. (3.4) one has $|(\hat{\mathbf{l}}\cdot\vec{\nabla})\hat{\mathbf{l}}| = \sin\eta\,\partial_r\eta$, so the normal component contribution to the vortex mass should be

$$M_{\text{bound states}}\delta_{\perp ij} = \int d^3r(\rho_n)_{ij} = L\,\frac{k_F^4}{2\pi\Delta_A}\int_0^\infty dr\; r\,\sin^3\eta\;\partial_r\eta. \tag{3.6}$$

Equation (3.6) for the vortex mass in terms of the local normal component coincides with the general equation (3.2) for the vortex mass in terms of $\omega_0(k_z)$. The interlevel spacing for this continuous vortex was found by Kopnin:[18]

$$\omega_0(k_z) = \frac{\Delta_A}{k_F r(k_z)}, \quad \cos\,\eta(r(k_z)) = \frac{k_z}{k_F}. \tag{3.7}$$

Here $r(k_z)$ is the radius at which the energy of the fermion, $E(r,\vec{k}) = \sqrt{v_F^2(k-k_F)^2 + \Delta_A^2(\hat{\mathbf{l}}(r)\times\hat{\mathbf{k}})^2}$, is zero at a given k_z. Equation (3.2) gives[18]

$$M_{\text{bound states}} = L\int_{-k_F}^{k_F}\frac{dk_z}{4\pi}\,\frac{k_\perp^2}{\omega_0(k_z)} = \frac{k_F}{4\pi\Delta_A}\int_{-k_F}^{k_F} dk_z(k_F^2-k_z^2)r(k_z).$$

After inverting the function $r(k_z)$ in Eq. (3.7) into $k_z(r) = k_F\cos\eta(r)$, one obtains Eq. (3.6).

VORTEX MASS FROM THE KINETIC EQUATION

The above results for the vortex mass can be proved using the kinetic equation for the fermions bound to the core.[2,18,19] The inertial term in the force balance for the vortex is obtained by replacing $1/\tau$ by $1/\tau - i\omega$ in the equation for the longitudinal (dissipative friction) force acting on the vortex line, where ω is external frequency identified with the frequency of the oscillations of the vortex line. In the temperature region $\omega_0 \ll T \ll T_c$ one has[18]

$$\mathbf{F}_{\text{long}} = -\mathbf{v}_L\,\frac{k_F^3}{4\pi}\,L\int d\,\cos\,\theta\,\sin^2\,\theta\left(\frac{1}{\tau} - i\omega\right)\,\frac{\omega_0}{\omega_0^2 + \left(\frac{1}{\tau} - i\omega\right)^2}. \tag{3.8}$$

In the limiting case $\omega_0 \gg \omega \gg 1/\tau$ one obtains $\mathbf{F}_{\text{long}} = i\omega\mathbf{v}_L M_{\text{bound states}}$, with the vortex mass

$$M_{\text{bound states}} = \frac{3\pi}{4}\,LC_0\int d\,\cos\,\theta\,\sin^2\,\theta\,\frac{1}{\omega_0(\theta)}, \tag{3.9}$$

where $C_0 = k_F^3/3\pi^2$ is close to the particle density n. This corresponds to Eq. (3.2).

In the high-frequency limit $\omega \gg \omega_0 \gg 1/\tau$, Eq. (3.8) leads to the ''dielectric'' behavior with the ''pinning potential''

$$U = \frac{1}{2}\,\alpha\mathbf{r}_L^2, \quad \alpha = \frac{k_F^3}{4\pi}\int d\,\cos\,\theta\,\sin^2\,\theta\;\omega_0(\theta). \tag{3.10}$$

DISCUSSION

The vortex inertia is essentially enhanced due to the fermion zero modes in the vortex core. This fermionic contribution to the vortex mass appears when the characteristic frequency is small compared to the interlevel distance $\omega \ll \omega_0$. The characteristic frequency of the tunneling process can satisfy this condition, since $\omega \sim \sqrt{F_{\rm vortex}(R_0)/M(R_0)R_0^2} \sim \omega_0 \xi/R_0 < \omega_0$. If $\omega > \omega_0$ the more general contribution of the core fermions, Eq. (3.8), is to be applied. But even in this case the effect of the fermions is always larger than the contribution of the hydrodynamic mass in Eq. (2.1). This is because the frequency ω of the vortex motion cannot exceed the magnitude of the gap Δ, otherwise the simple approach to the vortex dynamics is not valid. This means that the hydrodynamic mass in Eq. (2.1) never enters the tunneling rate in Fermi superfluids and superconductors.

On the other hand, because of the limited frequency the effect of the inertial mass on the vortex tunneling is still small compared to the effect of the Magnus force. Since $\omega \ll \omega_0$ the kinetic term $M\dot{\mathbf{v}}_L = -i\omega M \mathbf{v}_L \sim \hbar n L(\omega/\omega_0)$ is always smaller than the Magnus force $\pi\hbar n L \hat{z} \times \mathbf{v}_L$. That is why the volume law for the tunneling exponent in Eq. (1.1) is still dominant.

The situation can change in the regime $\omega_0 \tau \ll 1$, where the Magnus force is suppressed by the spectral flow of fermions: $\pi\hbar n L \hat{z} \times \mathbf{v}_L \to \pi\hbar(n - C_0) L \hat{z} \times \mathbf{v}_L$ (Refs. 27, 28, 19, 20).

The vortex mass can be also important in d-wave superconductors, where the effect of the fermions on the vortex is more pronounced due to gap nodes.[29] In these superconductors, with a highly anisotropic gap, the interlevel spacing depends on the azimuthal angle α between the momentum $\mathbf{k}$ in the $a-b$ plane and the direction of the gap nodes:[29]

$$\omega_0(\alpha) \approx \alpha^2 \frac{\Delta_0^2}{E_F} \ln \frac{1}{|\alpha|}, \tag{4.1}$$

where Δ_0 is the gap amplitude. The vortex mass in Eq. (3.2) is:

$$M \delta_{\perp ij} = L \int_{-k_F}^{k_F} \frac{dk_z}{2\pi} \int_0^{2\pi} \frac{d\alpha}{2\pi} k_{\perp i} k_{\perp j} \frac{1}{\omega_0(k_z, \alpha)}. \tag{4.2}$$

With Eq. (4.1) for $\omega_0(\alpha)$ the integral over α diverges near the gap nodes. The cutoff $\alpha_{\rm min} \sim \xi/R_v$, where $R_v \sim \xi\sqrt{B_{c2}/B}$ is the intervortex distance, gives a $\sqrt{B_{c2}/B}$-fold enhancement of the vortex mass:

$$M \sim m k_F^3 \xi^2 L \sqrt{\frac{B_{c2}}{B}}. \tag{4.3}$$

This equation holds if $1 \gg B/B_{c2} \gg T^2/T_c^2$ and $B/B_{c2} \gg E_F/\tau\Delta_0^2$.

I thank N. B. Kopnin for illuminating discussions. This work was supported through the ROTA co-operation plan of the Finnish Academy and the Russian Academy of Sciences and by the Russian Fund for Fundamental Research, Grant No. 96-02-16072.

[1] Ü. Parts, V. M. H. Ruutu, J. H. Koivuniemi *et al.*, Europhys. Lett. **31**, 449 (1995).
[2] N. B. Kopnin, JETP Lett. **27**, 390 (1978).
[3] G. E. Volovik, JETP Lett. **15**, 81 (1972).
[4] E. B. Sonin, Zh. Éksp. Teor. Fiz. **64**, 970 (1973) [Sov. Phys. JETP **37**, 494 (1973)].
[5] M. Rasetti and T. Regge, Physica A **80**, 217 (1975).
[6] E. M. Lifshitz and Yu. Kagan, Zh. Éksp. Teor. Fiz. **62**, 385 (1972) [Sov. Phys. JETP **35**, 206 (1972)].
[7] S. V. Iordanskii and A. M. Finkelstein, Zh. Éksp. Teor. Fiz. **62**, 403 (1972) [Sov. Phys. JETP **35**, 215 (1972)].
[8] G. Blatter, V. B. Geshkenbein and V. M. Vinokur, Phys. Rev. Lett. **66**, 3297 (1991).
[9] R. L. Davis, Physica B **178**, 76 (1992).
[10] H-c Kao and K. Lee, hep-th/9503200; R. Iengo, and G. Jug, cond-mat/9506062.
[11] F. Lund and T. Regge, Phys. Rev. D **14**, 1524 (1976).
[12] J. M. Duan, Phys. Rev. B **48**, 4860 (1993); Phys. Rev. Lett. **72**, 586 (1994).
[13] A. Nikiforov, E. B. Sonin, Zh. Éksp. Teor. Fiz. **85**, 642 (1983) [Sov. Phys. JETP **58**, 373 (1983)].
[14] R. L. Davis and E. P. S. Shellard, Phys. Rev. Lett. **63**, 2021 (1989).
[15] J. M. Duan, Phys. Rev. Lett. **75**, 974 (1995).
[16] C. Wexler and D. J. Thouless, cond-mat/9612059.
[17] C. Caroli, P. G. de Gennes and J. Matricon, Phys. Rev. Lett. **9**, 307 (1964).
[18] N. B. Kopnin, Physica B **210**, 267 (1995).
[19] A. van Otterlo, M. V. Feigel'man, V. B. Geshkenbein, and G. Blatter, Phys. Rev. Lett. **75**, 3736 (1995).
[20] M. Stone, Phys. Rev. B **54**, 13222 (1996).
[21] M. M. Salomaa and G. E. Volovik, Rev. Mod. Phys. **59**, 533 (1987).
[22] A. J. Manninen, T. D. C. Bevan, J. B. Cook *et al.*, Phys. Rev. Lett. **77**, 5086 (1996).
[23] G. E. Volovik, and V. P. Mineev, Zh. Éksp. Teor. Fiz. **81**, 989 (1981) [Sov. Phys. JETP **54**, 524 (1981)].
[24] G. E. Volovik, in *Helium Three*, eds. W. P. Halperin, L. P. Pitaevskii, Elsevier Science Publishers B. V., p. 27, 1990.
[25] M. J. Stephen, Phys. Rev. Lett. **72**, 1534 (1994).
[26] N. B. Kopnin and V. E. Kravtsov, JETP Lett. **23**, 578 (1976); Zh. Éksp. Teor. Fiz. **71**, 1644 (1976) [Sov. Phys. JETP **44**, 861 (1976)].
[27] G. E. Volovik, JETP Lett. **57**, 244 (1993).
[28] N. B. Kopnin, G. E. Volovik and Ü. Parts, Europhys. Lett. **32**, 651 (1995).
[29] G. E. Volovik, JETP Lett. **58**, 469 (1993).

Published in English in the original Russian journal. Edited by Steve Torstveit.

An optical method for simulating nonuniform systems

L. S. Al'perovich
Tel Aviv University, Ramat-Aviv 69978, Israel

S. A. Grachev, Yu. A. Gurvich, L. B. Litvak-Gorskaya, and A. P. Mel'nikov
Moscow State Pedagogical University, 119882 Moscow, Russia

I. A. Chaĭkovskiĭ
Ben-Gurion University of the Negev, Beer-Sheva 84105, Israel

(Submitted 11 December 1996)
Pis'ma Zh. Éksp. Teor. Fiz. **65**, No. 2, 207–211 (25 January 1997)

Model experiments of a new type in the physics of nonuniform systems are proposed. The method is based on the production of a randomly nonuniform distribution of charge carriers in a uniform semiconductor by means of photoexcitation with a nonuniform radiation flux. The method makes it possible to vary easily the character of the nonuniformities over wide limits. It has been used to investigate the effective transverse conductivity of nonuniform *p*-Si plates in a magnetic field (H). An anomalous transverse conductivity, previously predicted in a number of theoretical works, has been observed. As the electric field (E) increases, the anomalous conductivity decreases as a result of smoothing of the nonuniformities. The nonuniformities have virtually no effect on the conductivity in an open Hall circuit regime. © *1997 American Institute of Physics.* [S0021-3640(97)01802-1]

PACS numbers: 72.20.Jv, 72.40.+w

1. Transport processes in nonuniform systems are very difficult to study experimentally. It is quite difficult to fabricate samples with prescribed parameters characterizing the nonuniformity. It is even more difficult, and sometimes simply impossible, to change these parameters in the course of an experiment or even from one experiment to another. It is necessary to resort to artificial models. For example, some results have been obtained on a square metal grid whose conducting paths were cut randomly,[1] on a three-dimensional cubic lattice consisting of resistances and capacitances,[2] and on sheets of electrically conducting graphite paper with randomly distributed openings.[3] In these experiments the ratio between the volume fractions of the conducting and dielectric phases could be varied. However, it was impossible to control the conductivities of the two phases, specifically, to simulate the situation of a metal with good and poor conduction.

2. We propose to use nonuniform illumination of uniform semiconductors to produce a conducting medium with a nonuniform carrier density distribution $n(r)$. One way to achieve this is to illuminate a semiconductor plate through a special film — a mask having different transparency in different sections. The method makes it possible to model not only metal–dielectric systems but also systems containing two conducting phases with different conductivities. It is easy to vary the dimensions, shape, and density

of the nonuniformities and the degree of correlation in their arrangement. All this is achieved by adjusting the appropriate masks, which are easily fabricated. One mask can be replaced by another during an experiment. This distinguishes our method advantageously from previous methods employed for simulating disordered systems.

Our objective in the present work was to investigate the effective transverse electrical conductivity in the fields E and H by means of an optical method.

3. The experiments on high-mobility semiconductors, for example, InSb, showed that the transverse magnetoresistance in them increases linearly with H, while according to the classical theory the magnetoresistance saturates in strong H. Herring[4] indicated that this is due to the effect of nonuniformities which are small compared with the dimensions of the sample but much larger than the carrier mean free path.

In the experimental study of nonuniform media the effective conductivity σ^{eff} defined by the relation

$$\langle \mathbf{j}(\mathbf{r})\rangle = \sigma^{\text{eff}} \cdot \langle \mathbf{E}(\mathbf{r})\rangle, \tag{1}$$

where **j(r)** and **E(r)** are the local current density and field and the angle brackets indicate averaging over the volume of the sample, is measured. For weakly nonuniform media σ^{eff} differs very little from $\langle \sigma(\mathbf{r})\rangle$. The conductivity becomes strongly anisotropic in a classically strong field H ($\beta = \mu H/c \gg 1$, μ is the mobility): The diagonal components of the local transverse conductivity tensor $\sigma_{xx}(\mathbf{r}) = \sigma_{yy}(\mathbf{r}) = \sigma_{\perp}(\mathbf{r})$ (the field H is parallel to Z) are proportional to H^{-2}, the off-diagonal elements $\sigma_{xy}(\mathbf{r}) \propto H^{-1}$, and the longitudinal element $\sigma_{zz}(\mathbf{r})$ does not depend on H. The average values $\langle \sigma_{ik}(\mathbf{r})\rangle$ exhibit the same behavior. In this case $\sigma_{\perp}^{\text{eff}}$ can differ substantially from $\langle \sigma_{\perp}(\mathbf{r}, H)\rangle$. Herring calculated the difference $\delta\sigma_{\perp}^{\text{eff}} = \sigma_{\perp}^{\text{eff}} - \langle \sigma_{\perp}\rangle$ to lowest order in the quantity

$$\xi^2 = \langle \delta\sigma^2\rangle / \langle \sigma\rangle^2, \tag{2}$$

considering it to be small. Here $\langle \sigma\rangle$ is the average conductivity and $\langle \delta\sigma^2\rangle$ is the mean-square fluctuation of the conductivity for $H = 0$. It was found that $\sigma_{\perp}^{\text{eff}}$ decreases with H more slowly than $\langle \sigma_{\perp}\rangle$: $\delta\sigma_{\perp}^{\text{eff}} \sim H^{-1}$. Therefore, in strong fields the correction $\delta\sigma_{\perp}^{\text{eff}}$ can exceed $\langle \sigma_{\perp}\rangle$ even for $\xi^2 \ll 1$: Anomalous transverse conduction appears. Herring's results are correct for $1 < \beta < \xi^2$. For $\beta > \xi^2$ one has $\delta\sigma_{\perp}^{\text{eff}} \sim H^{-4/3}$ (Refs. 5–7). This refers to three-dimensional infinite samples. In a finite sample a size effect appears — $\sigma_{\perp}^{\text{eff}}(H)$ depends on the dimension L_z of the sample in the direction of H.[6,7] For two-dimensional nonuniformities $\sigma(r) = \sigma(x, y)$ there is no size effect. In this case $\delta\sigma_{\perp}^{\text{eff}}$ does not depend on H for $\beta < \xi^{-1}$ (Ref. 4), while for $\beta > \xi^{-1}$ one has[5,8]

$$\delta\sigma_{\perp}^{\text{eff}} \approx \frac{\xi}{\beta}\sigma_0, \tag{3}$$

where $\sigma_0 = \langle \sigma_{zz}(r)\rangle$.

Calculations have been performed for two-phase systems.[8,9]

One can see from this brief review that there are a large number of theoretical results concerning this question. However, we know of no works which are specially devoted to an experimental check of the theory. Apparently, the problem lies in the difficulties which were discussed above.

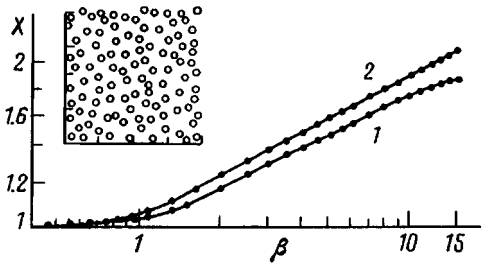

FIG. 1. $X(\beta)$ for sample 1: *1* — negative, *2* — positive. Inset: Enlarged fragment of the mask.

We underscore the fact that according to the theory in all cases for $\beta>1$, $\sigma_{\perp}^{\text{eff}}$ decreases more slowly with H than does $\sigma_{\perp}$ in a uniform sample.

4. Here we present the first results of the application of the optical method of simulation. We studied the effect of nonuniformities on the effective transverse conductivity of crystalline p-Si plates placed in a field H in liquid He. At liquid-helium temperatures T the free carrier density is determined entirely by photoexcitation.

The measurements were performed on a modified Corbino disk — a thin plate (500 μm) in the form of a disk with an opening at the center. The outer diameter of the plate was equal to 10 mm and the inner diameter was equal to 4 mm. A potential difference was applied between the end surfaces with the large and small radii. The magnetic field was perpendicular to the plane of the plate. In this configuration a Hall current exists in the disk, circulating around the axis of the disk. The radial current is determined by the conductivity $\sigma_{\perp}^{\text{eff}}$. The use of a disk with a hole instead of a ''solid'' disk made it possible to avoid a high electric field density near the center of the disk.

The mask consisted of a $\sim$200 μm thick sapphire plate on which niobium was deposited. The nonuniformities — bright spots against a general gray background — were obtained by a photolithographic method. The mask was prepared so that a large number of nonoverlapping nonuniformities would fit within the area of the sample. A 4×4 mm section contained 100 transparent spots of size $2R_p\sim200$ μm (Fig. 1, inset). The average distance between the centers of the spots was $2R_c\sim440$ μm. The distance between the edges of the spots was $L_k\sim(2R_c-2R_p)\sim240$ μm. The ratio of the transmission in a spot to the transmission outside a spot was $\sim1/0.7\approx1.4$. Negatives of the masks — dark spots on a bright background — were also used.

Free carriers were generated by means of foreign (background) radiation passing parallel to H through a pure Si filter and a mask, pressed to the metallized side to the disk, and through a 5 μm insulating polyethylene film (wavelength range 1–7 μm). In this range the experimental samples are practically transparent and the excitation is uniform over the depth of the sample. To avoid reflections of radiation, which would smear the nonuniformities, an absorber with a permittivity close to that of the sample was pressed to the back surface.

The experiments were performed on weakly doped Si:B samples with a main impurity density $N\sim6\cdot10^{15}$ cm^{-3}. For weak fields E, the mobility was determined by scat-

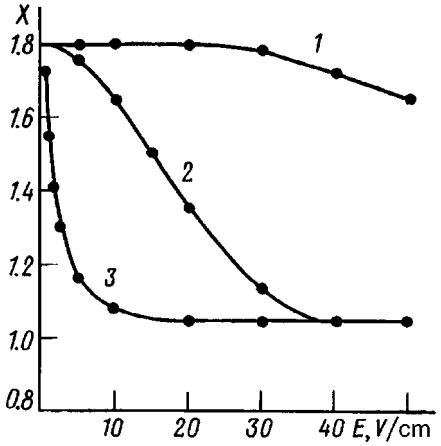

FIG. 2. X versus E for $H=18$ kOe for samples *1*, *2*, and *3*. Mask — positive.

tering by neutral impurities: $\mu=5\cdot10^4$ cm^2/V·s. The density N_k of the compensating impurity, determining the free-carrier lifetime τ, was chosen so as to reduce to a minimum the diffusional smearing of the density nonuniformities ($L_d \ll L_k$, L_d is the diffusion length). The field E corresponded to the Ohmic region of the current–voltage characteristic under uniform excitation. The field H was varied in the range $0<H<30$ kOe ($0<\beta<15$, the quantization parameter for heavy holes $\hbar\omega_c/kT<0.5$, and ω_c is the cyclotron frequency).

The effect of the nonuniformities was determined from the ratio of $\sigma_\perp^{\text{eff}}$ to $\langle\sigma_\perp\rangle$ for the same values of H. The transverse conductivity ($\sigma_\perp^h$) under uniform excitation, chosen so that $\langle\sigma_\perp\rangle=\sigma_\perp^h$ at $H=0$, was used for $\langle\sigma_\perp\rangle$. It is easy to show that this equality remains essentially valid in classically strong fields H.

The experimental results are illustrated for Si:B samples with close values of N ($\sim6\cdot10^{15}$ cm^{-3}) but different compensation: 1) $N_k\sim5\cdot10^{13}$ cm^{-3}; 2) $N_k\sim10^{13}$ cm^{-3}; and, 3) $N_k\sim2\cdot10^{12}$ cm^{-3}. The ratios $X=\sigma_\perp^{\text{eff}}/\sigma_\perp^h$ as a function of β for small E ($=1$ V/cm) for sample 1 are presented in Fig. 1 for the following cases: ''negative'' masks (curve *1*) and ''positive'' masks (curve *2*). One can see that the presence of the nonuniformities cause the relative magnetoresistance to decrease (X to increase); X starts to increase for $\beta>1$, reaching values of 1.9 and 2.1 for $\beta=15$.

The functions $X(E)$ for $H=18$ kOe (positive) for samples 1, 2, and 3 (curves *1*, *2*, and *3*) are presented in Fig. 2. One can see that the lower the value of N_k, the more X decreases with increasing E.

5. We shall first give a qualitative discussion of the results obtained. One can see from Fig. 1 that in the presence of nonuniformities the transverse conductivity decreases with H more slowly than for the uniform case: $X(H)>1$. This is observed for $\beta>1$, i.e., when conductivity anisotropy appears. The ratio $\delta\sigma_\perp^{\text{eff}}/\sigma_\perp^h$ reaches 1 for $\beta=15$: An anomalous transverse conductivity is present ($\sigma_\perp^h=\langle\sigma_\perp\rangle$!).

As E increases at $H=$ const, the ratio X decreases (Fig. 2). The lower the value of N_k (the longer the lifetime τ), the greater the decrease is. This is completely understandable. In the presence of a field E the nonuniformities drift in the Hall direction. If E is sufficiently large, the nonuniformities are smoothed and ξ decreases, and the effect decreases accordingly.

6. We now consider the quantitative aspect of the problem. The density $n(r)$ is proportional to the local transparency of the mask. Simple calculations give in our case

$$\xi=\begin{cases} 0.13 & \text{(negative);} \\ 0.15 & \text{(positive).} \end{cases} \tag{4}$$

Therefore, the conductivity $\sigma_\perp^{\text{eff}}$ in strong fields H ($\beta=15$) is twice the conductivity $\langle\sigma_\perp\rangle$ even for small ξ (≈ 0.1). We note that for the negative and the positive the dependences $X(H)$ for close values of ξ are close, although in these cases the nonuniformities themselves differ substantially in character. This agrees with the fact that according to the theory the effect of nonuniformities is determined solely by the parameter ξ.

The configuration of the experiment is such that the nonuniformities which arise are two-dimensional: $n(r)=n(x,y)$. Then for $\xi\beta>1$, using Eq. (3) and the fact that $\langle\sigma_\perp\rangle=\sigma_0\beta^{-2}$ and $\sigma_\perp^{\text{eff}}\approx\delta\sigma_\perp^{\text{eff}}$, we obtain the estimate

$$X(H)\approx\beta\xi. \tag{5}$$

For the maximum value $\beta=15$ formula (5) gives

$$X_{\max}=\begin{cases} 2.0 & \text{(negative);} \\ 2.4 & \text{(positive).} \end{cases} \tag{6}$$

The experimental values are $X_{\max}\approx 1.9$ and 2.1, respectively. This is fairly good agreement. However, since the experimental situation is complicated by a number of factors (the presence of light holes, weak quantization in H) and since the dependence of $\langle\sigma_\perp\rangle$ on β is weaker than predicted by the theory, it is more accurate to say that agreement obtains in order of magnitude.

7. We now briefly discuss the effect of E. It is easy to show that for $\beta\gg 1$ there is enough time over the lifetime τ for a carrier to be displaced in the Hall direction by a distance $L_{dr}\approx\mu E\tau\beta^{-1}$. For $E=10$ V/cm and $\beta=10$ one has $L_{dr}\approx 2$ μm and 100 μm for samples 1 and 3, respectively. In the first case $L_{dr}\ll L_K$, and drift plays no role. In the second case $L_{dr}\approx L_K$, and the smoothing is substantial. The experimental results agree completely with these estimates (see Fig. 2).

8. We also performed a series of experiments in the absence of a Hall current. In this case, with H varying in the range 0–30 kOe, the nonuniformities have virtually no effect on the conductivity.

Let us now summarize: 1) The optical method for simulating a nonuniform medium in application to the problem of transverse conductivity in a magnetic field was found to be completely adequate for the problem posed, and 2) the method made it possible to obtain a direct proof of the existence of anomalous transverse conductivity in a classically strong magnetic field.

[1] P. L. Watson, Leath, Phys. Rev. B **9**, 4893 (1974).
[2] V. E. Dubrov, M. E. Levinshteĭn, and M. S. Shur, Zh. Éksp. Teor. Fiz. **70**, 2014 (1976) [Sov. Phys. JETP **43**, 1050 (1976)].
[3] M. E. Levinshteĭn, M. S. Shur, and A. L. Éfros, Zh. Éksp. Teor. Fiz. **69**, 2203 (1975) [Sov. Phys. JETP **42**, 1120 (1976)].
[4] C. Herring, J. Appl. Phys. **31**, 1939 (1960).
[5] Yu. A. Dreĭzin and A. M. Dykhne, Zh. Éksp. Teor. Fiz. **63**, 942 (1972) [Sov. Phys. JETP **36**, 127 (1973)].
[6] Yu. M. Gal'perin and B. D. Laĭkhtman, Fiz. Tverd. Tela (Leningrad) **13**, 2102 (1971) [Sov. Phys. Solid State **13**, 1760 (1971)].
[7] O. E. Kvyatkovskiĭ, Zh. Éksp. Teor. Fiz. **85**, 202 (1983) [Sov. Phys. JETP **58**, 120 (1983)].
[8] A. M. Dykhne, Zh. Éksp. Teor. Fiz. **59**, 641 (1970) [Sov. Phys. JETP **32**, 348 (1971)].
[9] B. Ya. Balagurov, Zh. Eksp. Teor. Fiz. **108**, 2202 (1995) [JETP **81**, 1200 (1995)].

Translated by M. E. Alferieff

ERRATA

Erratum: Experimental observation of the interference of three- and five-wave mixing processes in optical second harmonic generation in a solution of bacteriorhodopsin [JETP Lett. 64, No. 10, 718–723 (25 November 1996)]

A. V. Balakin, D. Boucher, N. I. Koroteev, P. Masselin, A. V. Pakulev, E. Fertein, and A. P. Shkurinov
Pis'ma Zh. Eksp. Teor. Fiz. **65**, No. 2, 218 (25 January 1997)

PACS numbers: 42.65.Ky, 42.25.Hz, 99.10.+g

The authors gave the incorrect grant number. Instead of Grant No. 93.02.15-026, the correct grant number is 96.02-16596. [S0021-3640(97)01902-6]

Instructions for authors

Pis'ma Zh. Éksp. Teor. Fiz. **65**, No. 2, 216–217 (25 January 1997)

[S0021-3640(97)02002-1]

PACS numbers: 01.90.+g

The journal Pis'ma Zh. Éksp. Teor. Fiz. publishes short articles which require rapid publication and are of interest to a wide range of physicists. Rapid publication is for first observations of new physical phenomena and theoretical works containing fundamentally new results.

The complete text should not exceed 20 kB in TeX, allowing 1 kB for each figure. If there are no figures, this is approximately 8 or 9 double-spaced type-written pages, including the abstract and references. As a rule, tables are not published.

The first page of the manuscript should look like this:

Title.

Initials and last names of the authors.

Institutions where the authors are employed (including the city and postal code; it is recommended that the e-mail address of one author be given).

Abstract.

The main text follows after skipping one line.

The last names of foreign authors are written in the Russian transcription, but the original spelling must be indicated in a footnote. The names of foreign institutions are written in English.

We call to the attention of Russian authors the fact that the transliteration of last names from Russian into English is done according to strict rules (see Pis'ma Zh. Éksp. Teor. Fiz. **58**, No. 8, p. 699). If for some reason the authors desire a different transcription of their last names, they must indicate it on a separate sheet of paper.

Due to technical constraints on the publication of the journal and in keeping with the point of a brief communication, articles should not be overloaded with a large number of formulas, and the results should not be duplicated in the formulas, tables, and figures. All figures must be drawn clearly in a format ensuring that all details can be clearly understood. Gray-scale figures should be submitted only if absolutely necessary, since their preparation delays publication. The figure captions should be listed on a separate sheet of paper. The last names of the authors and the figure number should be indicated on the back of the figure.

Upper case letters (with no periods) should be used for the common abbreviations and their combinations, and each abbreviation should be explained the first time it appears. Footnotes should be numbered sequentially throughout the entire article.

The references should be listed at the end of the article and numbered in the text, for

example, Ref. 1. The references are listed in the order in which they appear in the text. The following format should be used for the references:

a. For journal articles, first the initials and then the last name of the authors, the title of the journal, the number of the volume (underlined or boldface), the page, and then the year in parentheses are given. If there are more than four authors, then only the first three are listed. For example:

1. A. B. Ivanov, V. G. Petrov, I. M. Sergeev *et al.*, Zh. Éksp. Teor. Fiz. **92**, 290 (1990).

b. In the case of books the initials and last names of the authors, the complete title of the book, the year and location of publication are given (if the book is a translation, then the information for the original must be indicated in parentheses).

Since no proofreading is done, the manuscripts must be prepared extremely carefully. Special care must be taken in showing accurately the indices and exponents, marking them with a half-arc. Primes must be carefully distinguished from the number 1, and the number 1 must be distinguished from a comma. When possible, cumbersome notation should be avoided and the composition of the formulas should be simplified (for example, by using exp). *Russian letters should not be used in the designations and indices.* For example, $P_{\rm opt}$ should be written instead of $P_{\rm опт}$.

To avoid misunderstandings and errors, upper and lower case letters should be clearly distinguished in formulas, if necessary, by marking with a pencil upper case letters with two underbars and lower case letters with two overbars. Greek letters should be underlined in red and vectors should be underlined with a thick blue line (do not use arrows above the letters).

Manuscripts with figures should be submitted in two copies, one of which must be signed by all authors. Gray-scale figures should be submitted in three copies. (Publication could be expedited by submitting in addition diskettes with the text in TeX or LaTeX.) In addition, for countries in the Commonwealth of Independent States the institution that is to appear in the title of the article as the principal institution should be indicated.

The exact address with the postal code, the last name, full first name, and patronymic of the author to whom correspondence should be addressed as well as his telephone number at work and at home should be attached to the manuscript.

The editorial office mails out (to Muscovites gives out) reprints of articles (25 copies of the Russian version and 15 copies of the English translation).

Reprints are kept in the editorial offices for not more than three months from the date of publication.

In connection with the rapid translation of the journal into English, the editors request that, when possible, the authors indicate in the articles the PACS classification (the classification scheme of the American Institute of Physics adopted in American journals). The classification is published in Pis'ma Zh. Éksp. Teor. Fiz. **58**, Nos. 7 and 9.

Pis'ma Zh. Éksp. Teor. Fiz. also accepts articles in English. Therefore the journal is bilingual. Authors desiring to publish their article in English must submit two copies of the English text, three copies of the figures with the English designations, on a separate

sheet of paper the title of the article and the last names of the authors in Russian, and a diskette with the text prepared using the TeX or LaTeX programs.

The editorial staff will not engage in editing the language. However, the editorial staff reserves the right to reject an article if there are any doubts concerning the correctness of the English. In this case a Russian version of the article can be submitted.